The Dissertation Committee for Ge Wang
certifies that this is the approved version of the following dissertation:

Rapid Frequency Chirps of an Alfvén Wave in a Toroidal Plasma

Committee:

Herbert L. Berk, Supervisor

Boris N. Breizman

François L. Waelbroeck

Philip J. Morrison

Milos Milosavljevic

Rapid Frequency Chirps of an Alfvén Wave in a Toroidal Plasma

by

Ge Wang, B.S.; M.S.

DISSERTATION

Presented to the Faculty of the Graduate School of

The University of Texas at Austin

in Partial Fulfillment

of the Requirements

for the Degree of

DOCTOR OF PHILOSOPHY

THE UNIVERSITY OF TEXAS AT AUSTIN

May 2013

Dedicated to my wife Zhenjun Shen and our daughter Sheryl X. Wang.

Acknowledgments

First of all, I indeed present the great appreciation to my supervisor Prof. Herbert Berk. I can't complete my current research work without his daily helpful discussions. When I came to USA six years ago, I had a dream to learn better plasma physics. I detoured my way in the middle from plasma physics to biological physics and returned plasma two and half years ago. I really appreciate Prof. Berk directs me toward the right way and pushes me to have a better understanding of plasma physics.

Prof. Boris Breizman also greatly influences me on the understanding of the physical world. His class of plasma physics is one of the best classes I have taken in the University of Texas at Austin. I always found I have got an insight into a problem which has been confusing to me for a long time during his class and discussion.

I wish to thank Prof. James Van Dam, Prof. François Waelbroeck, Prof. Philip Morrison and Prof. Milos Milosavljevic who were or are serving on my doctoral committee who have helped me during my studies.

And now, last but not least, I'd like to present my thanks to Dr. Eugene Chen, Dr. Tianchun Zhou, Dr. Bo Li , Dr. Xiaoming Wang and Dr. Xiaohui Gao, who are good friends in my life I met here. They have spread over the world but I will keep their unforgettable memories in my mind.

Rapid Frequency Chirps of an Alfvén Wave in a Toroidal Plasma

Publication No. _____

Ge Wang, Ph.D.
The University of Texas at Austin, 2013

Supervisor: Herbert L. Berk

Results from models that describe frequency chirps of toroidal Alfvén eigenmode excited by energetic particles are presented here. This structure forms in TAE gap and may or may not chirp into the continuum. Initial work described the particle wave interaction in terms of a generic Hamiltonian for the particle wave interaction, whose spatial dependence was fixed in time. In addition, we have developed an improved adiabatic TAE model that takes into account the spatial profile variation of the mode and the finite orbit excursion from the resonant flux surfaces, for a wide range of toroidal mode numbers. We have shown for the generic fixed profile model that the results from the adiabatic model agree very well with simulation result except when the adiabatic condition breaks down due to the rapid variations of the wave amplitude and chirping frequency. We have been able to solve the adiabatic problem in the case when the spatial profile is allowed to vary in time, in accord with the structure of the response functions, as a function of frequency. All the models

predict that up-chirping holes do not penetrate into the continuum. On the other hand clump structures, which down chirp in frequency may, depending on detailed parameters, penetrate the continuum. The systematic theory is more restrictive than the generic theory, for the conditions that enable clump to penetrate into the continuum. In addition, the systematic theory predicts an important finite drift orbit width effect, which eventually limits and suppresses a down-chirping response in the lower continuum. This interruption of the chirping occurs when the trapped particles make a transition from intersecting both resonant points of the continuum to just one resonant point.

Table of Contents

List of Figures

Chapter 1

Overview

1.1 Fusion power

Fusion power is believed to be the ultimate solution to civilization's energy needs because the fusion fuel, such as deuterium, are plentiful on the earth or can be bred from the other abundant resources (e.g. tritium can be bred from lithium). Fusion shares with fission the advantage of high energy capacity and freedom from the greenhouse gases. Fusion is much safer than fission, problem with an uncontrolled chain reaction cannot occur and the radiation hazard is significantly lower than fission. One kilogram of deuterium (**D**) and tritium (**T**) fuels would release 10^8 kWh of energy and would provide the requirements of a 1 GW power station for a day.

On the other hand controlled fusion requires the confinement of a hot plasma dilute gas rather than compact fission rods. Though in principle feasible, the confinement issue has proved to be so difficult that the scientists have devoted more than one half century to study and are still attempting to achieve their goal. In order to achieve a fusion reaction, the fuels are heated to a very high temperature to overcome the repulsive force between the positive charged nuclei. Therefore, the most challenging problem of controlled nuclear

fusion is how to maintain a stable equilibrium of the fusion system and suppress all the instabilities driven by the free energy sources (current, gradient of density and temperature, etc.) that degrade the fuel's confinement time.

Ironically, mankind's civilization has developed by taking the fusion power generated in the sun's core, which leads to photon production in its photosphere to shower photons on the earth which have been absorbed to enable life to develop. Unfortunately this energy is not concentrated or necessarily available on demand. Hence, there is a need to search for a more compact energy source.

It is physically impossible to squeeze fusion fuel together on the earth using the sun's trick of gravitational attraction. Instead, we can compress and heat the fuel using high-energy beams of laser light, electrons or ions, which is called inertial confinement. The other magnetic approach is more highly developed and is usually considered more promising for energy production, called magnetic confinement fusion [38, 75].

Many magnetic confinement devices have been designed and built for last half a century. The tokamak, thus far the most successful device, generates its poloidal field B_P entirely through plasma current and its toroidal field B_T through the external coils with the safty factor $q \equiv rB_T/RB_T \sim 1$ [74]. Other configurations such as the stellarator, reversed field configuration, or spheromak have either externally generated poloidal fields or self-generated fields producing a very different range of q values than a tokamak, and different stability criteria. All of these devices have faced considerable challenges related

as to how to confine the high temperature plasma and then control the particle flux and heat load deposited on the first wall facing to fusion plasma.

Indeed the magnetic fusion research is now building a burning plasma experiment at the ITER (International Thermonuclear Experimental Reactor) facility in Cadarache, France, where a large tokamak is now under construction. The ITER tokamak has the 18 niobium-tin toroidal field coils and the superconducting central solenoid coil with producing a field of 13.5 teslas. At their maximum field strength of 11.8 teslas, they will be able to store 41 gigajoules and they are expected to have the needed confinement to generate a burning plasma [43, 56].

The most promising fusion reaction is that in which the nuclei of deuterium and tritium fuse to produce an alpha particle with the release of a neutron, that is

$$\mathbf{D} + \mathbf{T} \rightarrow \mathrm{He}(3.5\mathrm{MeV}) + \mathrm{n}(14.1\mathrm{MeV}). \tag{1.1}$$

The neutron is lost directly from the system carried away with a large amount of fusion power but alpha particles are trapped in plasma and then heat the system to sustain the fusion reaction. When the balance is reached where the plasma temperature can be maintained against the energy losses solely by alpha particle heating, the burning plasma is self-heated and ignites a self-sustaining fusion reaction. In principle, no external heating is needed, though auxiliary heating will be used for the startup and burn control.

Although the population of alpha particle is relatively small compared

to the background density, Alpha particles generated from the reaction might have important consequences to the stability and turbulence through the wave-particle interactions. So far it is known that some waves, in tokamak, such as Alfvén waves, become unstable due to the energetic alpha particles which transfer kinetic energy and momentum of alpha particles to the waves. The momentum transfer causes alpha particles to cross field lines and possibly be lost to the walls. The loss of energetic particles means that the heat source of the plasma is being drained which can quench the fusion burn. In addition energetic alpha particle bombardment of wall facing material can cause wall degradation, which is of considerable concern. Therefore, the understanding of nonlinear coupling processes involved in fast ion interaction with thermal particles is important to global stability, confinement, heating and current drive, alpha channeling, burn control, Helium ash removal , thermal instabilities, etc. [17, 40, 41]

A burning plasma is considered to be self-heated by the 3.5 MeV alpha particle byproduct, alpha particles from the fusion reaction. However, the conventional collision theory predicts that most of the alpha particle energy heats electrons through the electron drag process. Only about 10% of the alpha particle energy directly heats ions, which is the fuel that needs to be hot (between 10 -20 KeV) to have reasonable fusion production (ions are only heated secondarily through electron ion thermal equilibration processes). In addition as the collision time is rather long, (0.5s in ITERs targeted burning plasma), the alpha particle pressure can build up to the point that it can effect

plasma stability. It has been proposed to use the alpha particles tendency to produce instability in a constructive way. In particular there is a benefit to extract energy from alpha particles in a controlled manner so that energy is transferred to the background plasma significantly faster than occurs with electron drag. If this can be done without the alpha particles being lost to the plasma edge, there is the benefit that the alpha particle pressure will remain below any particle kinetic pressure instabilities that might otherwise arise. In addition, if the alpha particle can be controlled to primarily heat ions, the fusion efficiency can be significantly improved at fixed plasma pressure when ions are hotter than electrons, a larger rate of fusion production then arises [3, 26].

1.2 Toroidal Alfvén eigenmodes

The Alfvén continuum is intrinsically modified due to toroidicity [20]. Gaps in the continuum arise, which in turn leads to weakly damped toroidal Alfvén eigenmodes (TAE). Previous studies found that the energetic particle pressure gradient supplies the free energy source that can destabilize waves which resonantly interact with the periodic motion of the energetic particles [30, 33].

In a slab the shear Alfvén wave is usually strongly stable because of the phase mixing arising from the interaction with shear Alfvén continuum, where the mode structure is singular and the wave spectrum spreads continuously in the range of $\min(k_\parallel^2 v_A^2) \leq \omega^2 \leq \max(k_\parallel^2 v_A^2)$ ($k_\parallel$ is the shear Alfvén wave

number parallel to the equilibrium magnetic field and v_A is Alfvén velocity in an inhomogeneous plasma). However, the poloidal symmetry breaking in the toroidal confinement device leads to the couplings between neighboring poloidal harmonics, which not only opens a gap in the continuous shear Alfvén spectrum, but also produces discrete Alfv'en eigenmodes [20]. These discrete modes, known as TAEs, are linearly excited as discrete shear Alfvén-like modes in the gap region. As a consequence, TAE is undamped to the lowest order in the gap. Dissipation however may be present due to weak viscosity, resistivity and remnant interaction with the continuum in spatial regions where the wave amplitude is weak.

The resonance condition $\omega - k_{\|} v_A \approx 0$, shows that moderately high $n(\sim 10)$ Alfvén waves are in a frequency range that can resonantly interact with alpha particles. If the intrinsic diffusion mechanisms acting on the alpha particles are low enough, the instability produced will lead to a chirping response that arises as a consequence of the background dissipation mechanisms that are present [37, 66].

Rosenbluth, et.al. developed an MHD model TAE waves for a low-beta plasma ($\beta \equiv 8\pi p/B^2 \ll 1$, p is the plasma thermal pressure and B is the magnitude of magnetic field) and a small inverse aspect ratio tokamak ($\epsilon = r/R \ll 1$, r is minor radius and R is major radius of tokamak) with circular cross section to describe high toroidal mode number n TAE waves

(RBV tip model) [67]:

$$(\mathbf{b}\cdot\nabla)[\nabla^2(\mathbf{b}\cdot\nabla)\phi]+\nabla\cdot[(\omega^2/v_A^2)\nabla\phi]=0, \tag{1.2}$$

where $v_A = B/\sqrt{4\pi\rho}$ is the Alfvén speed, with ρ the mass density and $\mathbf{b}$ directs the unique direction of magnetic fields. In the toroidal geometry, the equilibrium magnetic field is modified by a poloidal angle θ dependence $B = B_0[1+\epsilon\cos\theta]$, which causes the coupling among the poloidal harmonics and then the poloidal m-number is not a good 'quantum number'. In the case of a small inverse aspect ratio, wave potential ϕ_m essentially couples only to its neighboring sidebands $\phi_{m\pm1}$ due to toroidicity. The reduced MHD equation is given by [67],

$$\frac{d}{dr}[(\frac{\omega^2}{v_A^2}-k_{\|m}^2)\frac{d\phi_m}{dr}]-\frac{m^2}{r^2}(\frac{\omega^2}{v_A^2}-k_{\|m}^2)\phi_m+\hat{\epsilon}\frac{\omega^2}{v_A^2}(\frac{d^2\phi_{m-1}}{dr^2}+\frac{d^2\phi_{m+1}}{dr^2})=0. \tag{1.3}$$

Here, $\hat{\epsilon}\approx 5r/2R$ is the toroidicity coupling strength for a low-beta tokamak plasma.

An Alfvén gap opens in the Alfvén continuum due to the degeneracy condition at the resonant surface $r = r_m$ where $k_{\|m-1}(r_m) = -k_{\|m}(r_m) = 1/(2q_mR)$ ($q_m = q(r_m)$ is the safety factor at the resonant surface) as shown in Fig. 1.1, whose center frequency is $\omega_A = v_A(r_m)/2q_mR$.

Away from the gap, it is accurate to approximate the MHD equations as if the plasma was cylinder where both the toroidal harmonic n and poloidal harmonic m are good quantum numbers. The toroidal coupling is significant only in the vicinity of the TAE gap locations at the resonant surface where

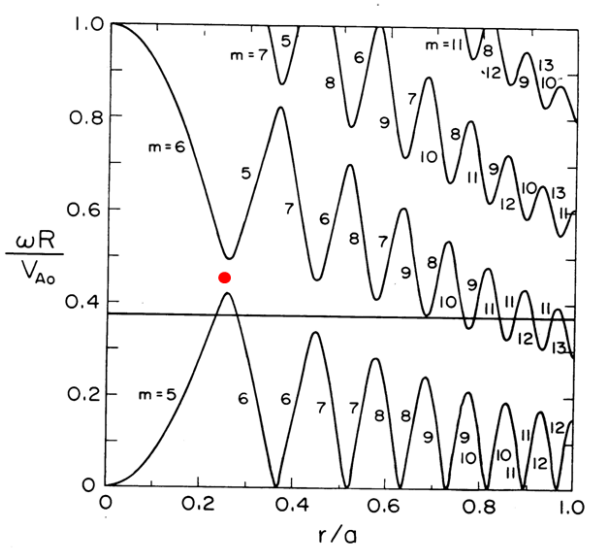

Figure 1.1: The degeneracy due to toroidicity opens a frequency gap in the continuum spectrum of shear Alfvén wave. TAE wave formed in the gap region can be excited due to the energetic particles.

there is the strong interaction between the m^{th} and $m+1^{th}$ harmonics due to toroidicity. A boundary layer method is used to match the outer and inner solution. Let,

$$x = n[q(r) - m_0/n] \approx nq'(r_l)(r - r_m) + m + 1/2.$$

Then we obtain the following coupled equations valid in the narrow layers in the vicinity of the gaps:

$$(\frac{1}{2} + x_m + \frac{\epsilon'_m g_m}{4})\frac{d\phi_m}{dx_m} + \frac{\epsilon'_m}{4}\frac{d\phi_{m+1}}{dx_m} = C^-_m \tag{1.4}$$

$$(\frac{1}{2} + x_m - \frac{\epsilon'_m g_m}{4})\frac{d\phi_{m+1}}{dx_m} - \frac{\epsilon'_m}{4}\frac{d\phi_m}{dx_m} = C^+_{m+1}. \tag{1.5}$$

The Berk-Mett quadratic form [11] is derived by connecting 'jumps' in

the perturbed radial displacement across the tips to the outer region where cylindrical solutions away from tips apply as shown in the work of RBV tip model [67].

$$-\sum_m \frac{\pi^2 R c^2 q'_m r_m n}{q_m^2 \omega_A} \begin{bmatrix} C^-_{m+1}\widetilde{C}^-_{m+1}(\overline{\Delta}^-_{m+1} + \alpha^-_{m+1}) \\ +C^+_m \widetilde{C}^+_m(\overline{\Delta}^+_m + \alpha^+_m) + \beta^-_{m+1}\widetilde{C}^+_m C^-_{m+1} \\ +\beta^+_m \widetilde{C}^-_{m+1} C^+_m - \widetilde{\Delta}^+_{m+1}\widetilde{C}^+_{m+1} C^-_{m+1} \\ -\widetilde{\Delta}^-_m C^+_m \widetilde{C}^-_m \end{bmatrix}, \tag{1.6}$$

where q'_m are the derivation of safety factor with respect to r at $r = r_m$ where $q_m \equiv (m + 1/2)/n$. The symbol '$\sim$' above $C^{\pm}$ represents the adjoint of this amplitude and we will show the detail in our discussion of the equivalence of Hamilton principle in real space and frequency domain in chapter 4. The external constants $\overline{\Delta}_m$ and $\widetilde{\Delta}_m$ (with the subscript indicating the corresponding poloidal harmonic component) are obtained from the outer MHD equations and can be numerically calculated as described in reference[67]. The analytic function $\alpha^{\pm}(\omega) = -\omega/\sqrt{1-\omega^2}$, $\beta^{\pm}(\omega) = -1/\sqrt{1-\omega^2}$ are derived from the inner layer equations in terms of the TAE order-ϵ frequency shift ω of the m^{th} couplet primarily consisting of the m^{th} and $m+1^{th}$ poloidal harmonics.

In addition, the radial homogeneous plasma in tokamak leads to the relevant radial structure of a TAE mode, which is of the integral form [9],

$$\phi_m(r) = \frac{\Phi_m}{\pi} \int_{r_m}^{r} dr' \frac{a_m + b_m(r' - r_m)}{(r' - r_m)^2 + a_m^2}, \tag{1.7}$$

which expresses in terms of $C^{\pm}$ in the expression written above in Eq. 1.4, the coefficients Φ_m and a_m, b_m are obtained in chapter 4.

With a sufficiently strong energetic particle free energy source, another class of instability called Energetic Particle Modes (EPMs), may arise. They

typically occur inside the Alfvén continuum so that in the absence of a drive a long lived plasma oscillation would not arise. The EPM occurs only with a strong enough energetic particle drive to overcome continuum damping. An example of such a mode is the fishbone oscillation which is an $n = 1$ internal mode with dominant poloidal mode number $m = 1$ which is resonantly destabilized by energetic trapped particles. Chen et al. [19] proposed that the mode is destabilized by energetic trapped ions via processional drift resonance ($\omega = \omega_d$) and that the mode is intrinsically an energetic particle mode. This non-perturbative scenario for linear instability is out of the scope of this investigation and will not be discussed in this thesis.

1.3 Bump-on-tail instability

Bump-on-tail is a very common instability in plasma physics. When the energetic particles have an inverted distribution, forming a bump on the tail of the thermal particle distribution, it will induce an instability with the strong wave excitation. In the linear theory, the bump-on-tail instability can be thought of as the inverse of Landau damping, where the existence of a greater number of particles that move faster than the wave phase velocity as compared with those that move slower, leads to an energy transfer from the particles to the wave. The instability driving mechanism of the bump-on-tail instability is a fully kinetic phenomenon and cannot be described in a fluid model which can treat the properties of the background wave in the absence of the resonant drive. The free energy induced bump-on-tail instability is associated with the

spatial gradients of the inverted particle distribution[1, 39].

The distribution of alpha particles also is indeed inverted and provides a free energy source for the bump-on-tail-like instability. As an example even in slab geometry, we take a Maxwellian distribution with a gradient in the x direction in a uniform magnetic field along the z direction. The simplest such alpha particle distribution is nearly isotopic in phase space. The distribution can depend on the particle energy E and the guiding coordinate $X = x - v_y/\omega_c$ (ω_c is the gyro-frequency),

$$f(E, x) = \int dv_x \exp(-\frac{E}{T}) \exp(-\frac{x - \frac{v_y}{\omega_c}}{L}),$$

where T is the particle thermal temperature and L is the length scale of system. Then notice that $\partial f/\partial v_y$ is proportional to $-v_y/v_{th}^2 + (\omega_c L)^{-1}$. Hence, the distribution is inverted ($\partial f/\partial v_y$ is positive for $v_y > 0$) for $0 < v_y < v_{th}^2/(\omega_c L)$ and then this region of phase space is a drive promoting instability. This inversion arises in a very similar way for more complicated problems.

When the bump-on-tail instability evolves into its nonlinear stage, Bernstein-Greene-Kruskal (BGK) modes [13] are formed due to nonlinear properties of the instability resonances, provided that each resonance is sufficiently separated so that mode overlap does not arise. The interplay between the wave field, which tends to flatten the distribution of resonant particles, and the source and sink relaxation processes, which tend to restore the unstable distribution function, leads to various nonlinear effects. When extrinsic, as well as intrinsic dissipation is present, particles with inverted distribution do no cause

instability of the energetic particle drive is too weak to overcome the dissipative processes present. Instability arises when the population of energetic particles reaches a critical value. Around this critical value is a near-threshold regime of wave excitation for which a rich family of nonlinear phenomena have been revealed. Berk et.al. found as they decreased their relaxation rates: steady saturation, pulsation, a frequency pitchfork splitting sequence and an explosive solution in their cubic equations[6]. Later on, a full kinetic numerical simulation of the bump-on-tail instability near-threshold showed that the explosive state evolved into hole and clump phase space structures moved in the phase space causing frequency chirping signals to appear [8].

Late in the nonlinear evolution, particles are trapped in slowly moving potential wells which allows the adiabatic approximation to be used to describe the dynamics. The treatment leads to a predicted wave saturation amplitude and a specific chirping rate if the frequency shift during the initial nonlinear stage is assumed to be small compared to the separation of different linear frequencies [4]. The time scale of chirping events is much shorter than the frequency variation of equilibrium profile. The Berk-Breizman model (BB model) predicts that emerging frequency shifts vary with the square root of time and saturation amplitude is $(0.54\gamma_L)^2$ (γ_L is the mode linear growth rate) for the marginal instability. The rate of frequency shift is determined by the balance between the rate of energy being nonlinearly extracted from the resonant particles and the power dissipated into the background plasma through the various damping mechanisms present in the system.

Figure 1.2(a) shows the time sequence of chirping structures that form after linearly unstable excitation. When the particles are fully trapped in the resonant region, the wave is saturated and the distribution function flattens in the resonance region but the chirping causes steep gradients with the ambient region of phase space that is outside the trapped region.

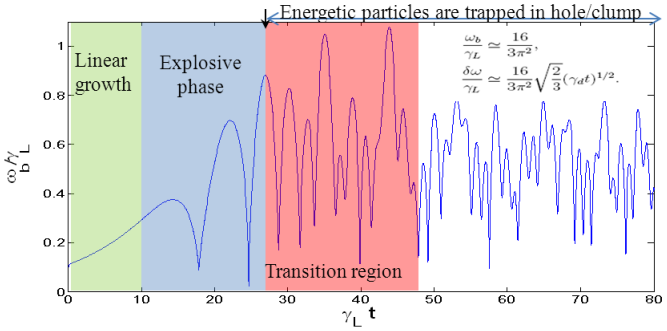

(a)

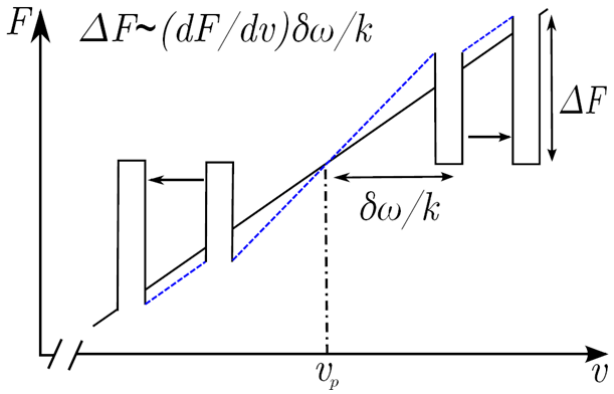

(b)

Figure 1.2: (a) The time sequence of chirps; (b) The formation of hole/clump in phase space.

Candy et.al. attempted to apply the hole-clump mechanism to nonlinear simulations of two-species plasma, fishbone bursts and beam-driven TAE

problems [18]. Recently, Lilley et.al. studied the effects of particle relaxation process due to dynamical friction (drag). It is found that drag greatly expanded and enhanced the regimes for explosive solution for the waves. When diffusion dominates, the waves exhibit regimes of steady-state, amplitude modulation, chaotic and explosive regimes near marginal stability [50]. Later simulations showed that the combined effect of dynamical friction and diffusion produces a diverse range of nonlinear behaviors including hooked frequency chirping, undulating, and steady state regimes [51]. A marginally unstable energetic particle population in dissipative plasma is found to change globally due to wave chirping of a single wave-particle resonance, whose convection motion in phase space results in continual "burrowing" the holes and clumps in the continuous production of nonlinear hole and clump pairs [49].

Frequency chirp has been extensively observed on several fusion related plasma experiments [27, 28, 54, 64]. The development of chirping events has been quantitatively described as a result of the generation of phase space structures (holes and/or clumps) and their chirps due to the presence of background dissipation[14, 48, 51, 61, 70]. Spontaneous nonlinear coherent frequency chirping structures arise in response to the dynamics of the trapped particles in these phase space structures. Specially, the rapid frequency chirp is observed in MAST experiments as shown Fig. 1.3 [35].

In this thesis, we explores TAE chirps which arise from spontaneous formation of nonlinear phase-space structures (holes and clumps) sweeping in the phase space. If dissipation in the background plasma is present, and

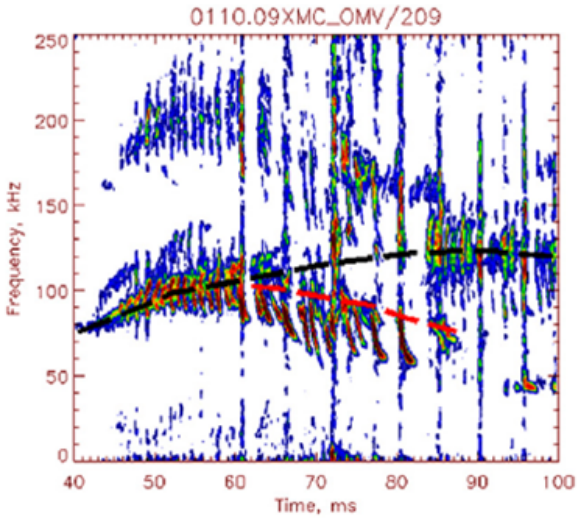

Figure 1.3: Hole-clump modes before t=60ms as have been interpreted signals from hole-clump structures arising from perturbative modes, in much same as hole-clump structures formed in the bump-on-tail model. The later chirping signals (red dashed line) between t=60ms and t=85ms do not follow the scaling of the BB model and the starting frequency may not even be in the gap. These modes are likely to be non-perturbative EPM's.

if the plasma is at low enough collisionality, TAE waves are likely to form resonant phase space structures in the frequency gap which may then chirp into the continuum. The initial evolution of the phase space structure is quite similar to the most simplified model described by the electrostatic bump-on-tail instability [8, 50, 60]. However, when TAE approaches the Alfvén tip, the assumptions for the chirping frequency used in the initial theory fail and a more sophisticated evaluation needs to be made. In chapter 2, a Vlasov simulation is developed to simulate TAE frequency chirping in the Alfvén gap and continuum, with a generic form for the particle-wave interaction and a fixed spatial dependence of the TAE mode structure. In chapter 3 we show

that the results of the simulation can be replicated by using an adiabatic model for the particle-wave interaction except where the adiabatic approximation breakdowns. Specifically, the asymmetric downward and upward chirps near the tip regions are analyzed quantitatively. In chapter 4, we take the spatial dependence of the TAE mode structure into account and use a systematic procedure, based on the map model [9, 10] to describe the dynamics of the mode. A variational method for the wave-particle interaction is formulated with the test functions for the waves constrained to be those linear MHD solution that minimize the variational form. It is expected that this method is accurate if the width of the separatrix in momentum space (normalized to the resonant frequency as is discussed later) is much less than the TAE gap.

Chapter 2

Simulation for Spontaneous Frequency Chirps of Toroidal Alfvén Eigenmode

2.1 Introduction

In this chapter, we model spontaneous chirps that can arise when TAE waves are excited by energetic particles[20]. The chirping TAE wave can deviate significantly from the bulk plasma eigenfrequency and it should even be possible for the phase space structures to enter the Alfvén continuum as is indicated in some experiments[28, 64]. The description of a chirping mode is a drastically different wave response from that predicted by linear or the usual nonlinear theory.

The presently developed analytic theory for a TAE mode[4, 8] is justified only when the mode is excited in the TAE gap with a frequency shift significantly less than the difference between the continuum and linear frequencies. The transition from the TAE gap region to the continuum, demonstrated here, is in a regime not described by the standard theory. Here we construct a 'toy model' for the wave-particle interaction, and a plausible model of the background wave properties. This wave model is derived from a small inverse aspect ratio tokamak theory to examine the possibility of achieving chirping

events that are formed in the TAE gap and continue chirping into the continuum. We note that in the continuum we have a strong damping mechanism. An issue then arises if a chirp can continue in the continuum. Our simulations show that the chirp does continue. To match the strong dissipation of the continuum, the chirping rate increases together with the field amplitude of the chirping signal. This increase is enabled by the free energy in the particle distribution, which is released to balance the strong dissipation that exists in the continuum. Indeed, the wave can be viewed as a catalyst. As the wave chirps, resonant particles release energy from the inverted distribution to the background in a manner described in references[4, 8]. In the simulation we also observe an initial formation of the phase space structures with their subsequent chirps. Initially the characteristic of the chirp is similar to what has been described for the bump-on-tail problem [8]. However in the subsequent evolution, new chirping properties appear as the excited wave chirps towards the continuum and then often into the continuum.

In the below discussion, we obtain the linear TAE background wave equation from the Berk-Mett quadratic form[11] derived from the RBV model[67] which is valid for a small inverse aspect ratio and low beta tokamak and study the interactions between the linear waves and the nonlinear response of energetic particles. For the present study we assume that waves can be described by a single symmetric couplet and a simplified model of a two-dimensional phase space distribution is used to describe the energetic particles. The RBV theory leads to a Volterra integral equation in the time domain for the evolution of

the wave. To this equation we add, using a simplified model, an interaction term of the wave and energetic particles. The particles are taken to satisfy a one dimensional Vlasov equation given in terms of action-angle variables. The dynamics of the resonant particles is then the same as the dynamics in the bump-on-tail problem. Integrating in phase space we then calculate the particle-wave interaction term. This term is formally a source for the linear wave equation for TAE excitations. In the time domain the TAE excitation has been shown to be described by a Volterra equation [72]. Without dissipation, the Volterra equation coupled to the energetic particle interaction term, produces a linear instability with a growth rate γ_L. We then add to the equation two extrinsic dissipation mechanisms which will be described here and next chapter. The dissipation produces a damping rate γ_d. We select enough dissipation to create an initial system with energetic particles close to marginal stability, with a growth rate $\gamma = \gamma_L - \gamma_d \ll \gamma_L$.

In order to resolve the fine structure in phase space, the numerical scheme integrates the Vlasov equation in the Fourier transformed phase space using a numerical method originally developed by Breizman and Petviashvili[62]. The algorithm is improved through the shifting to the wave frame and the calculation is accelerated by avoiding the time expensive iteration steps. Our present simulation results replicate the saturated wave amplitude and square root law of the initial chirping rate associated with the previous analytic theory. We demonstrate the self-consistency of the filtered chirped signal and the dynamics of the clump throughout its evolution using a WKB-like analysis of

the signal. Plots of the phase space structure correlate well with the shape of the separatrix of a chirping structure.

2.2 Basic equations

We begin with the Berk-Mett quadratic variational form as the basis for constructing a TAE wave theory for arbitrary mode numbers in the large aspect ratio low-beta circular tokamak limit. The general expression was derived in the frequency domain[11] by using a boundary-layer method to combine an ideal MHD outer region approximated as a response in cylindrical geometry and matched to the inner layer response that accounts for the toroidicity of the geometry. For large toroidal mode number n, the quadratic form of a TAE wave is the following:

$$\mathbf{Q_{TAE}} = -\sum_m \frac{\pi^2 R c^2 q'_m r_m n}{q_m^2 \omega_A} \begin{bmatrix} C^-_{m+1}\widetilde{C}^-_{m+1}(\overline{\Delta}^-_{m+1} + \alpha^-_{m+1}) \\ +C^+_m\widetilde{C}^+_m(\overline{\Delta}^+_m + \alpha^+_m) + \beta^-_{m+1}\widetilde{C}^+_m C^-_{m+1} \\ +\beta^+_m\widetilde{C}^-_{m+1}C^+_m - \widetilde{\Delta}^+_{m+1}\widetilde{C}^+_{m+1}C^-_{m+1} \\ -\widetilde{\Delta}^-_m C^+_m \widetilde{C}^-_m \end{bmatrix}, \quad (2.1)$$

The symbol '$\sim$' above $C^{\pm}$ represents the adjoint of this amplitude. In the ideal MHD limit, the m^{th} and $m+1^{th}$ poloidal coupling in the narrow inner layer determine the form $\alpha^{\pm}$ and $\beta^{\pm}$ as a function of frequency, which are analytic on the upper half complex plane.

$$h = \frac{\omega^2/\omega_A^2 - 1}{\hat{\epsilon}_m},$$
$$\alpha^+_m = \alpha^-_{m+1} = -\frac{h_m}{(1-h_m^2)^{1/2}},$$
$$\beta^+_m = \beta^-_{m+1} = -\frac{1}{(1-h_m^2)^{1/2}}.$$

Here, h represents a frequency shift from ω_A normalized by the gap width. In the adiabatic models, a notation ω is used to replace h_m to avoid the confusion.

With the RBV tip theory the m^{th} and $m+1^{th}$ poloidal harmonics are intrinsically linked together when the frequencies are close to and within the gap. As the chirping frequency moves away from the gap frequency, the two mode components decouple. For example, if the safety factor increases with minor radius, then for downward chirp of a clump into the continuum, the mode structure becomes more dependent on the m^{th} component as the $m+1^{th}$ component reduces in amplitude. Similarly, the $m+1^{th}$ poloidal harmonic will eventually dominate as a hole chirps into the upper continuum. The results that emerge from the tip model are justified as long as the inverse aspect ratio is small, $\omega(t)-\omega_A \ll \omega_A$ and the MHD excitations at the nearest neighboring tip positions (e.g. at $r \sim r_{m+1}$, where $q(r_{m+1}) = (m+3/2)/n$) is negligible.

The present form indicates that a "string" of m couplet components of the TAE response can be excited by the energetic particles with the distribution function $\hat{f}(\theta, p; h)$ ((θ, p) is a pair of action-angle variables describing the resonant coordinates of the energetic particles in tokamak) at the frequency of h. In addition the TAE wave couples with the interaction Lagrangian term for the energetic particles. We model this interaction with the form,

$$\begin{aligned} Q_{TAE} = -Q_{int} = -\int d^3r\, \mathbf{A}\cdot\delta\mathbf{j} \approx -\frac{1}{i\omega_m}\int d^3r\, \mathbf{E}\cdot\delta\mathbf{j} \\ = -\frac{i\eta}{2\pi}\int_{-\infty}^{\infty} \hat{f}(\theta,p;h)(C_m^+ + C_{m+1}^-)e^{-i\theta}\, dpd\theta. \end{aligned} \tag{2.2}$$

Then $Q_{TAE}+Q_{int}$ represents the quadratic form, whose variation with respect to $\widetilde{C}_m$ (for all m), produces the wave equation. Here $h = h_m$, $\mathbf{A}$ is the vector potential in the gauge where $\mathbf{E} = -\partial\mathbf{A}/\partial t = i\omega_A\mathbf{A}$ and η is the wave-particle coupling strength that is used to determine the linear growth rate γ_L of the TAE wave. The trapped energetic particles, interacting with TAE waves, are described by a single pair of action-angle variables. The Hamiltonian associated with the particle motion is,

$$\mathcal{H} = \frac{p^2}{2} + \Re[e^{i\theta}(C_m^+ + C_{m+1}^-)].$$

The notation $\Re$ indicates the real component. Then the equations of motion obtained from Hamilton's equations are: $\dot{p} = -\frac{\partial\mathcal{H}}{\partial\theta}$, $\dot{\theta} = \frac{\partial\mathcal{H}}{\partial p}$. Note, if we assume that the couplet interaction term $\widetilde{\Delta}_m$ is small, the spatial integral in Eq.(2.2) need only to be taken over the space of a single couplet. The interaction we have described is essentially the same as the bump-on-tail problem[62]. The new aspect here is that we describe waves that form in a gap, which then chirp into the continuum.

By taking the functional variation with respect to $\tilde{C}_m^+$ and $\tilde{C}_{m+1}^-$, one can readily obtain the wave equations for the TAE/energetic particle interaction in the frequency domain.

$$(\overline{\Delta}_m^+ + \alpha_m^+)C_m^+ + \beta_{m+1}^- C_{m+1}^- = -\frac{i\eta}{2\pi}\int_{-\infty}^{\infty}\hat{f}(\theta,p;h)e^{-i\theta}\,d\theta dp, \tag{2.3}$$

$$\beta_m^+ C_m^+ + (\overline{\Delta}_{m+1}^- + \alpha_{m+1}^-)C_{m+1}^- = -\frac{i\eta}{2\pi}\int_{-\infty}^{\infty}\hat{f}(\theta,p;h)e^{-i\theta}\,d\theta dp. \tag{2.4}$$

We are interested in the time evolution behavior of these equations. Therefore, the inverse Fourier transformation is applied to the above two

equations (2.3) and (2.4) to convert from h space to the time domain. Then the equations for the independent mode amplitudes $A^+ = C_m^+ + C_{m+1}^-$ and $A^- = C_m^+ - C_{m+1}^-$ are found to be,

$$A^+(t) = \frac{1}{\Delta_m - i}\int_0^t (J_0(t-\tau) - iJ_1(t-\tau))A^+(\tau)\,d\tau - \frac{2i\eta}{\Delta_m - i}\int_{-\infty}^{\infty} f_1(p,t)\,dp,$$
$$A^-(t) = -\frac{1}{\Delta_m - i}\int_0^t (J_0(t-\tau) + iJ_1(t-\tau))A^-(\tau)\,d\tau, \qquad (2.5)$$

where J_0 and J_1 are the zero-order and first-order Bessel functions, respectively and $f_1(p,t) = \int_{-\pi}^{\pi} \frac{d\theta}{2\pi} f(\theta,p;t)e^{-i\theta}$. The $A^-(t)$ decouples from the dynamics of the energetic particles (it can be shown that this amplitude decays as $t^{-3/2}$ and thus has negligible long time behavior). Therefore only the evolution of the A^+ amplitude is followed. Henceforth, the superscript '+' will be suppressed without ambiguity. In addition to the equations of motion that are produced by the Berk-Mett variational form, we add rather arbitrarily linear damping term. We assume that this term is produced by an extrinsic physical mechanism. There are several ways to model the added damping in Eqs. (2.3) and (2.4). One way is to set $h \to h + i\gamma_d$, which is the way we have usually run. An alternative way is to let $\Delta_m \to \Delta_m - i\kappa$, with $\kappa > 0$. We can then choose γ_d or κ to have the values needed to study a system near marginal stability. Most of our results are obtained by letting $h \to h + i\gamma_d$ with $\kappa = 0$. However, we show that we obtain very similar agreement of the evolution by letting $\Delta_m \to \Delta_m - i\kappa$ with $\gamma_d = 0$. With $\kappa = 0$ and γ_d finite, the wave equation in

the time domain becomes,

$$A(t) = \frac{1}{\Delta_m - i}\int_0^t (J_0(t-\tau) - iJ_1(t-\tau))e^{-\gamma_d(t-\tau)}A(\tau)\,d\tau - \frac{2i\eta}{\Delta_m - i}\int_{-\infty}^{\infty} f_1(p,t)\,dp. \tag{2.6}$$

This wave equation is non-local in time requiring detailed knowledge of the time history from the past. Similar non-local wave equations for the internal kink mode have previously been derived [15, 18].

The kinetic Vlasov equation is used to describe the dynamics of collisionless particles with a distribution function characterized by a single pair of action-angle variables (p, θ) of the unperturbed orbits. Then the Vlasov equation is given by,

$$\frac{\partial f}{\partial t} + p\frac{\partial f}{\partial \theta} - \Re\{A(t)e^{i\theta}\}\frac{\partial f}{\partial p} = 0. \tag{2.7}$$

In our work we consider the equilibrium distribution is to be smooth and the localized behavior modeled as a linear function. With a suitable choice of η, we can take $\partial f_0(p)/\partial p = 1$ where $f_0(p)$ is the unperturbed distribution. The complete set of equations for the model is then described by equations (2.6) and (2.7).

2.3 Linear analysis and nonlinear saturation

The linear mode analysis is an important tool in the plasma physics, where the individual zero eigenvalue in the dispersion matrix represents one independent wave mode. Because the damping or growth rate of a mode is

usually much smaller than the real frequency, the perturbative method is used to calculate the damping/growth rate.

The linear analysis of equations (2.6) and (2.7) allows the determination of the TAE growth during the initial excitation. The linear stage is readily described in the frequency domain. The wave equation takes the form,

$$[\Delta_m - (\frac{1-\tilde{h}}{1+\tilde{h}})^{\frac{1}{2}}]\hat{A}(h) = -\frac{i\eta}{\pi}\int_{-\infty}^{\infty}\hat{f}(\theta,p;h)e^{-i\theta}\,d\theta dp, \tag{2.8}$$

where $\tilde{h} = h + i\gamma_d$. The TAE wave is excited by resonant energetic particles with a momentum $p = h$. To solve for perturbed distribution function, we need to solve the linearized Vlasov equation:

$$\frac{\partial f}{\partial t} + p\frac{\partial f}{\partial \theta} - \Re(A(t)e^{i\theta})\frac{\partial f_0(p)}{\partial p} = 0. \tag{2.9}$$

Using $\partial f_0(p)/\partial p = 1$ and $A = \hat{A}e^{-iht}$, we find

$$f_1 = \frac{\Re[\hat{A}e^{i(\theta-ht)}]}{-i(h-p)}. \tag{2.10}$$

Taking the limit h is nearly real, Eq.(2.10) becomes

$$f_1 = \Re[\frac{i}{h-p} + \pi\delta(h-p)]\hat{A}e^{i(\theta-ht)}. \tag{2.11}$$

The non-trivial solution $\hat{A}(h)$ is determined when Eq. (2.10) is inserted into Eq.(2.9). In the p-integration, the principle part term vanishes because the integrand is odd in p and only the delta function term contributes. We then obtain a dispersion relation with the approximate root given by,

$$h = (\Delta_m^2 - 1)/(\Delta_m^2 + 1) + i(\gamma_L - \gamma_d),$$

where γ_L is the linear growth rate in absence of dissipation when $\gamma_L \ll 1-|h|$. The parameter η is chosen to obtain the desired γ_L and then η is approximately given by,

$$\eta = \frac{(\Delta_m^2+1)^2}{4\pi\Delta_m}\gamma_L.$$

Physically, the growth of an instability will finally terminate to be a saturation due to the finite excitation from a free energy source. The analysis of the nonlinear saturation for a single BGK mode was discussed in [4]. The authors treated the particles trapped in the potential well in the adiabatic approximation and obtained the following expression for trapping frequency ω_b ($\omega_b^2 = |A|$ is the wave amplitude in terms of the square of the bounce frequency of the most deeply trapped particles) and the frequency shift $\delta\omega$ during the initial nonlinear stage (the adiabatic model will be discussed in detail in chapter 3),

$$\begin{aligned}
&\frac{\omega_b}{\gamma_L} \simeq \frac{16}{3\pi^2}, \\
&\frac{\delta\omega}{\gamma_L} \simeq \frac{16}{3\pi^2}\sqrt{\frac{2}{3}}(\gamma_d t)^{1/2}.
\end{aligned} \tag{2.12}$$

Also note that wherever there is no damping, the mode amplitude in the steady-state regime is estimated by the following well known result[29],

$$\frac{\omega_b}{\gamma_L} \simeq 3.2, \tag{2.13}$$

which was verified in the code we developed.

The analytic results derived from the linear and saturation stages provide good benchmarks for our following numerical calculations.

2.4 Numerical scheme

Several different numerical schemes have been developed to study the Berk-Breizman model directly in the action-angle space [47, 70] and in Fourier space, respectively. We use the numerical scheme in Fourier space developed by Breizman and Petviashvili [62], which is able to resolve the fine structure of a nonlinear developing distribution. This numerical scheme integrates the Vlasov equation in the Fourier transform space (s, n) of the action-angle variables (p, θ), respectively. The periodicity in θ allows n to be an integer while the infinite domain of p imposes that s be continuous. Then in this 'double' Fourier space the distribution is written as $\widetilde{F}_n(s, t)$. The functional dependence of s is obtained by using a numerical grid that is fitted to a cubic spline.

Our algorithm used to solve the Vlasov equation has been changed from the original Petviashvili's work [62]. In Petviashvili's numerical scheme, the Vlasov equation is solved in the Fourier space (s, n) of the action-angle variables (p, θ). The integration was based on an iterative scheme where the implicit part of the inversion arises from the free streaming terms while the interaction term is treated as a source term whose form is updated during the iteration. The iteration comes at a cost of computational time that prevents efficient code parallelization. Our present Vlasov solver avoids the iterative process and solves the Fourier transformed Vlasov equation along each individual free streaming characteristic line as a tri-diagonal matrix equation. The spatial dependence $e^{i\theta}$ in the wave-particle interaction models the mode coupling only between $n - 1$, n and $n + 1$ in the Fourier space, which gives the

tri-diagonal matrix. The complicated spatial dependence has to involve more mode number coupling and then decelerates the linear algebra calculation. The resulting code is then suitable for parallelization along a set of characteristic lines, where the individual characteristic line is independent and free of communication between them. In this method the computational time is reduced by an order of magnitude.

The distribution function is not usually a smooth function around the separatrix region of a structure. As a result, a Gibbs phenomenon is found when the distribution function in the Fourier space is converted to the physical space. Gibbs ripples appear inside the resonant structure. Fortunately, the source term $-\frac{i\eta}{\pi}\int_{-\infty}^{\infty} f(p,\theta,t)e^{-i\theta}dpd\theta$ appearing in the wave equation still maintains accuracy for a long time even with the Gibbs ripple phenomenon present as has been investigated in Ref. [34]. Therefore, we apparently obtain the correct wave response, though the Gibbs phenomenon becomes more pronounced as time evolves especially when viewing the distribution function in the (p,θ) phase space. An additional approximation is to set a non-reflection boundary condition at the boundary positions of $s = \pm s_{max}$ to avoid largely false signals from being reflected from these boundaries. However, even this boundary condition can lead to trouble late in time when an aliasing problem sometimes develops. With an alternate procedure that smoothly filters the large s data, we have largely removed this aliasing problem.

In the computational frame the chirping signal of interest only oscillates at a low frequency. Then in accord with Nyquist Shannon sampling theorem

[68], a moderately large time step Δt can be taken and the targeted phase space structure can evolve and be accurately described even when the phase space structure of interest produces a large frequency shift in the laboratory frame. To avoid this problem, which normally would require a reduced time step to retain $|h|\Delta t \ll 1$, we have developed a procedure that calculates the wave/particle interactions in a calculation frame that is nearly the same as the momentum of the phase space structure being tracked. Then a moderately large time step can be taken and the target phase space structure can evolve and remain accurate even with a fixed Δt. The integro-differential equation for the interaction of the TAE is straightforwardly modified, as will be shown, to enable the tracking of the phase space structure in the moving reference frame.

To obtain the equations in the reference frame, we rewrite Eqs. (2.6) and (2.7) in terms of the following variables,

$$\begin{aligned} a(t) &= A(t)\exp(-i\int_0^t dt'\, h_{cf}(t')), \\ \tilde{\theta} &= \theta - \int_0^t dt'\, h_{cf}(t'), \\ \tilde{p} &= p - \frac{dh_{cf}(t)}{dt}, \end{aligned} \tag{2.14}$$

where $h_{cf}(t) = p$ is the 'velocity' (which in this model is identical to the momentum) in the calculation frame. The equations for the system then

become,

$$(\Delta_m - i)a(t) - \int_0^t (J_0(t-\tau) - iJ_1(t-\tau))e^{i\int_\tau^t dt' h_{cf}(t')}a(\tau)e^{-\gamma_d(t-\tau)}\,d\tau$$
$$- \lambda(J_0(t) - iJ_1(t))e^{i\theta_{cf}(t)}e^{-\gamma_d t} = -i4\pi\eta\tilde{f}_1(0,t), \quad (2.15)$$

$$\frac{\partial\tilde{f}_n}{\partial t} + n\frac{\partial\tilde{f}_n}{\partial s} + is\frac{dh}{dt}\tilde{f}_n = -\frac{is}{2}(a(t)\tilde{f}_{n-1} + a^*\tilde{f}_{n+1}) + \frac{1}{2}a(t)\delta_{n,1}\delta(s), \quad (2.16)$$

where a small term λ is added to perturb the initial system. The chirping rate $dh/dt \equiv dh_{cf}/dt$ appears in Eq.(2.16) because the calculation is being performed in a non-inertial reference frame and the chirping rate plays a role of a non-inertial force in the new frame. The phase of the calculation frame is defined as $\theta_{cf}(t) = \int_0^t dt'\, h_{cf}(t')$.

In practice, we search for the maximum amplitude of the wave spectrum generated from a Fourier time window over one hundred wave periods. A relaxation procedure, to produce only a slowly varying calculation frame, is employed to fill in the time gap between two adjacent time windows.

$$\frac{dh_{cf}(t)}{dt} = \frac{h(t_n) - h_{cf}(t)}{\tau},$$

where τ is a numerical relaxation time parameter and $h(t_n)$ is the central frequency in the spectrum for the target phase space structure taken at the last evaluated time window centered at time $t = t_n$. The typical mismatch achieved between $h(t_n)$ and h_{cf} is 0.1 radians per unit time. For the convenience of visualization the data is shifted back to the lab frame using the appropriate inverse transformation.

Other more sophisticated method to track the velocity frame of the phase space structure is implemented in our numerical scheme. This tracking

allows a shift of the computation frame from the 'lab' frame to a wave frame. The tracking region is localized to lie within $-\pi \leq \theta \leq \pi$ and $p_- \leq p \leq p_+$, where p_- and p_+ are defined as the lower and upper bounds of a velocity window transferring to the wave frame. For a clump/hole that is in the tracking region, the velocity of the wave frame v_f is determined by demanding that the overall relative acceleration of the region vanishes.

$$dv_f/dt = -\int_{-\pi}^{\pi}\int_{p_-}^{p_+} f(p,\theta,t)\Re(A(t)e^{i\theta})dpd\theta / \int_{-\pi}^{\pi}\int_{p_-}^{p_+} f(p,\theta,t)dpd\theta = 0. \tag{2.17}$$

Note that in the above equation we are using coordinate information only within the tracking region. The method of tracking given in Eq. (2.17) was developed after we found unacceptable tracking error emerging when we attempted to use band-pass filter to extract the frame of the wave by tracking the peak intensity of the wave spectrum as we discussed. The spectral method was particularly deficient during the early stages of the evolution, when the frequencies from different structures are close together. Then the mixing of signals from adjacent structures produces a great deal of noise which leads to difficulty to obtain an early comparison of the simulation results with that of adiabatic theory. This problem is greatly alleviated when the frame of the wave is determined at every time step by Eq. (2.17).

The distribution function is saved in (s, n) space. To solve the Vlasov equation, the method of characteristics followed by iteration is used. The integral along the characteristic lines from $(s - n\Delta t, t)$ to $(s, t + \Delta t)$ in one

time step Δt takes the form,

$$\tilde{f}_n(s,t+\Delta t) = \tilde{f}_n(s-n\Delta t,t) - \frac{i}{2}\int_0^{\Delta t} d\tau\,(s-n\tau)$$
$$\cdot\,[a(t+\Delta t-\tau)\tilde{f}_{n-1}(s-n\tau,t+\Delta t-\tau) + 2\frac{dh}{dt}\tilde{f}_n(s-n\tau,t+\Delta t-\tau)$$
$$+\,a^*(t+\Delta t-\tau)\tilde{f}_{n+1}(s-n\tau,t+\Delta t-\tau)]$$
$$+\,\frac{1}{2}a(t+\Delta t-s)\sqcap(\frac{s}{\Delta t})\delta_{n,1}. \qquad (2.18)$$

Where we have introduced the notation for a rectangle function, $\sqcap(x) = \theta(x)\theta(1-x)$, with a step function $\theta(x)$. We will implement an alternative iteration, where the dh/dt term is part of the leading order iteration. Such a procedure should lead to faster convergence and perhaps more accuracy. (Note that the equilibrium distribution only directly appears in the $n = 1$ term.)

The wave equation is a Volterra equation of the second kind, which is readily solved by numerical integration where old values are saved and only the newest value for the distribution function are then calculated at each time step [65]. The Vlasov and wave equations is then solved simultaneously to describe the interaction of the wave and particles. To achieve sufficient accuracy, several iterations is needed until the prescribed convergence criteria is reached. A successive over-relaxation method (SOR) is implemented to accelerate the rate of convergence and the optimized extrapolation factor is verified with numerical checks [65].

2.5 Results and discussion

2.5.1 Verification of the code

We have verified our code by comparing with the theoretical linear growth rate and the levels of saturation when damping is either excluded or included.

The linear growth rate is calculated by the linear fitting of the logarithm of the mode amplitude $|A|$ shown in the Fig. 2.1. The simulation parameters we takes here for the time step is $\Delta t = 0.1$, the s grid size is $\Delta s = 0.1$, the domain of s grid is $-s_{max} \leq s \leq s_{max} = 100$ and total number of mode is$-20 \leq n \leq 20$. The observed growth is in agreement with linear theory as shown in Fig. 2.1.

Depending on the background dissipation, two different levels of saturation are expected. These two saturations levels are found in the simulation and they are shown in Fig. 2.2(a) and 2.2(b). The numerical results can be compared with those expected from the expected results given in the equations (2.12) and (2.13). For $\gamma_d = 0$, the case in Fig. 2.2(a), the mode amplitude climbs quickly to the expected saturation level and the simulation data fluctuates around the predicted value. To observe the saturation level of the chirping mode, a chirping signal filter is applied to the wave amplitude $A(t)$ over the bandwidth of the chirping frequency. Chirping starts at around $t = 100$ time units. However, in order to filter a chirping band accurately, we need to wait until 1000 time units. The Fig. 2.2(b) only shows the wave amplitude after $t = 1000$. At this time the saturation level is slightly below the expected level

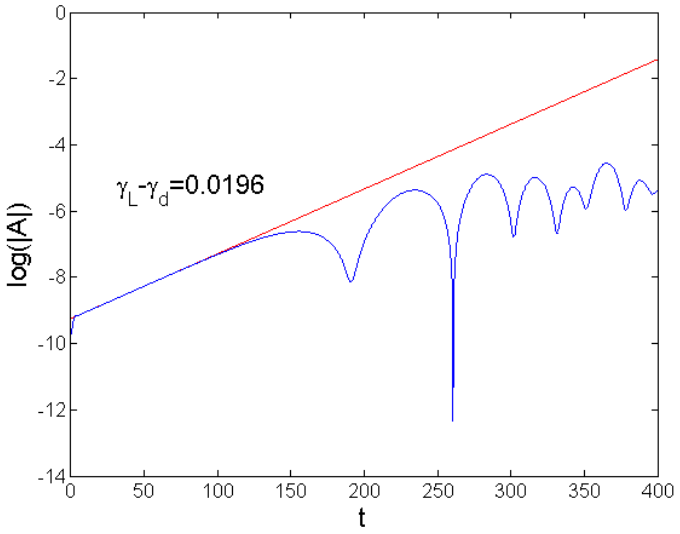

Figure 2.1: Time evolution of the logarithm of the mode magnitude $|A|$. The initial parameters are chosen to obtain a mode near marginal stability with $\gamma_L = 0.1$, $\gamma_d = 0.08$, which is achieved with $\Delta_m = 0.654$ and $\eta = 0.0248$. During the linear stage the growth rate agrees with the analytic growth rate $\gamma_L - \gamma_d = 0.02$(shown by the red curve).

and falling, while the frequency has shifted from $h = -0.45$ to $h = -0.8$. Hence, even with the relatively large change from the initial frequency, an agreement of 80% of the theoretical waterbag model used[8] is observed. Later the wave amplitude falls, reaches a stationary level and finally increases after the clump has entered the Alfvén continuum. The chirping rate of the signal in Fig. 2.2(c) shows the strong chirping also accompanies the clump that has entered the continuum.

We also tested the sensitivity of our results to the manner extrinsic dissipation is described. In model 1 dissipation is obtained by adding the

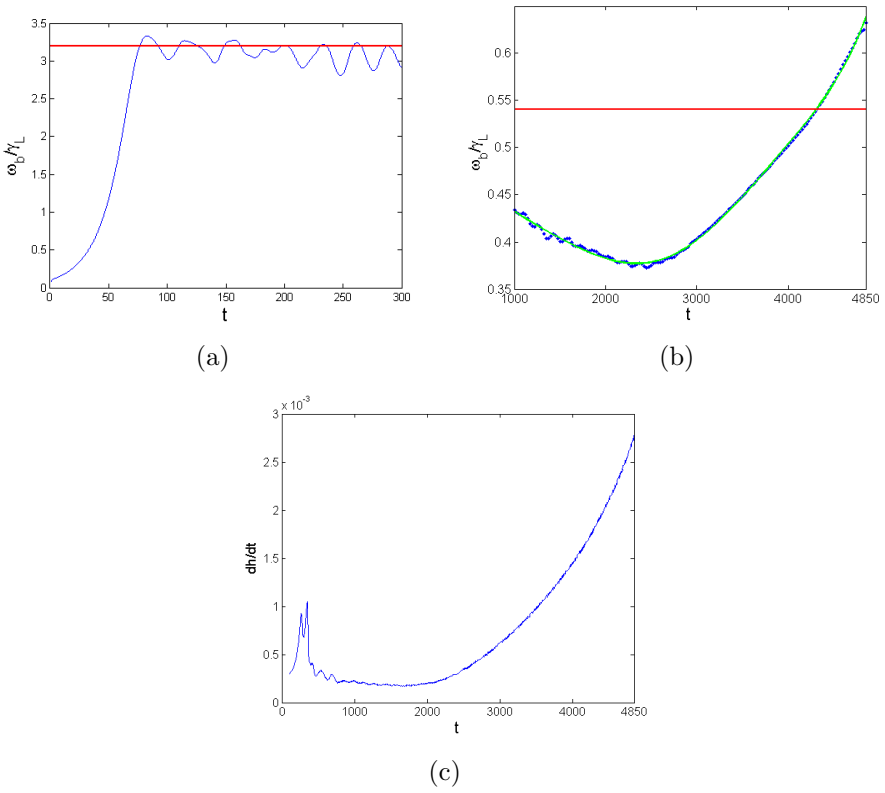

Figure 2.2: Different saturation levels depending on the presence or absence of γ_d. (a) For the zero damping case $\gamma_L = 0.1$; (b) for the near marginal instability case, where $\gamma_L - \gamma_d \ll \gamma_L$, $\gamma_L = 0.1, \gamma_d = 0.08$; (c) the chirping rate dh/dt is shown. The red line indicates the expected initial saturation value and the green one shows the best 6th order polynomial fit to the scatter of measured data for $\omega_b/\gamma_L = |A|^{1/2}/\gamma_L$.

factor $exp[-\gamma_d(t-\tau)]$ in Eq. (2.6) (model 1). An alternative model is to omit this exponential factor and choose Δ_m to be complex so as to produce a damping factor $e^{-\gamma_d t}$ in the linear solution when there are no energetic particles present (model 2). These two dissipative models will continue to be elaborated in our adiabatic model. Thus these two models are essentially the same when

$|h - h_0| \ll |1 + h_0|$ (h_0 is the linear eigenfrequency of TAE), but then differ in details when $|h - h_0| \geq |1 + h_0|$. These figures show that these models give very similar results as can be observed in Fig. 2.3(a) and 2.3(b).

2.5.2 Rapid chirping frequency

The chirping frequencies shown in Fig. 2.4 in the rest frame is the salient feature of our nonlinear system. These frequencies stay in resonance with the driving perturbations from the energetic particles. A continual phase-locking takes place in the clump and the drag-like force due to dissipation forces a change of velocity of the phase space structure. Thus the chirping frequency is intrinsic and self-sustainable with no external driving force.

The chirping frequency is determined by a short-time Fourier transform (STFT) method, which is a modified Fourier transform over a finite time window. The initial chirping spectrum initially vary as the square root of time ($h_0 - h \approx 0.44\gamma_L(\gamma_d t)^{1/2}$) and surprisingly this dependence lasts until the chirping frequency approaches the continuum frequency boundary. Afterward the clump signal takes on a more complex time dependence.

2.5.3 Verification of understanding from filtered response

The adiabatic approximation accounts for a two time-scale representation of the simultaneous response of the mode and trapped particle dynamics. The phase of the mode amplitude A is a fast variable while the slowly varying quantities are the magnitude of the wave amplitude, the instantaneous bounce

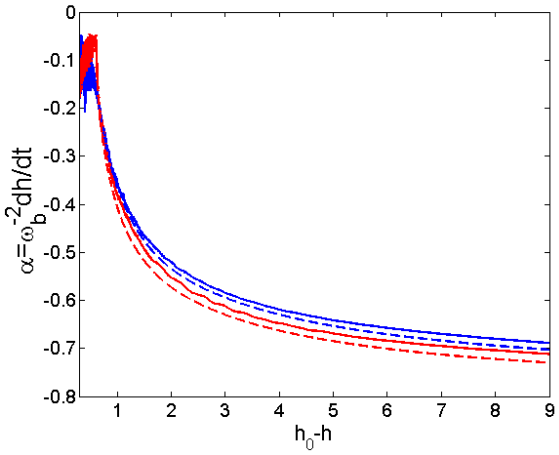

(a)

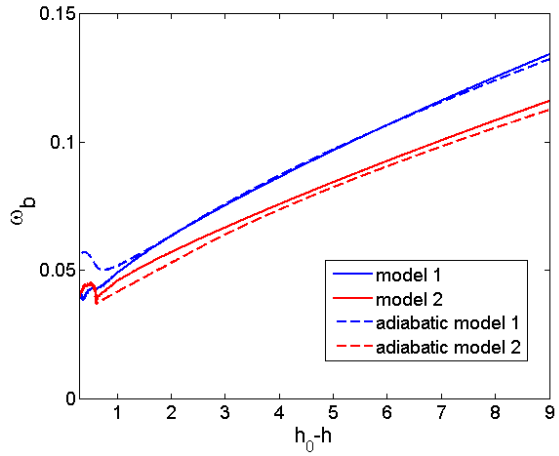

(b)

Figure 2.3: Comparisons between two different dissipation models. The damping rate is chosen as $\gamma_d = 0.08$ in model 1, where the imaginary part κ of Δ_m is zero. In model 2, for the same linear damping rate $\kappa = -0.623$ and $\gamma_d = 0$. The analytic models (dash lines) based on the adiabatic approximation (which is discussed in chapter 3) correlate extremely closely to the simulations.

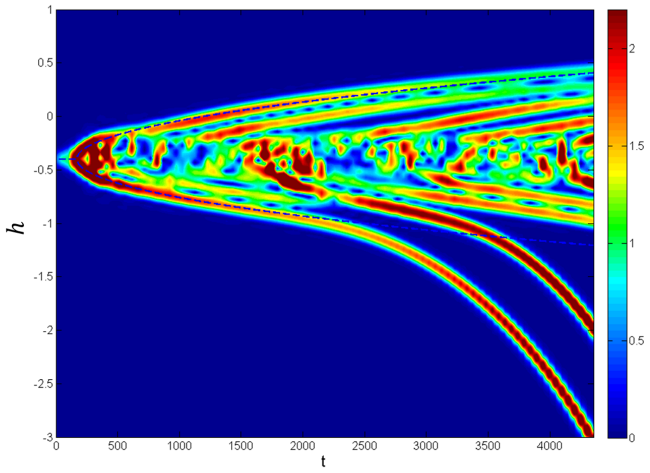

Figure 2.4: The evolution of the wave spectrum. The TAE gap is located between $h = -1$ and 1 while the initial frequency starts at $h \approx -0.4$. The dashed curve is the predicted frequency shift that increases as the square root of time.

frequency ω_b and the chirping rate dh/dt. The dynamics of trapped particles in a chirping wave potential can be reduced to a Hamiltonian for the particle motion given by[4],

$$\mathcal{H} = \frac{\Omega^2}{2} - \omega_b^2 \cos q + \frac{dh}{dt} q. \tag{2.19}$$

We define $\alpha \equiv \omega_b^{-2} dh/dt$. Both coordinate and momentum are defined as functions varying slowly with time.

A Hamiltonian has its O- and X-points determined by $\frac{\partial \mathcal{H}}{\partial q} = 0$, where $\frac{\partial^2 \mathcal{H}}{\partial q^2} > 0$ for an O-point and $\frac{\partial^2 \mathcal{H}}{\partial q^2} < 0$ for an X-point. For this Hamiltonian there is a solution for these points when $|\alpha| \lesssim 1$. The values of $\mathcal{H}' \equiv \frac{\mathcal{H}}{\omega_b}$ at q_O and q_X are (the subscripts O and X refer to the O and X points respectively.)

:

$$
\begin{aligned}
q_O &= -\sin^{-1}\alpha \quad (here, -\frac{\pi}{2} \leq \sin^{-1}\alpha \leq \frac{\pi}{2}),\\
q_X &= -\pi sg(\alpha) + \alpha \sin^{-1}\alpha + (1-\alpha^2)^{1/2},\\
{\mathcal{H}'}_O &= -\alpha \sin^{-1}\alpha - (1-\alpha^2)^{1/2},\\
{\mathcal{H}'}_X &= -\pi sg(\alpha) + \alpha \sin^{-1}\alpha + (1-\alpha^2)^{1/2},
\end{aligned} \tag{2.20}
$$

$sg(z) = \frac{z}{|z|}$ is the sign function. Note that ${\mathcal{H}'}_X$ is the value of the $\mathcal{H}'$ on the separatrix. For our application q and Ω are given by,

$$
\begin{aligned}
q &\equiv \theta - \omega_0 t - \int_0^t dt' \delta\omega(t'),\\
\Omega &\equiv p - \omega_0 - \delta\omega(t).
\end{aligned}
$$

Here ω_0 is the initial linear frequency ($\omega_0 = h_0$) and $\delta\omega$ indicates the the instantaneous shift of frequency.

In order to verify the suitability of an adiabatic approximation, we use a band filter about the frequency of interest, to filter the left hand side of Eq. (2.15). Then we use this signal to evaluate the left hand side of Eq. (2.8), as the filtered signal to lowest order, should be described by a WKB wave. The equality of the left hand side to the right hand side of Eq. (2.15) is numerically checked where particle distribution is filtered by a momentum band to obtain the distribution around the resonance $p = \omega_0 + \delta\omega(t)$. We then calculate the complex amplitude,

$$
A_{clump}(t) = \frac{-2i\eta \oint_{clump} f(\theta, p, h) e^{-i\theta} d\theta dp}{\Delta_m - \sqrt{\frac{1+h}{1-h}}}. \tag{2.21}
$$

where the symbol 'clump' under the integral denotes an integration that uses the filtered distribution in p. The result of the filtered right hand side is then compared with $A_{chirp}(t)$, which has been extracted by filtering the raw $A(t)$ with a frequency band window about the target chirping frequency.

The WKB description predicts that, in principle the complex ratio $A_{chirp}(t)/A_{clump}(t)$, is unity. Thus to the extent this ratio is $1 + i0$, indicates the appropriateness of the adiabatic approximation in Fig. 2.5. The agreement is observed with a reasonable uncertainty throughout t from the first appearance of the isolating clump to the final chirping state. Before the target structure enters the continuum the ratio is nearly unity but with a fair amount of fluctuation, perhaps due to the proximity of nearby structures. In the continuum, fluctuation from unity is considerably less. Overall, the lowest order WKB description is good. Perhaps improvement can be achieved when interactions with neighboring structures are accounted for.

2.5.4 Phase space structure

In this section we view the created phase space structures in more detail. We note again that without background damping the mode would remain at the linear frequency of the wave, and the instability would simply flatten the resonance region. A damping mechanism is required to enable the spontaneous generation of the clump and/or hole structures from the resonance region. The damping absorbs the extra wave energy and allows the phase space structures to move to lower energy states (in this TAE model the higher frequencies

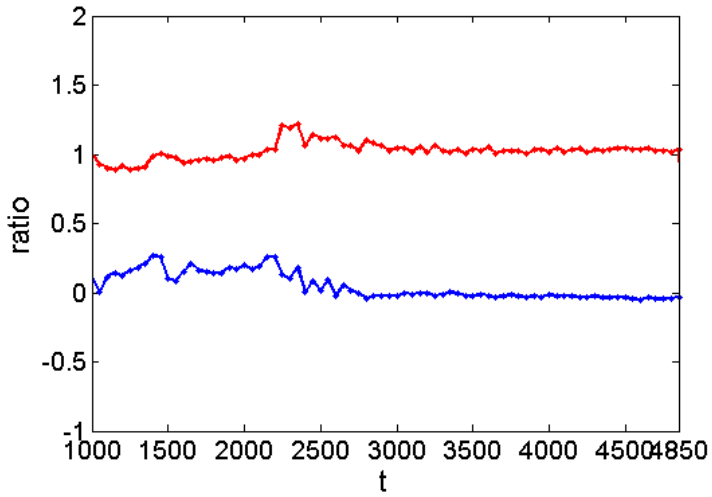

Figure 2.5: Verification of the suitability of the adiabatic approximation, achieved by testing the extent to which the complex ratio $A_{chirp}(t)/A_{clump}(t) = 1$. The real part is the red line and the imaginary part is the blue line.

correspond to holes and the lower frequencies correspond to clumps). Initially phase mixing develops in the resonant region at the frequency predicted by the linear wave theory, so that the resonance condition occurs at $p \approx h_0 = -0.4$. The trapping structure that forms during the early linear stage is observed in Fig. 2.6(a). Later on, the chirp of the frequency becomes apparent and a clump structure of trapped particles emerges in the phase space (Fig. 2.6(b)) due to the phase locking of the trapped particles to the excited wave. Then the clumps propagate towards the Alfvén gap-contiuum boundary; first approaching (Fig. 2.6(c)) and then penetrating the Alfvén continuum (Fig. 2.6(d)). The chirping rate substantially increases within the Alfvén continuum (Fig. 2.6(e)). Finally, the clump moves far from the gap-continuum boundary deep into the continuum region (Fig. 2.6(f)). The relationship between the chirping fre-

quency and the time evolution is shown in Fig. 2.6(g). We have focused on the clump formed closest to the lower continuum. In addition a hole simultaneously formed to give increasing frequency chirps, but we have not observed these waves reach $h = 1$, the upper continuum frequency. Secondary, tertiary, etc. structures continually emerge from the linear resonant region.

The clump is locked and continually accelerates in synchronism with the continuously chirping wave. As we can directly measure ω_b^2 and dh/dt of a clump, we can determine how the separatrix should look like. In figure 2.7 we show how the separatrix shape and amplitude compare with the phase space structures that can be calculated from the data. We see good agreement, though there is deviation. The deviation may be due to the neglect of effects coming from the slowly changing values of d^2h/dt^2 and $d\omega_b/dt$. Also the tails seen by the phase structure are due to non-adiabatic behavior in the phase space region near the separatrix.

Physically, the chirping wave is strongly correlated with the trapped structure in phase space. We found the width of trapped structure $\Delta\theta$ reflects the chirping parameter α,

$$\alpha = \frac{1}{\sqrt{2 + \Delta\theta^2 - 2\cos\Delta\theta - 2\Delta\theta\sin\Delta\theta}}. \tag{2.22}$$

Figure 2.8 indicates the strong correlation between the chirping wave and trapped structure.

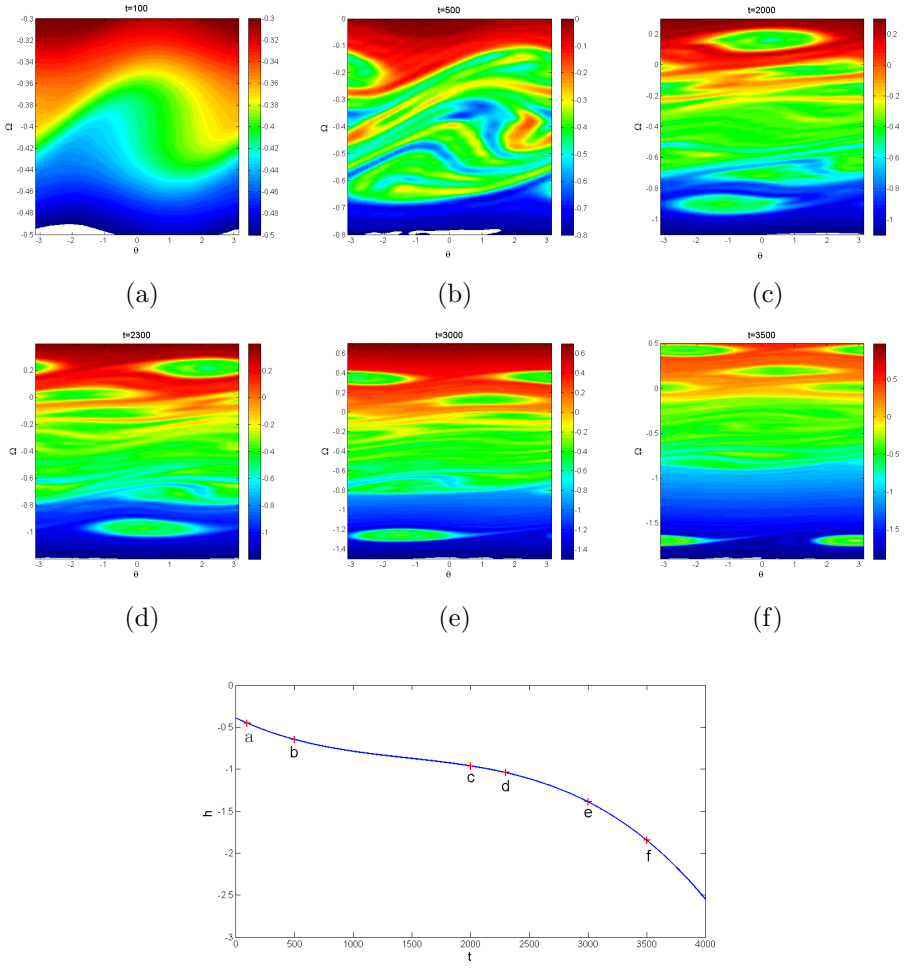

Figure 2.6: 2.6(a)-2.6(f) are snapshots of the phase space at indicated times as shown on 2.6(g).

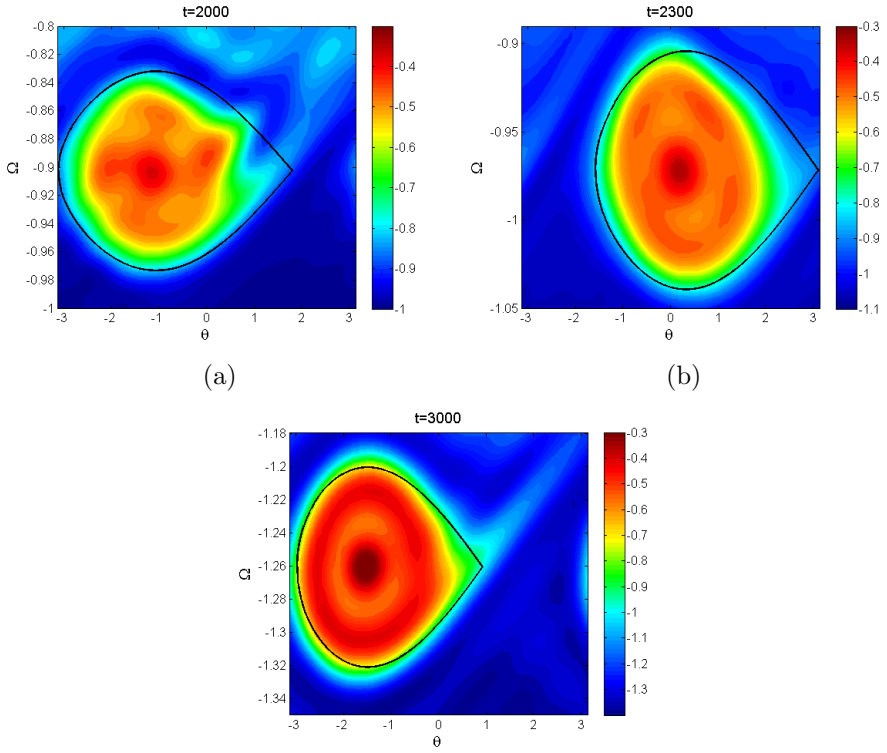

(a) (b) (c)

Figure 2.7: The black closed curve shows the separatrix of the clump in the description of Eq. (2.19). The portraits of the clumps are enclosed by these theoretical separatrix.

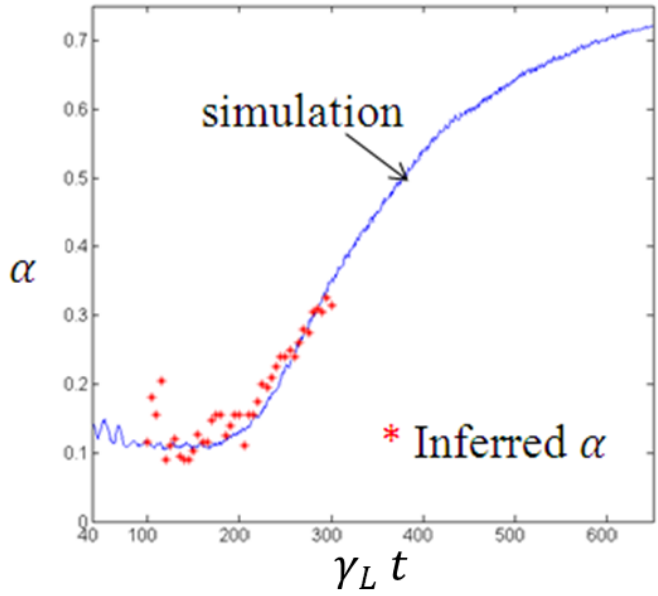

Figure 2.8: The correlation test is a good sign to verify the frequency shifts due to the formation of clump/hole pairs instead of other nonlinear effects. The red scattering dots show the chirping rates calculated from the structure width and the blue curve is the wave data of chirps.

2.6 Summary

A special property of a TAE mode is that in linear theory the wave exists in a frequency gap surrounded by a region with a continuous spectrum. The continuum regime gives rise to an intrinsic dissipative response to an external excitation. The initial excitation reproduces nonlinear features that are nearly independent of the detailed wave model. These are the formation of hole/clump pair at a characteristic saturation level and a characteristic spontaneous chirping frequency shift proportional to $\sqrt{t}$ that is due to the phase

locking between the phase space structure and the wave. The phase locking and particle trapping continues during the entire evolution of the phase space structures. What we have investigated here is for how long the characteristic frequency shift remains proportional to $\sqrt{t}$ (this continues until frequency reaches the continuum/gap boundary), whether the phase space structure can penetrate into the continuum from the gap region (we find that there is penetration) and whether the evolution of the phase space structure can be approximated by an adiabatic (WKB) theory (it can and when clump is in the continuum and well separated from other phase space structures the agreement is especially good). If one assumes the initial distribution is a waterbag, as was assumed in [8], the adiabatic theory can be solved to obtain the time evolution of the system. We have found in next chapter that if we choose a waterbag distribution, where for a constant unit slope of the normalized equilibrium distribution, $f(h) - f(h_0) = h - h_0$, we obtain very good agreement.

An important innovation of our calculation, is to perform the computations in the frame of the targeted phase space structure. Then the numerical step size, Δt, does not have to get smaller as the chirping continues, since in this frame, $h\Delta t$ can remain small, even when there is the chirping present.

Chapter 3

Adiabatic Model of Rapid Frequency Chirps of Toroidal Alfvén Eigenmode

3.1 Introduction

The simulation shows a large frequency shift where the TAE chirp becomes comparable to the frequency shift between the linearly predicted frequency and the continuum frequency, and as a result the standard chirping theory [4, 8] is inapplicable. Here we will exhibit a new model for describing the phase space chirp of TAE modes that has the possibility of chirping into the surrounding continuum. The governing equations for this model are based on the linear RBV tip model, which describes the TAE excitation in a large aspect ratio, circular tokamak at low beta. To simplify the calculation we deal with a case where the TAE excitation is primarily from a single couplet which consists of wave with a poloidal structure consisting dominantly of the m and $m+1$ poloidal harmonics localized near the region around $q(r_m) = (m+1/2)/n \equiv q_m$. We assume that the interaction with neighboring couplets can be ignored which is easiest to satisfy at low shear.

The original theory for the tip model was derived in frequency space. Using the Fourier transform, the frequency form can be converted into a con-

volution integral with a temporal kernel producing a non-local time response for the wave. The governing theory for the time representation of the RBV tip model has been described in chapter 2 [72]. In the present chapter we show how to develop an adiabatic theory for the RBV-resonant particles and waves. During the adiabatic evolution of a TAE wave amplitude and its chirping rate, parameters need to evolve slowly in one bounce period in the wave trapping fields. The adiabatic dynamics of energetic particles in the trapping region of a hole or clump can be described with action-angle variables, where the canonical action variable J is an adiabatic invariant [58]. The distribution function of energetic particles is given by $f(J)$ which remains constant in time, except for the change of the distribution function near the separatrix where particles are entrapped by or lost from the trapping region. This theory leads to results which for the most part closely replicate the results of Vlasov simulations.

3.2 Adiabatic invariant

Adiabatic invariants are crucial to the understanding of a single charged particle motion in a complex geometry of magnetic and electric fields. Kaufman [45] used the three adiabatic invariant actions of a particle in a toroidal plasma with axial symmetry: the magnetic moment μ, the canonical angular momentum P_ϕ and the toroidal flux enclosed by the drift surface to build up a quasi-linear theory. The Hamiltonian for the unperturbed motion of a single particle only relies on these three adiabatic invariants. Then the interaction introduces the perturbed parts in the form of a interaction-Hamiltonian, such

as was used by Kaufman [45]. Canonical perturbation theory can be used to construct plasma kinetic theory in action-angle variables [52]. In our investigation of the wave-particle interaction of shear Alfvén-like wave, the magnetic moment remains constant due to the low frequency compared to the ion cyclotron frequency of the TAE waves. The resonant condition also requires $E - \omega/nP_\phi$ to be a constant, which is implicitly related to a second adiabatic invariant. Moreover, if the resonances are well separated in the particle's phase space, we only keep a single resonant harmonic in the Hamiltonian with the resonant interaction.

A third adiabatic invariant J of the perturbed Hamiltonian system arises from the periodic motion of trapped particles in a resonance. The adiabatic approximation assumes that the action J is an invariant during the entire evolution, which is a good approximation when the physical parameters in the system vary slowly. The variation of the action can be evaluated from the slowly varying parameters in our model, from which we can check whether the rate of time variation of the various calculated quantities is indeed small compared to the bounce rate of a typical trapped particle.

3.3 Dissipative models for TAE wave

The chirping events are observed when the physical system is near marginal instability, i.e. the instability drive and background dissipation are nearly comparable to each other. Without chirping, when the bounce time of a deeply trapped particle is comparable to the growth time, the distribution

will flatten and the instability drive will be quenched. However, when there is chirping, the energy of chirping waves is supplied not only from newly trapped energetic particles but also from the downward or upward motion in phase space of the hole and/or clump structures that have formed. Two external damping mechanisms are implemented in the adiabatic theory in the same way as in the previous chapter which described our simulation.

The wave equation, including the interaction with the resonant particles, takes the form [72],

$$(\Delta_m - i)A(t) - \int_0^t (J_0(t-\tau) - iJ_1(t-\tau))e^{-\gamma_d'(t-\tau)}A(\tau)d\tau = -\frac{i\eta}{\pi}\int_{-\infty}^{\infty} f(p,\theta,t)e^{-i\theta}dpd\theta, \tag{3.1}$$

where the left hand side (LHS) is the linear response due to the electromagnetic field and the background plasma, and the right hand side (RHS) describes the interaction of the resonant particle currents with the linear wave. The factor η is proportional to the linear growth rate and later will be explicitly defined. The real component of the parameter Δ_m ($\Delta_r = \Re\Delta_m$) is obtained from the ideal MHD contribution of the predominant poloidal m^{th} and $m+1^{th}$ components of an Alfvénic mode outside the gap region, while the frequency dependent terms represent the ideal MHD contribution in the vicinity of the gap. Parameters are scaled so that the band frequency in the gap lies between $-1 \leq \omega \leq 1$. With this frequency normalization the linear TAE frequency is given by $\omega_0 = (\Delta_r^2 - 1)/(\Delta_r^2 + 1)$ when there is no instability drive. In ideal MHD theory there is no dissipation when the eigenmode frequency is in the gap

and never intersecting any continuum curves. To produce damping in the gap region, extrinsic dissipation is added to our model with the parameters chosen to produce a given damping rate γ_d close to the linear growth rate γ_L, when there is no dissipation. Two dissipative parameters are chosen to capture the dissipation due to non-ideal MHD effects. The parameter γ_d' mocks up damping arising from non-ideal MHD effects, such as viscosity or resistivity at spatial positions near the tip region, while the imaginary component of the parameter Δ_m ($\Delta_i = \Im\Delta_m$), is used to capture dissipation arising from non-ideal MHD effects outside the TAE interaction region that is remote from the 'tips'. In general we can treat a combination of the two parameters, using a single parameter β, with $0 \leq \beta \leq 1$ where the two dissipative parameters are given by $\gamma_d' = \beta\gamma_d$ and $\Delta_i = (1-\beta)\Delta_{i0}$, with $\Delta_{i0} = -\lambda\gamma_d$ where $\lambda = (\Delta_r^2+1)^2/(4\Delta_r)$. Note that for any β the sum of these two terms gives the same damping rate γ_d when $\gamma_d \ll 1$. To see if there is any sensitivity to the nonlinear results with the choice of dissipation models, the simulations have primarily been performed for the two extremes : cases (I) $\gamma_d' = \gamma_d$, and $\Delta_i = 0$ and case (II) $\gamma_d' = 0$ and $\Delta_i = \Delta_{i0}$ (Δ_{i0} is finite and negative). Both models produce nearly the same response in the linear phase and the early chirping response where the theory of Ref. [8] applies. However with increasing frequency shift, the choice of the dissipation model changes the quantitative dynamical evolution though not the qualitative conclusion.

To test the sensitivity to the dissipation mechanism, the results for a downshifting clump for the two alternative damping mechanisms, cases (I)

and (II), are compared in Figs. 3.1(a) and 3.1(b) where a clump is tracked using the Vlasov solver discussed in chapter 2. The parameters chosen for the simulations in the figures are $\gamma_L = 0.1$ and $\Delta_r = 0.56$ with $\gamma_d = 0.08$ in case (I) and $\Delta_i = -0.0623$ in case (II). We see that there is the same general tendency for the two curves, but there are quantitative differences arising between the results of the two dissipation models. Similar results are found for an upshifting hole.

3.4 Adiabatic model

The particle-wave resonant structure can be derived from Hamilton-Jacobi theory. In systems where the Hamilton-Jacobi equation for the unperturbed orbits is separable, one can use the method, similar to the Schwarzschild transformation [25], to obtain action-angle variables to reduce the dimensions of a resonant system. For a sufficiently small perturbation, one can isolate a single resonance and select a transformation to the frame of the resonance structure, in the process of reducing the dynamics of the motion to a single action variable and its conjugate angle variable. One finds the following Hamiltonian [72] for a frequency sweeping structure,

$$\mathcal{H} = \frac{P^2}{2} - \omega_b^2(\cos\theta - \alpha\theta). \tag{3.2}$$

Here, P is the momentum of particles that are nearly resonant with the wave field, and θ is a phase angle in the wave field. This Hamiltonian is a function of the wave amplitude ω_b^2 and chirping parameter $\alpha \equiv \omega_b^{-2} d\omega/dt$, which leads

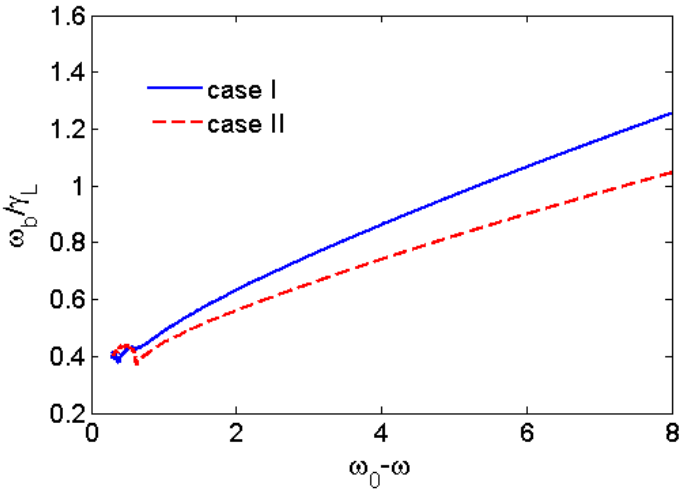

(a)

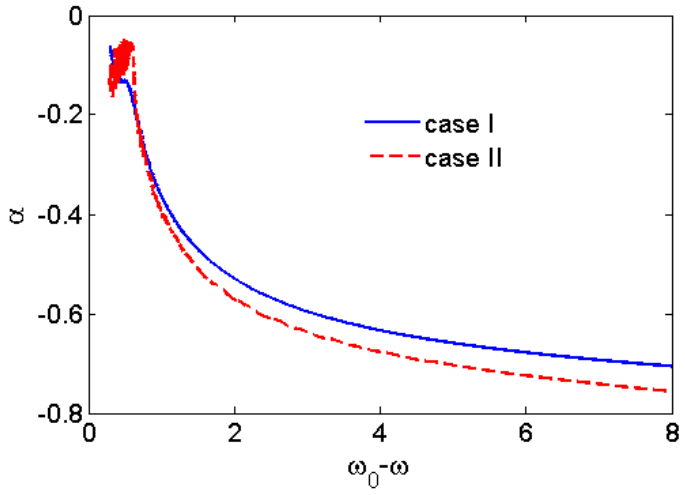

(b)

Figure 3.1: Comparison of the evolution of trapping frequency ω_b (panel a) and chirping parameter α (panel b) for two alternative damping cases in Vlasov simulations. The solid blue line depicts dissipation case (I) where the frequency is offset with an imaginary component $\gamma_d' = \gamma_d = 0.08$. The dashed line is for dissipation case (II) where the Δ_m parameter is offset with an imaginary component $\Delta_{i0} = -0.0623$.

to an asymmetric separatrix in θ about the O-point, where the energetic particles are deeply trapped. A normalized Hamiltonian-like form can be used to simplify the analysis to one parameter α,

$$h = \frac{p^2}{2} - \cos\theta + \alpha\theta \tag{3.3}$$

where $p = P/\omega_b$, $h = \mathcal{H}/\omega_b^2$. When the parameters α and ω_b^2 evolve slowly, the appropriate action J is an adiabatic invariant and is given by,

$$J = \frac{j\omega_b}{2\pi} = \frac{1}{\pi}\int_{\theta_{min}}^{\theta_{max}} P d\theta = \frac{\sqrt{2}\omega_b}{\pi}\int_{\theta_{min}}^{\theta_{max}} \sqrt{e(J) + \cos\theta - \alpha\theta}\, d\theta. \tag{3.4}$$

Here $e = h(p,\theta)$ is a normalized energy which for trapped particles takes on the range of values from $-\alpha\arcsin\alpha - \sqrt{1-\alpha^2}$ to $-|\alpha|\pi + \alpha\arcsin\alpha + \sqrt{1-\alpha^2}$ and j is a normalized action variable. It is worth noting that J is an adiabatic invariant but j is not. The angles θ_{max} and θ_{min} are the points on the separatrix where the momentum p vanishes. The positions of O and X points θ_O, θ_X, and range of e are determined by the conditions:

$$\begin{aligned} &\frac{\partial h(p,\theta_{O,X})}{\partial\theta} = 0 \\ &\frac{\partial^2 h(p,\theta_O)}{\partial^2\theta} > 0; \quad \frac{\partial^2 h(p,\theta_X)}{\partial^2\theta} < 0 \\ &h(p,\theta_O) \le e \le h(p,\theta_X) \end{aligned} \tag{3.5}$$

During the evolution, the action J is assumed to be conserved from a time t to $t+\Delta t$, which is constructed exactly from the numerical calculation without approximations. The distribution only depends on the action value but is independent of time when the bounce average on the trapped trajectory is

applied. Hence, $f(J)$ only changes due to the evolution of the separatrix value, $J_{spx}(t)$. If J_{spx} increases, the new distribution at the separatrix becomes, $f[J_{spx}(t+\Delta t)] = F_0[\omega(t+\Delta t) \pm J_{spx}(t+\Delta t)]$, with the + sign for $\omega > \omega_0$ and a minus sign for $\omega < \omega_0$, where ω_0 is the frequency predicted from linear theory. For example, the newly created value of the trapped distribution function at $t = t_1$, $f(J_{spx}, t = t_1)$ then remains constant in time (i.e. $f(J = J_{spx}, t) = f(J_{spx}, t = t_1)$) as long as the value of J_{spx} at a time $t > t_1$ satisfies $J_{spx}(t) > J_{spx}(t_1)$. This value $f(J_{spx}, t_1)$ is stored and used for the subsequent evolution of the phase space structure. On the other hand, if J_{spx} decreases, the distribution at the separatrix changes with the new $f(J_{spx})$ coming from a previously interior J-value in the trapped region whose J-value is equal to the new J_{spx}. Hence, this stacked data structure is part of the evolutionary rules for the distribution function. If the newly formed action at the separatrix is greater than the action previously topping the stack, push the new action to the top of the stack. Otherwise keep popping the top actions until the new action can be pushed.

The adiabatic response of the LHS of the wave equation, Eq.(3.1), is approximately the band filtered signal in the wave frame. The form for the

RHS was derived in [4, 8]. The resulting adiabatic equations are given by,

$$\Re(\Delta_m - \sqrt{\frac{1+\widetilde{\omega}}{1-\widetilde{\omega}}})\omega_b = \frac{\eta}{\pi}\int_0^{\frac{J_{spx}}{\omega_b}} dj(f(\omega_b j) - F_0(\omega_b j))\int_0^{2\pi} d\phi\cos\theta, \quad (3.6)$$

$$\Im(\Delta_m - \sqrt{\frac{1+\widetilde{\omega}}{1-\widetilde{\omega}}})\omega_b = -\frac{\eta}{\pi}\int_0^{\frac{J_{spx}}{\omega_b}} dj(f(\omega_b j) - F_0(\omega_b j))\int_0^{2\pi} d\phi\sin\theta$$

$$= 2\alpha\eta\int_0^{\frac{J_{spx}}{\omega_b}} dj(f(\omega_b j) - F_0(\omega_b j)).$$

$F_0(J)$ is the unperturbed distribution function normalized with the property that $\frac{dF_0(J)}{dJ} = 1$, and $\widetilde{\omega} = \omega + i\gamma_d'$. The canonical angle ϕ for the perturbed system is determined from the relation,

$$d\phi = \frac{\pi d\theta}{\sqrt{e(J) + \cos\theta - \alpha\theta}} / \int_{\theta_{min}}^{\theta_{max}} \frac{d\theta}{\sqrt{e(J) + \cos\theta - \alpha\theta}}. \quad (3.7)$$

In absence of dissipation and drive ($\eta = 0$), one finds (see [20, 72]) from the linear theory of Eqs. (3.1) and (2.7), that the linear frequency ω_0, is given by $\omega_0 = (\Delta_r^2 - 1)/(\Delta_r^2 + 1)$. When we take into account drive and dissipation under the assumption $\gamma_L \ll 1$, we find a growth rate γ given by $\gamma = \gamma_L - \gamma_d$, with $\gamma_L = 4\pi\Delta_r\eta/(\Delta_r^2+1)^2 = \pi\eta/\lambda$, $\gamma_d = \gamma_d' - 4\Delta_r\Delta_i/(\Delta_r^2+1)^2$. Case (I) discussed in the previous section has $\Delta_i = 0$ so then $\gamma_d' = \gamma_d$, while case (II) has $\gamma_d' = 0$, and then $\Delta_i = -\gamma_d(\Delta_r^2+1)^2/(4\Delta_r) = -\lambda\gamma_d \equiv \Delta_{i0}$. In general we have $\gamma_d' = \beta\gamma_d$ and $\Delta_i = (1-\beta)\Delta_{i0}$ with $0 \le \beta \le 1$. We also assume that the contribution of the untrapped particles to the perturbation is small, so that their contribution outside the separatrix is negligible and hence neglected.

To evaluate the angular integration in the RHS of the first term in

Eqs.(3.6), we consider the function M and its derivative.

$$M(e) = 2\sqrt{2}\omega_b \int_{\theta_{min}}^{\theta_{max}} \sqrt{e(J) + \cos\theta - \alpha\theta}\cos\theta d\theta, \tag{3.8}$$

$$\frac{dM(J)}{dJ} = \frac{dM(J(e))/de}{dJ(e)/de} = \frac{2\pi \int_{\theta_{min}}^{\theta_{max}} \frac{\cos\theta d\theta}{\sqrt{e(J)+\cos\theta-\alpha\theta}}}{\int_{\theta_{min}}^{\theta_{max}} \frac{d\theta}{\sqrt{e(J)+\cos\theta-\alpha\theta}}} = \int_0^{2\pi} \cos\theta d\phi.$$

Then, the double integral can be written as,

$$\Re(\Delta_m - \sqrt{\frac{1+\widetilde{\omega}}{1-\widetilde{\omega}}})\omega_b = \frac{\eta}{\pi}\int_0^{\frac{J_{spx}}{\omega_b}} dj(f(J) - F_0(J))\frac{dM}{dJ} \tag{3.9}$$

Here, the functions M and J are calculated near the separatrix on a fine grid of $e(J)$ and the derivative dM/dJ is constructed with high accuracy in use of a cubic spline. A trapezoidal rule is used in the J integration from 0 to J_{spx}.

During the evolution of the system, the time scale for change is much longer than a wave period, while the time step in Vlasov simulation has to be smaller than the wave period. Therefore, if the adiabatic assumption for the phase space structure is fulfilled, the adiabatic equations enable more rapid predictions of the wave evolution than one would obtain from direct Vlasov simulation. However, the accuracy of the adiabatic equations is assured only if the response remains adiabatic during the evolution.

In the simulation, the adiabatic approximation is never formally justified at the birth of a resonant structure as the quantities ω_b and α initially change too rapidly. Nonetheless, we initiate our problem early in the formation process, where the adiabatic approximation is not valid and we find, as will be shown below, that the subsequent adiabatic evolution is close to numerical

simulation results. To begin with, a small resonant waterbag structure is assumed present centered at an initial frequency $\omega_0 + \Delta\omega$ slightly shifted from the linear frequency ω_0. This waterbag distribution is constant for all particles trapped inside the separatrix region, given by F_0 for all J values less than the separatrix value $J = J_{spx}$, while the distribution just outside separatrix discontinuously changes to $F_0 = \omega_0 + J_{spx}$. The two relations in Eqs.(3.6) are then solved for ω_b and α. We find that a solution to Eqs.(3.6) can be obtained even for small value of the deviation $\Delta\omega$ from the linear frequency, such as $\Delta\omega \sim 0.2\gamma_L$. Having found an initial solution, we scan the frequency ω and solve for $\omega_b(\omega)$ and $\alpha(\omega)$. The time dependence of the solution can also be found by integrating, $\omega_b^{-2} d\omega/dt = \alpha$.

The numerical results, arising from the choice of case (I), are shown in Fig.3.2(a) for the clump and Fig. 3.2(b) for the hole. These solutions show that the TAE waves, initially excited in the gap $-1 \leq \omega \leq 1$, chirp as clumps move towards the lower continuum ($\omega = -1$) and as holes move towards the upper continuum ($\omega = 1$). The clump shown in Fig.3.2(a) penetrates the lower tip and then evolves with an increasing wave amplitude. The sensitivity of the response to the initial frequency displacement $\Delta\omega$ has been investigated. There is sensitivity in the early response to $\Delta\omega$. We will see in the next section that the best fit, of the adiabatic theory with the simulation, results when $\Delta\omega \sim 0.5\gamma_L$.

Figures 3.2(a) and 3.2(b) also show the results predicted from treating the distribution function as a waterbag, whose discontinuity is at the separatrix

of the trapped particles. One then finds the following equations determining the evolution,

$$\Re(\Delta_m - \sqrt{\frac{1+\widetilde{\omega}}{1-\widetilde{\omega}}})\omega_b = \frac{\lambda\gamma_L}{\pi^2}(1-\alpha^2)^{7/4}d_1(\alpha)\Delta f(J) \tag{3.10}$$
$$\Im(\Delta_m - \sqrt{\frac{1+\widetilde{\omega}}{1-\widetilde{\omega}}})\omega_b = \frac{\lambda\gamma_L}{\pi^2}\alpha(1-\alpha^2)^{5/4}d_2(\alpha)\Delta f(J).$$

where the functions $d_1(\alpha)$ and $d_2(\alpha)$ are smooth monotonic and slowly varying functions of α, given by,

$$\begin{aligned} d_1(\alpha) =& 2\sqrt{2}(1-\alpha^2)^{-7/4} \\ & \cdot \int_{\theta_{min}}^{\theta_{max}} d\theta \sqrt{(1-\alpha^2)^{1/2} - |\alpha|\pi + \alpha \arcsin\alpha + \cos\theta - \alpha\theta}\cos\theta = 16c_1(\alpha), \\ d_2(\alpha) =& 2\sqrt{2}(1-\alpha^2)^{-5/4} \\ & \cdot \int_{\theta_{min}}^{\theta_{max}} d\theta \sqrt{(1-\alpha^2)^{1/2} - |\alpha|\pi + \alpha \arcsin\alpha + \cos\theta - \alpha\theta} = 16c_2(\alpha), \end{aligned} \tag{3.11}$$

whose values, as the magnitude of α goes from 0 to 1, vary from $\frac{1}{3}$ to $\frac{3}{14}$ for $c_1(\alpha)$ and from 1 to $\frac{3}{10}$ for $c_2(\alpha)$ along the separatrix determined from the normalized Hamiltonian Eq.(3.3). We also note that there is error in Ref. [4] for values of c_1 and c_2 as $|\alpha|$ approaches unity, and in particular c_1 does not change sign contrary to Ref. [4] as $|\alpha|$ goes from 0 to 1.

In obtaining Eq.(3.10) we have assumed that the distribution remains a waterbag with $f(J)$ constant in the trapping region at the value $F_0(J) = \omega_0$ where ω_0 is the J value of the unperturbed particles at the original linear frequency. Just outside the separatrix $f = F_0(\omega \pm J_{spx})$, so there is a discontinuity $\Delta f(J) = \omega \pm J_{spx} - \omega_0$ at the separatrix. The assumption of a discontinuous

waterbag distribution at the separatrix is maintained, even when the bounding separatrix increases during the evolution. In contrast the consistently evaluated distribution is continuous as J_{spx} increases. Nonetheless we see that there is general qualitative agreement of the mode amplitude and chirping parameter with the consistent theory but with a significant quantitative difference, particularly early in the evolution.

3.5 Comparison of adiabatic theory with kinetic model

The adiabatic model is derived from our basic equations assuming that the adiabatic approximation is valid during the entire evolution of the phase space structure. Agreement of the predictions of the adiabatic and simulation results, implies that the adiabatic model captures the essential dynamics being produced in the simulation.

First we compare the theoretical adiabatic response of a down-chirping clump to the results found in the simulation. The initial adiabatic solution is obtained by assuming an initial waterbag distribution at the bounding separatrix present with a frequency, $\Delta\omega$, shifted slightly from the linear mode frequency. One can then solve the adiabatic equations given by Eqs.(3.6) for $\omega_b(\omega)$ and $\alpha(\omega)$. A comparison for a clump of $\omega_b(\omega)$ and $\alpha(\omega)$ between what is predicted by the adiabatic theory and simulations is shown for dissipative case (I) in Figs.3.3(a) and 3.3(b). Similar good comparisons, not shown here, have been obtained for dissipative case (II) as well.

We find very good results for a hole in the mid-range of $\omega - \omega_0$, as is

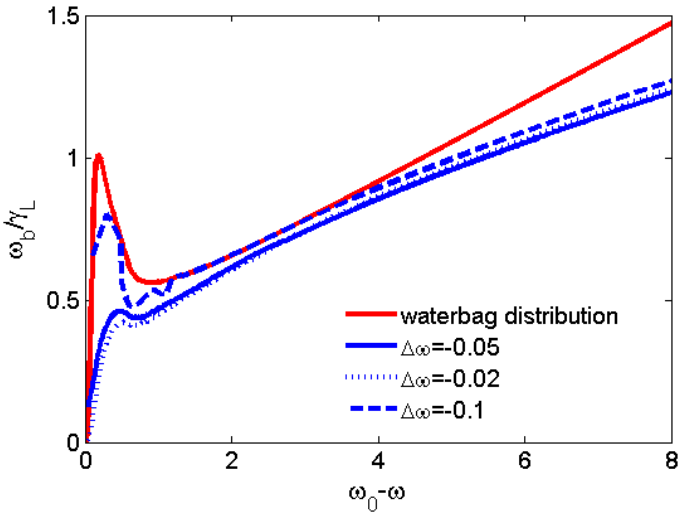

(a)

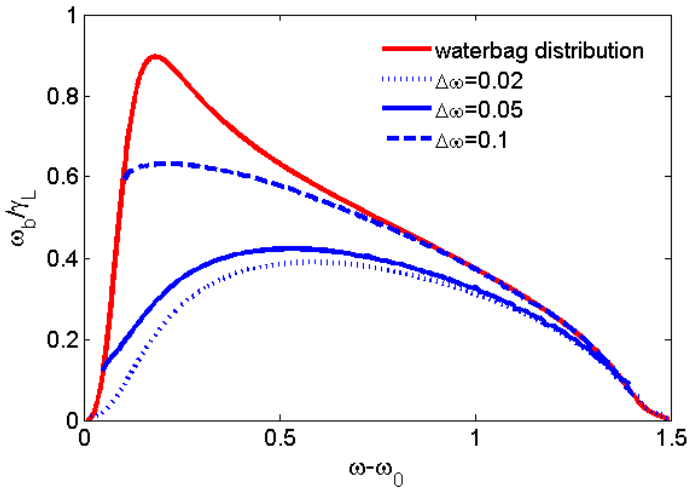

(b)

Figure 3.2: Adiabatic prediction (for dissipation case (I)) for amplitude evolution of a clump (panel a) and hole (panel b). $\gamma_L = 0.1$, $\gamma_d = 0.08$, $\Delta_m = 0.654$ and $\eta = 0.0248$. The blue curves are for self-consistent adiabatic responses that evolve from an initial waterbag distribution displaced from linear frequency by various $\Delta\omega$ values. The red curve is for a distribution constrained to be a waterbag with a discontinuity at the trapped particle separatrix.

seen in Figs. 3.4(a) and 3.4(b) which are the results for the dissipative case (I), where $\gamma_d' = \gamma_d$. However, for early times when the frequency shift is too small we do not extract reliable data from the simulation because the noise is high (higher than that for a clump with the same magnitude of frequency shift). Thus, for the simulation in Figs. 3.4(a) and 3.4(b), we only show the filtered results of $\omega_b(\omega)$ and $\alpha(\omega)$ when $\omega - \omega_0$ is larger than 0.25, when the filtering of the noise becomes manageable. In the frequency range $0.25 \leq \omega - \omega_0 \leq 1.05$ there is excellent correlation between the adiabatic theory's predicted values for $\omega_b(\omega)$ and $\alpha(\omega)$ compared to the values produced in the simulation. However, the hole appears to disintegrate when $\omega - \omega_0 > 1.05$.

Thus we conclude, for the down-chirping clump and the up-chirping hole, that the agreement between Vlasov simulation and consistent adiabatic model is impressively good for both cases, as long as the chirping structure stays intact in the simulation. The reason for the hole's disintegration is not firmly established. However a candidate explanation for the loss of the hole is the breakdown of the adiabaticity assumption as the hole approaches the upper continuum. In figures 3.5(a) and 3.5(b) we show an adiabaticity breakdown parameter, P_{adb}, where a smaller P_{adb} means better reliability of the adiabatic prediction (the definition of P_{adb} is discussed at the end of this section). We see in the figure on the top, that the breakdown parameter suddenly begins to rise at $\omega - \omega_0 \sim 1.2$, a number close to where the hole disintegrates in the simulation. We still need to confirm whether the deterioration of adiabaticity leads to the loss of the hole. Other candidate reasons is the onset of as yet

an unidentified instability, or simply the accumulation of numerical error. We also note that case (II) does not exhibit sudden deterioration, just a slow decay in amplitude as the frequency approaches the upper continuum. For this case, the adiabatic theory is consistent even for small amplitude, because the adiabatic parameter, P_{adb}, remains small.

There are several other points worth noting. In the early stages of evolution, it is seen in Fig. 3.5(a) that an initial small hole does not satisfy the adiabaticity condition as the parameters change too rapidly. The trapping frequency at the O-point, Ω_b, is given by $\Omega_b = \omega_b(1-\alpha^2)^{1/4}$. The simplest criterion to fulfill the adiabaticity condition for particles at the O-point is:

$$\frac{1}{\Omega_b^2}\frac{d\Omega_b}{dt} \ll 1. \tag{3.12}$$

Since $d/dt = \omega_b^2 \alpha d/d\omega$, this criterion is equivalent to

$$|\alpha(1-\alpha^2)^{-5/4}[(1-\alpha^2)\frac{d\omega_b}{d\omega} - \frac{1}{2}\omega_b\alpha\frac{d\alpha}{d\omega}]| \ll 1 \tag{3.13}$$

We see that if α^2 is close to unity it is likely that the adiabaticity criterion will fail. Nonetheless the comparison of the results from the adiabatic and simulation runs, from the creation of a phase space structure to its late evolution, is generally excellent. What appears to be important for an accurate prediction of the evolution, is that the distribution fills in smoothly, as it does both in the actual simulation and in the case of an initially small waterbag core where the separatrix surrounding the trapped particles grows during the chirp.

In addition the adiabatic approximation is suspect when a clump goes through the tip point at $\omega = -1$. In this case the local adiabatic approx-

imation for model (II) cannot be justified due to an abrupt change of the parameters of the adiabatic equations in Eqs.(3.6). We see in Fig.3.5(b) that adiabatic parameter P_{adb} decreases markedly as the frequency chirps toward $\omega = -1$, where $\omega_0 - \omega \approx 0.6$. However, close to $\omega = -1$, the adiabatic parameter suddenly begins to increase quite markedly for case (II) ($\gamma_d' = 0$) and only modestly for case (I) ($\gamma_d' = \gamma_d$). However, P_{adb}, still remains small, even for case (I). Hence, the disturbance producing an adiabaticity violation remains moderate, and the resulting comparisons of adiabatic theory with the simulation remain accurate even as the chirping structure goes through the continuum boundary as well as deep into the continuum.

A more restrictive adiabatic condition is based on the following considerations. First we note as the parameters, ω_b and α vary slowly in time, that a particle's action along its actual trajectory varies during a bounce time and it is only the mean value, which we have denoted as J, that remains constant during the evolution of the particle's motion. There is then a maximum variation of the action $\delta J(J)$ from the mean value J during a single bounce of the particle. We have analytically evaluated $\delta J(J)$ by standard means. Then if $\delta J(J)$, is larger than the difference between the separatrix J_{spx} and J, i.e. $J_{spx} - J$, this particle has a high probability of being untrapped, which is a violation in the assumption of the constancy of J. We then solve for that action, J_{cr} that satisfies the condition $\delta J(J_{cr}) = J_{spx} - J_{cr}$ which enables us to define P_{adb} as $P_{adb} \equiv \delta J(J_{cr})/J_{spx}$. Then as a criterion for the validity of adibaticity for most of the particles trapped in the phase space structure, we

require $P_{adb} \ll 1$.

The adiabaticity parameter, P_{adb}, for the hole and clump runs given in Figs. 3.5(a) and 3.5(b) show very small numbers for P_{adb} except for the initial states when $|\alpha|$ is somewhat less than unity and near the upper continuum for the hole in case (II). Hence the adiabatic model gives excellent results compared to the Vlasov simulation except for a hole near the upper continuum.

3.6 Analysis of adiabatic theory

The relatively complicated structure of Eqs.(3.6) makes them difficult to solve analytically over the entire domain of the chirp especially as it is difficult to analytically calculate the correct distribution function $f(J)$ when the separatrix is rising. We can simplify the problem by assuming that the distribution in the trapping region is always a waterbag distribution described in the previous section. We will use this waterbag assumption to study properties of the chirping mode for a clump structure at the lower continuum frequency and its later chirp when it is deep into the Alfvén continuum a great deal below the lower tip frequency. We also study the adiabatic chirping properties of a hole should the frequency get close to the upper tip.

The waterbag model from Eqs. (3.10) predicts the bounce frequency (i.e. square root of wave amplitude) and chirping parameter at the lower tip,

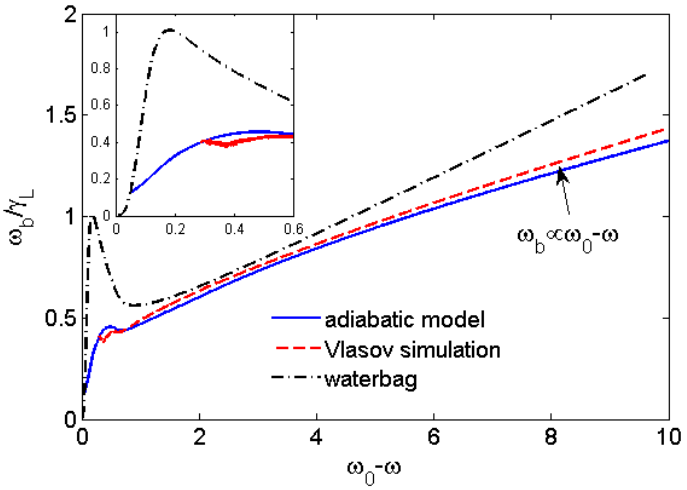

(a)

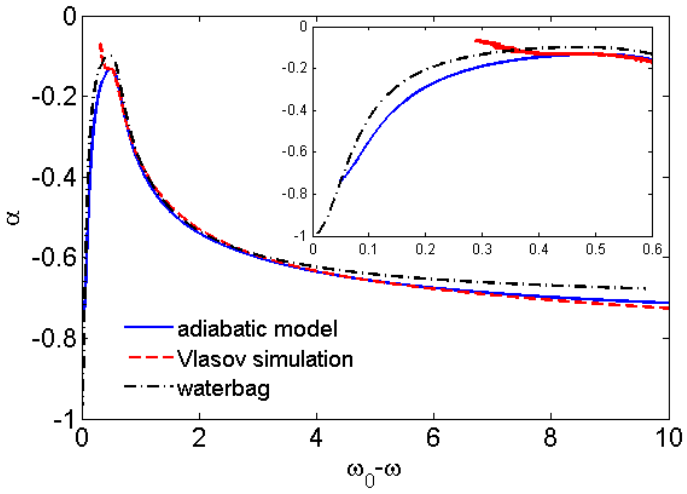

(b)

Figure 3.3: Comparison, using case (I), for a clump between the predications of adiabatic theory and simulation results, for the mode amplitude, ω_b (panel a) and chirping parameter α (panel b). Comparison of the results for the crude waterbag model is also shown. System parameters are : $\Delta_m = 0.654, \eta = 0.0248, \gamma_L = 0.1, \gamma_d = 0.08, \Delta\omega = 0.5\gamma_L$. The inserted figures resolve the response when the frequency is in the gap ($0 \leq \omega_0 - \omega \leq 0.6$).

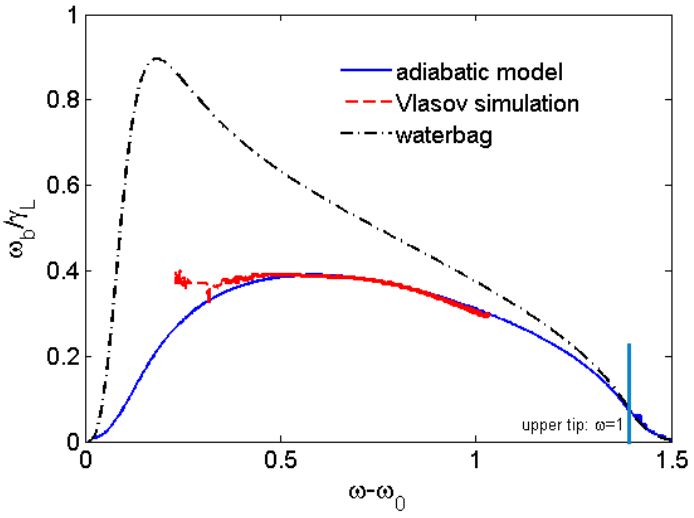

(a)

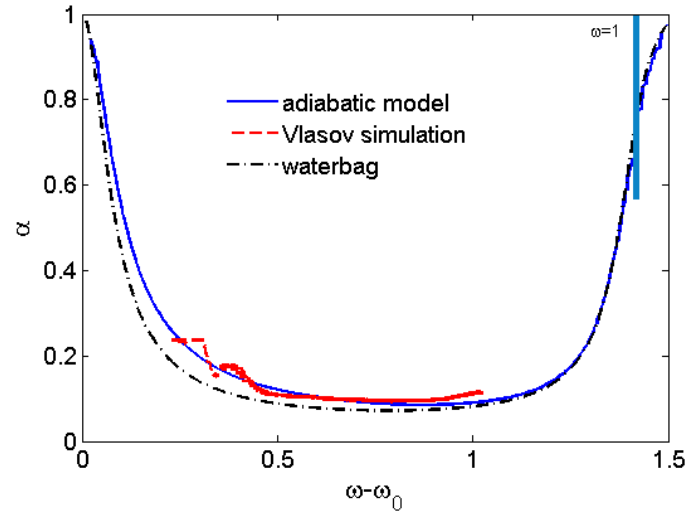

(b)

Figure 3.4: Comparison of predictions for ω_b (panel a) and α (panel b) between Vlasov simulation and adiabatic model for an evolving hole structure for dissipative case (I). Same input parameters as Figs.3.3(a) and 3.3(b).

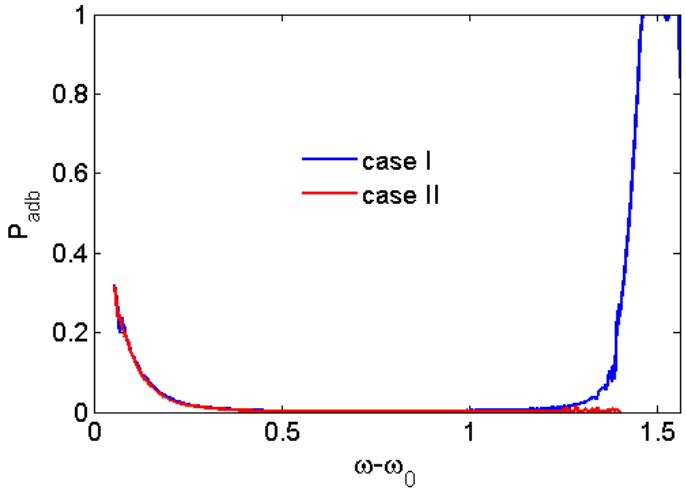

(a)

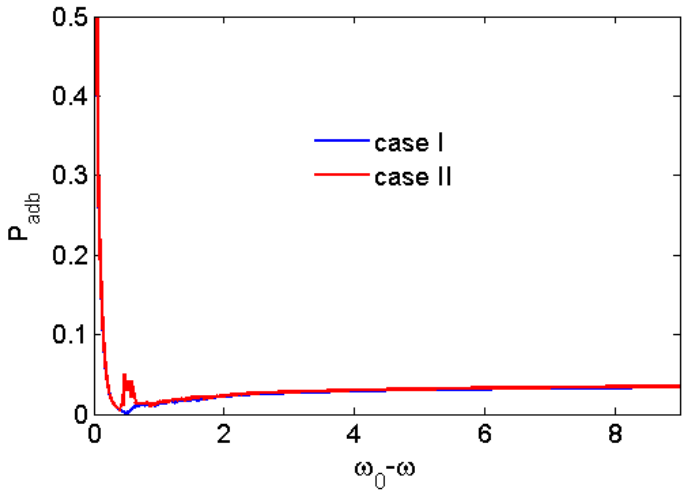

(b)

Figure 3.5: Study of evolution of the adiabaticity parameter as a function of frequency shift for both hole (panel (a)) and clump (panel (b)) for the two extreme dissipative cases (I) and (II).

is given by,

$$\frac{\omega_b}{\gamma_L} = \frac{\lambda(1+\omega_0)\Delta_r^{5/2} d_1(\alpha) d_2(\alpha)^{7/2}}{\pi^2((\Delta_i d_1(\alpha))^2 + (\Delta_r d_2(\alpha))^2)^{7/4}} = 0.62, \tag{3.14}$$

$$\alpha = \frac{\Delta_i d_1(\alpha)}{((\Delta_i d_1(\alpha))^2 + (\Delta_r d_2(\alpha))^2)^{1/2}} = -0.132.$$

where the numerical values are calculated using the parameters given in the caption of Figs.3.3(a) and 3.3(b). As can been seen in Fig.3.3(a), this predicted chirping parameter is quite similar to the simulation result, while ω_b/γ_L is a factor ~ 1.5 larger than the prediction of the consistent model. Also note in Fig.3.3(a), that the waterbag model prediction is significantly different from the consistent adiabatic results when the frequency is in the gap but much closer for frequencies in the continuum.

Deep in the continuum ($\omega_0 - \omega \gg 1$), the chirping parameter α, plotted in Fig. 3.3(b) approaches a constant value and the bounce frequency in Fig. 3.3(a) grows linearly with ω. This behavior is apparent from a local analysis of the equations for the waterbag model Eqs. (3.10), under the assumption $\omega \gg 1$, where one finds:

$$\omega_b \Delta_r = \frac{\lambda \gamma_L}{\pi^2}(1-\alpha^2)^{7/4} d_1(\alpha)(\omega_0 - \omega), \tag{3.15}$$

$$\omega_b = \frac{\lambda \gamma_L}{\pi^2}\alpha(1-\alpha^2)^{5/4} d_2(\alpha)(\omega_0 - \omega).$$

Dividing these two equations, we obtain an implicit function of α. A simplified expression is obtained if we use the value $\alpha^2 = 1$ in d_1 and d_2. Then we find that deep in the continuum,

$$\alpha \to \alpha_{-\infty} \doteq -\frac{1}{\sqrt{1.96\Delta_r^2 + 1}} = -0.74. \tag{3.16}$$

This value appears to be within 10% of the value found in the simulation as seen in Fig.3.1(b). Such a solution leads to an explosive growth in the time domain as follows from the evolution equation,

$$\alpha = \omega_b^{-2}\frac{d\omega}{dt} = \omega_b^{-2}\frac{d\omega_b}{dt}\frac{d\omega}{d\omega_b} = \frac{\pi^2\omega_b^{-2}}{\lambda\gamma_L\alpha(1-\alpha^2)^{5/4}d_2(\alpha)}\frac{d\omega_b}{dt} \tag{3.17}$$

This equation, solved for $\alpha = \alpha_{-\infty}$, has an explosive response, which is proportional to $(t_\infty - t)^{-1}$. The undetermined constants can be obtained by curve fitting to the numerical solutions of the adiabatic waterbag equations.

$$\omega_b(t) = \frac{\omega_{b0}t_\infty}{t_\infty - t}. \qquad (t_\infty = 6448, \omega_{b0} = 0.0322) \tag{3.18}$$

A similar procedure can be used to study the behavior of the adiabatic response of a hole near the upper continuum. Simulations indicate that the hole disappears before the frequency gets too close to continuum and thus the adiabatic theory for this case cannot be compared with simulation results. The analysis demonstrates that for dissipative case (II), where the dissipation Δ_i is finite and $\gamma_d' = 0$, the chirping mode does not penetrate the continuum. As the continuum is approached α becomes small and ω_b vanishes in proportion to $\sqrt{1-\omega}$. However, when γ_d' is nonzero, the hole slightly penetrates into the continuum, and then decays to zero amplitude when $\omega = 1 + (\frac{\gamma_d'}{\sqrt{2}\Delta_r})^{2/3}$.

3.7 Adiabatic theory for hole near upper continuum

The hole dynamics approaching the upper continuum is analyzed using the waterbag model while examining frequencies close to the upper continuum

where $|1-\omega| \ll 1$ and $\gamma_d \ll 1$, the two adiabatic equations can be written approximately as

$$\omega_b(\Delta_r - \Re(\frac{2}{1-\widetilde{\omega}})^{1/2}) = -\frac{\lambda\gamma_L}{\pi^2}(1-\alpha^2)^{7/4}d_1(\alpha)(1-\omega_0), \tag{3.19}$$
$$\omega_b(\Delta_i - \Im(\frac{2}{1-\widetilde{\omega}})^{1/2}) = -\frac{\lambda\gamma_L}{\pi^2}\alpha(1-\alpha^2)^{5/4}d_2(\alpha)(1-\omega_0),$$

with the d_1 and d_2 given in Eqs.(3.11). We also introduce a parameter β defined as $\beta = \gamma_d'/\gamma_d$, and then $\Delta_i = (1-\beta)\Delta_{i0}$, where $\Delta_{i0} = -\lambda\gamma_d$, with $\lambda = (\Delta_r^2+1)^2/(4\Delta_r)$, which produces the same damping rate γ_d, for all values of β. Then equation (3.19) can be written as,

$$\begin{aligned}
&\omega_b[\Delta_r - \sqrt{\frac{\sqrt{(1-\omega)^2+(\beta\gamma_d)^2}+1-\omega}{(1-\omega)^2+(\beta\gamma_d)^2}}] \\
&\quad = -\frac{\lambda\Delta_r}{\pi^2}\gamma_L(1-\alpha^2)^{7/4}d_1(\alpha)(1-\omega_0), \\
&\omega_b[(1-\beta)\Delta_{i0} - \sqrt{\frac{\sqrt{(1-\omega)^2+(\beta\gamma_d)^2}-1+\omega}{(1-\omega)^2+(\beta\gamma_d)^2}}] \\
&\quad = -\frac{\lambda\gamma_L}{\pi^2}\alpha(1-\alpha^2)^{5/4}d_2(\alpha)(1-\omega_0).
\end{aligned} \tag{3.20}$$

Dividing the two equations with each other to eliminate ω_b, we obtain

$$\begin{aligned}
&\frac{\sqrt{\sqrt{(1-\omega)^2+(\beta\gamma_d)^2}-(1-\omega)} - \Delta_{i0}(1-\beta)\sqrt{(1-\omega)^2+(\beta\gamma_d)^2}}{\sqrt{\sqrt{(1-\omega)^2+(\beta\gamma_d)^2}+(1-\omega)} - \Delta_r\sqrt{(1-\omega)^2+(\beta\gamma_d)^2}} \\
&= \frac{\alpha d_2(\alpha)}{(1-\alpha^2)^{1/2}d_1(\alpha)}.
\end{aligned} \tag{3.21}$$

As the upper continuum is approached from below, we first consider the region where $\beta\gamma_d \ll (1-\omega) \ll 1$. Then we find that in this region $\alpha \ll 1$ and is

approximately given by,

$$\alpha = \frac{1}{3\sqrt{2}}(1-\omega)^{1/2}(-\Delta_{i0}(1-\beta) + \frac{\beta\gamma_d}{\sqrt{2}(1-\omega)^{3/2}}). \tag{3.22}$$

For the dissipative case (II), where $\beta = 0$, we see that α goes monotonically to zero as ω approaches unity. Then from Eqs. (3.19), we find that $\omega_b = \frac{\lambda\gamma_L}{3\sqrt{2}\pi^2}(1-\omega_0)\sqrt{1-\omega}$.

If $\beta \neq 0$ it can also be shown that α continues to decrease as ω approaches unity as long as the inequality $1-\omega \gg \beta\gamma_d$ continues to be valid. However when this inequality is invalid, $1-\omega \sim \beta\gamma_d$ a rather complicated function of $1-\omega$ results where the solution for α increases to a value that is an order-unity fraction less than 1. In addition ω always penetrates the continuum for non-zero β. At $\omega = 1$, we find in the limit of $\gamma_d \ll \max(1, 1/\Delta_r^2)$, α satisfies,

$$\frac{\alpha d_2(\alpha)}{(1-\alpha^2)^{1/2} d_1(\alpha)} = 1, \tag{3.23}$$

with the solution $\alpha = 0.645$ independent of the value of β, while the bounce frequency is,

$$\omega_b = 0.69\beta^{1/2}\lambda\gamma_L\gamma_d^{1/2}(1-\omega_0). \tag{3.24}$$

After penetration into the continuum, α increases and heads towards unity. When $\beta\gamma_d \ll \omega - 1 \sim (\beta\gamma_d)^{2/3}$, α^2 is given by,

$$\alpha^2 = 1 - 1.96\left(\frac{\beta\gamma_d}{2(\omega-1)} - \frac{\Delta_r}{\sqrt{2}}(\omega-1)^{1/2}\right)^2. \tag{3.25}$$

The maximum frequency, ω_{mx}, is found to be,

$$\omega_{mx} = 1 + (\frac{\beta\gamma_d}{\sqrt{2}\Delta_r})^{2/3}. \tag{3.26}$$

In this region $\omega - 1 \sim (\beta\gamma_d)^{2/3}$, ω_b goes to zero as

$$\omega_b = 0.05\lambda\gamma_L(1-\omega_0)\sqrt{\omega-1}\left(\frac{\beta\gamma_d}{2(\omega-1)} - \frac{\Delta_r}{\sqrt{2}}(\omega-1)^{1/2}\right)^{5/2}. \qquad (3.27)$$

3.8 Summary

Frequency chirping frequently arises after the spontaneous excitation of waves in a plasma when there is a close balance of the drive from the free energy source present to amplify the waves together with a nearly matching sink of dissipation which causes wave damping in absence of a free energy source. The chirp is due to the formation of clump and/or hole structures as a result of wave trapping of resonant particles. Then, as an alternative to the amplitude damping, the energy released by the free energy source is absorbed by the dissipative sink while the phase space structures move to a lower energy state. This movement of the trapping structure in phase space produces the observed chirping signal which is locked to the phase space positions of the holes and clumps [4].

The constancy of the trapped particle action in a slowly evolving wave enables an adiabatic description of the system in terms of a relatively simple set of equations based on a Hamiltonian that explicitly includes the chirping term but implicitly includes time. Most other studies of this problem have assumed either $\alpha \ll 1$ or $\alpha \approx 1$. Whenever the adiabatic theory is justified we can avoid a more expensive simulation of studying chirps, based on solving the Vlasov equation by a direct numerical integration. Indeed we find that our

reduced adiabatic description usually gives impressive agreement with direct numerical simulation results. When we find a disparity of the adiabatic theory prediction with numerical observations, as occurred when holes attempt to reach the upper continuum, we find that the adiabatic solutions lead to an increase in value of the adiabaticity parameter, P_{adb}, which indicates that the adiabaticity theory could be failing. On the other hand, early in the simulation, we find that even though there is a large adiabaticity parameter that would lead one to distrust the validity of the early calculation when the phase structures are small, the best results of the simulation are achieved when very small initial seeds for holes or clumps are taken. Perhaps a reason for this, is that a small initial seed leads to a relatively smooth trapped distribution around the separatrix, rather than a waterbag distribution, with an abrupt transition at the separatrix. In the simulation one would expect that the intrinsic non-adiabatic behavior near the separatrix would cause a smooth distribution to develop. The development of a similar smooth distribution in the adiabatic calculation may then give a more accurate prediction during the later evolution when the adiabaticity assumption is justified because a more realistic distribution, than that from a waterbag, has formed.

As an example of missing physics that is essential to the theory, is that the interaction term of the particle Hamiltonian does indeed depend on the wave frequency and particle momentum, as is the case for the Hamiltonian derived in [10] for using eigenfunctions derived for near the tips of the RBV model. Inclusion of these effects will now be investigated in next chapter. This

addition to the model adds an essential sense of realism to the calculation. Then a more reliable assessment can be made as to whether the hole-clump chirping theory gives an accurate physical model for interpreting experimental data.

Chapter 4

Rapid Frequency Chirps of TAE due to Finite Orbit Energetic Particles

4.1 Introduction

Our previous studies assumed a generic Hamiltonian interaction between the particles and the waves [72, 73]. Now we introduce a self-consistent interaction of particles with the wave in accord with map model developed in [9, 10]. For the moderately high m modes, the finite width of the orbit $\Delta_b \approx q\rho$, is accounted for as it can be comparable to the mode scale length $\Delta_{Gp} \approx r_m^2/ms_mR$. Here $\rho = (v_\parallel^2 + v_\perp^2/2)/(\omega_c v_\parallel)$ is a valid expression when $v_\perp/v_\parallel \ll \sqrt{\epsilon}$ (an approximation assumed throughout this work), r_m is the mode location where $q(r_m) = (m + 1/2)/n \equiv q_m$ which is the safety factor at the position of the TAE gap. $s_m \equiv r_m q'_m/q_m$ is the local magnetic shear and m denotes both the poloidal mode number and the gap number where there is a coalescence of the m^{th} and $m + 1^{th}$ poloidal harmonics. In these formula Δ_{Gp}/Δ_b is arbitrary but needs to satisfy the condition that Δ_b is smaller than the spatial distance between neighboring gaps, given roughly by $\Delta_b \ll r_m/m$ [16].

During a chirp into the Alfvén continuum, the orbit width under our

restriction, does not intersect the continuum when the frequency is in the gap. When the frequency enters the continuum the orbit will at first intersect the continuum twice, as seen in Fig. 4.1, and then with a continuing chirp, it will intersect just once essentially when the separation, at fixed frequency, of the two continuum curves becomes larger than half the total orbit width.

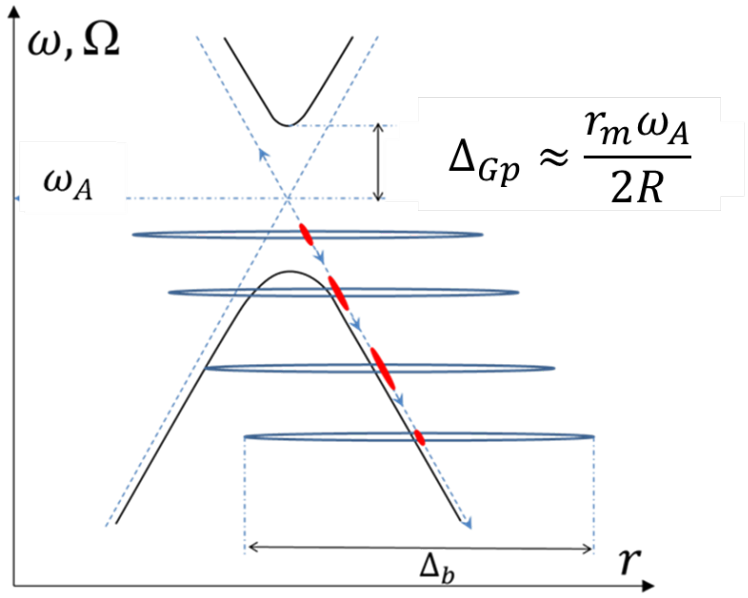

Figure 4.1: TAE mode is excited in the Alfvén gap with the width Δ_{Gp}. The horizontal elongated loops show the radial range of the oscillating trajectories of energetic particles. The red structures represent that the separatrix regions during a down chirp.

4.2 Model range of applicability

Our simulation neglects the coupling of the modes between adjacent gaps so that we limit our consideration of TAE excitation to a wave only in a

single Alfvén gap. This approximation is limited in applicability to low shear and serves as a rough model for higher shear.

The nonlinearities in our model only come from the particle kinetic behavior and not from the MHD equations. As typically the MHD nonlinearity, which scales as $(\delta B/B)^2$, can be neglected as the kinetic interaction scales as $\sqrt{\delta B/B}$. However, near the tip it is likely that the ordering breaks down in a manner similar to the way it does for fishbone modes caused by the internal kink [59]. However, if an MHD nonlinear structure can be prevented from developing due to plasma fluid viscous behavior (which could have an anomalous source), our model can still be applicable [4, 18].

An energetic particle of a mass m_p and a charge q_p in a tokamak rotates toroidally and poloidally as passing particles at rate $v_\parallel/R$ and $v_\parallel/(qR)$ respectively and with an additional unperturbed guiding center drift velocity $v_d \equiv (\frac{1}{2}v_\perp^2 + v_\parallel^2)/(\omega_c R)$, primarily in the toroidal direction. Here $v_\perp$ and $v_\parallel$ are the velocities of energetic particles perpendicular and parallel to the unperturbed magnetic field $\mathbf{B}$, respectively. These relations are accurate if $v_\perp/v_\parallel < \sqrt{\epsilon}$. The contributions from the banana-orbit particles are ignored. All the passing particles have nearly constant parallel velocity $v_\parallel$ along the magnetic field in the case $v_\parallel/v_\perp \gg \sqrt{R/r}$.

In our model, the magnetic moment is conserved due to the low frequency of the TAE waves. However, the energy E of energetic particles is not in principle conserved during the wave-particle interaction. Instead, the energetic particles are moving on the constant surface of $E' = E - \omega(t)P_\phi/n$

in the presence of the perturbed waves, whose frequency $\omega(t)$ evolves during a frequency chirp. To avoid the complicated analysis on the constant E' surface, we approximate the dynamics of TAE and energetic particles to arise on a constant E instead of the constant E' surface and therefore only P_ϕ changes during the wave particle interaction. The validity condition for this approximation is obtained as follows. The momentum excursion at constant E' and constant E are given respectively by,

$$< \delta P_\phi > |_{E'} = -\frac{\omega_c r_m \delta r}{q_m}(1 + \frac{\omega_A R}{n v_\parallel}),$$
$$< \delta P_\phi > |_{E} = -\frac{\omega_c r_m \delta r}{q_m},$$

where $\omega_A = v_A/2q_m R$ indicates the frequency in the middle of Alfvén gap and $<>$ takes the time average on the poloidal angle. When the toroidal mode number $n \gg \omega_A R/v_\parallel = v_A/2q_m v_\parallel$, the toroidal momentum excursion from the constant E' surface $< \delta P_\phi > |_{E'}$ is approximately equal to $< \delta P_\phi > |_E \approx -\omega_c r_m \delta r/q_m$. This is a condition that is readily satisfied for moderately large n values.

In addition, the weighting of the equilibrium distribution can be exactly written as a derivative of the toroidal momentum P_ϕ at constant E' surface, where the form of the energetic particle distribution is $g(E', P_\phi, t) = f(E = E' + \omega P_\phi/n, P_\phi, t)$. Often one can neglect the E derivative on P_ϕ, so that

$$\frac{\partial g(E', P_\phi, t)}{\partial P_\phi}|_{E'} - \frac{\partial f(E, P_\phi, t)}{\partial P_\phi}|_E = \frac{\omega}{n}\frac{\partial f(E, P_\phi, t)}{\partial E}|_{P_\phi} \approx 0.$$

if the Alfvén frequency satisfies $\omega_A \ll nq_m v_\parallel^2/\omega_c r_m^2 = \omega_{*\alpha}$, then $\partial g(E', P_\phi, t)/\partial P_\phi|_{E'} \approx \partial f(E, P_\phi, t)/\partial P_\phi|_E$. However, this approximation does not need to be restrictive in our model, as $\partial g(E', P_\phi, t)/\partial P_\phi|_{E'}$ is being considered constant in the gap region, where the simulation takes place.

Another approximation in the model is that the orbit width is well separated within the global mode width of the m^{th} and $m+1^{th}$ structure. The condition for the energetic particle-wave interaction to be dominated by the particle-wave interaction in the tip is given by [16],

$$\Delta r_b \frac{dq}{dr} < \frac{1}{n}.$$

Here $\Delta r_b = q_m R v_d / v_\parallel$ is the radial deviation from the resonant surface in one bounce period of the poloidal direction. The conditions we discussed above are combined to express the constraints on the toroidal mode number n,

$$\frac{v_A}{2q_m v_\parallel}, \frac{v_A \omega_c r_m^2}{2q_m^2 R v_\parallel^2} \ll n < \frac{\omega_c r_m}{s_m q_m^2 v_\parallel (1 + v_\perp^2/2v_\parallel^2)}.$$

In our work, the adiabatic condition for trapped energetic particles is assumed to be valid in the entire phase space and frequency domain. A breakdown condition for adiabaticity can be constructed to evaluate the appropriateness of adiabaticity, near the O-point based on checking whether the trapping frequency or chirping rate changes significantly in a time ω_{bO}^{-1}. This leads to the expression we use for the validity of the adiabatic analysis,

$$\begin{aligned} P_{adbO} =& |\frac{\alpha}{\sqrt{1-\alpha^2}} \frac{d}{d\omega} \omega_{bO} (1-\alpha^2)^{1/4}| \\ &+ |\frac{\alpha}{\omega_{bO}(1-\alpha^2)^{3/4}} \frac{d}{d\omega} \left(\alpha \omega_{bO}^2 \frac{d}{d\omega} \omega_{bO} (1-\alpha^2)^{1/4} \right)| \ll 1, \end{aligned} \tag{4.1}$$

where ω_{bO} is the bounce frequency for deeply trapped particles at O-point and α is the chirping rate, that we previously defined.

4.3 Variational principle with a wave-particle interaction

Hamilton's principle states that the dynamics of a physical system follows a trajectory from t_1 to a time t_2 that is an extremal path in a phase space of a physical system.

$$S[\mathbf{q}(\mathbf{r},t)] = \int_V d^3\mathbf{r} \int_{t_1}^{t_2} d\tau \mathcal{L}(\mathbf{q}(\mathbf{r},\tau), \dot{\mathbf{q}}(\mathbf{r},\tau), \tau), \tag{4.2}$$

where $\mathcal{L}(\mathbf{q}(\mathbf{r},\tau), \dot{\mathbf{q}}(\mathbf{r},\tau), \tau)$ is the Lagrangian density. Then employing the standard variational method, the Euler-Lagrange equations for the evolution of the system are determined. This method has also been extended to embrace fluid [23, 42] and Vlasov systems [55, 77].

The dynamical equations are derived by taking the variation of an action integral with respect to the coordinate $\mathbf{q}$, which require fixed values at endpoints of the trajectory. The endpoint contributions restrict the class of small perturbations on $\delta\mathbf{q}$ with $\delta\mathbf{q}(t = t_1) = 0$ and $\delta\mathbf{q}(t = t_2) = 0$.

The variational problem can be generalized by extending the time endpoints from zero to infinity and to apply the variational principle to an action density integrated over space and time.

$$S[\mathbf{q}(\mathbf{r},t)] = \int_V d^3\mathbf{r} \int_0^{\infty} d\tau \mathcal{L}(\mathbf{q}(\mathbf{r},\tau), \dot{\mathbf{q}}(\mathbf{r},\tau), \tau),$$

This action is reexpressed as a superposition of Fourier modes in ω complex plane with a Laplace transformation, where the small perturbations $\delta\mathbf{q}(\mathbf{r},\omega)$ are chosen to be analytic on the upper half complex plane of ω as imposed by the causality condition.

For our model, we begin with the Lagrangian density for an Alfvén-like wave interacting with energetic particles. This consists of the sum from contributions from the field and from the background plasma and the energetic particles $\mathcal{L} = \mathcal{L}_{em} + \mathcal{L}_p$ [22]. Here, $\mathcal{L}_{em} = (\mathbf{E}\cdot\mathbf{E} - \mathbf{B}\cdot\mathbf{B})/2 \approx -\mathbf{B}\cdot\mathbf{B}/2$ is the electromagnetic field Lagrangian density where it is appropriate to neglect the electric field term in $\mathcal{L}_{em}$ when the Alfvén velocity is much less than the speed of light. The electric and magnetic fields need to be expressed the scalar and magnetic potential, so that $\mathbf{E} = -\nabla\varphi - \partial_t\mathbf{A}$ is the perturbed electric field, $\mathbf{B} = \nabla\times\mathbf{A}$ is the perturbed magnetic field, φ and $\mathbf{A}$ are the perturbed scalar and vector potentials introduced in [44]. Then the Lagrangian density of charged particles in an electromagnetic field is,

$$\begin{aligned}\mathcal{L}_p &= \sum_i \frac{1}{2}m_p\mathbf{v}_i^2 - q_i\varphi(\mathbf{r},t) + q_i\mathbf{v}_i\cdot\mathbf{A}(\mathbf{r},t) \\ &= \frac{1}{2}n_p m_p\mathbf{v}^2 - \rho_p\varphi(\mathbf{r},t) + \mathbf{j}_p(\mathbf{r},t)\cdot\mathbf{A}(\mathbf{r},t),\end{aligned} \tag{4.3}$$

where a cold plasma model is used to represent the response of the background plasma so that individual particles are represented by the fluid kinetic energy times the plasma density, n_p. In addition, ρ_p and $\mathbf{j}_p$ are the charge density and the current of energetic particles, respectively. The summation is the addition of the contributions to the Lagrangian from individual particles [7], which is

then replaced with a fluid representation of the response.

Here we will use that the energetic particle dynamics satisfies a Vlasov equation where the field is determined by the wave-particle interaction term that was derived in the map model of [9, 10]. The action that satisfies the interactions of the MHD plasma with the magnetic field as well as the kinetic wave particle interactions of the fields with the energetic particle currents that are determined by the dynamics of the energetic particles which are governed by a Vlasov equation, is given by,

$$S \approx \int d^3\mathbf{r}dt \left\{ \frac{n_p m_p}{2} \frac{(\mathbf{E}\times\mathbf{b})^2}{\mathbf{B}^2} - \frac{\mathbf{B}^2}{2} + \mathbf{j}_p \cdot \mathbf{A} - \rho_p \varphi \right\}, \tag{4.4}$$

where $\mathbf{b}$ is the unit direction of the magnetic field. The fluid element of energetic particles mainly drifts with the $\mathbf{E}\times\mathbf{B}$ drift velocity and the equilibrium fields, are subtracted from this action expression.

In the reduced MHD theory [75], the vector and scalar potentials are represented by a single scalar function $G(\mathbf{r},t)$ so that $\mathbf{A} = -\mathbf{b}(\mathbf{b}\cdot\nabla)G(\mathbf{r},t)$, $\varphi = \partial G(\mathbf{r},t)/\partial t$. Then the perturbed electric and magnetic field can be expressed in the form of $G(\mathbf{r},t)$,

$$\begin{aligned}
\mathbf{E} &= -\nabla\varphi - \frac{\partial \mathbf{A}}{\partial t} = -\nabla\dot{G}(\mathbf{r},t) + \mathbf{b}\mathbf{b}\cdot\nabla\dot{G}(\mathbf{r},t), \\
\mathbf{B} &= \nabla\times\mathbf{A} \approx -\mathbf{b}\times\nabla[\mathbf{b}\cdot\nabla G(\mathbf{r},t)] + O(\frac{\epsilon}{n}),
\end{aligned}$$

where '$\dot{G}$' represents the partial time derivative acting on G. For small inverse aspect ratio or large toroidal mode number n, the correction term is indeed small and can be removed from the perturbed magnetic field. We observe the perturbed electric field along the magnetic field is shorted, i.e. $\mathbf{b}\cdot\mathbf{E} = 0$.

Substituting the fields from the reduced MHD model into the action 4.4, we find

$$S = \int d^3\mathbf{r}dt \left\{ \frac{[\mathbf{b}\times\nabla\dot{G}(\mathbf{r},t)]^2}{2v_A^2} - \frac{[(\mathbf{b}\cdot\nabla)(\mathbf{b}\times\nabla G(\mathbf{r},t))]^2}{2} \right.$$
$$\left. -\mathbf{j}_p\cdot\mathbf{bb}\cdot\nabla G(\mathbf{r},t) - \rho_p\dot{G}(\mathbf{r},t)\right\}. \tag{4.5}$$

The first and second terms in 4.5 are associated with the kinetic energy of particles and the perturbed magnetic field energy and the last two terms show the interaction between the energetic particles and waves. The last two terms can be altered as follows. The integral can be written as $\rho_p\dot{G} = d(\rho_p G)/dt - \dot{\rho_p}G$. As the full time derivative term can be dropped in the integral as a total derivative does not affect the equations of motion. Further, from the charge continuity equation,

$$\dot{\rho_p} + \nabla\cdot\mathbf{j}_p = 0.$$

Thus the wave-particle interaction terms are reduced to,

$$-\mathbf{j}_p\cdot\mathbf{bb}\cdot\nabla G(\mathbf{r},t) - \rho\dot{G}(\mathbf{r},t) = -\mathbf{j}_{p\|}\mathbf{b}\cdot\nabla G(\mathbf{r},t) + \mathbf{j}_p\cdot\nabla G(\mathbf{r},t) - \nabla\cdot[G(\mathbf{r},t)\mathbf{j}_p]$$
$$= \mathbf{j}_p\cdot(\mathbf{I}-\mathbf{bb})\cdot\nabla G(\mathbf{r},t) - \nabla\cdot[G(\mathbf{r},t)\mathbf{j}_p],$$

where the divergence term can be dropped as it does not contribute to the equations of motion. Then the action turns into a functional of $G(\mathbf{r},t)$,

$$S[G(\mathbf{r},t)] = \int d^3\mathbf{r}dt \left\{ \frac{[\mathbf{b}\times\nabla\dot{G}(\mathbf{r},t)]^2}{2v_A^2} - \frac{[(\mathbf{b}\cdot\nabla)(\mathbf{b}\times\nabla G(\mathbf{r},t))]^2}{2} \right.$$
$$\left. +(\mathbf{b}\times\mathbf{j}_p)\cdot(\mathbf{b}\times\nabla G(\mathbf{r},t))\right\}$$
$$= \int d^3\mathbf{r}dt \left\{ \frac{[\nabla_\perp\dot{G}(\mathbf{r},t)]^2}{2v_A^2} - \frac{(\mathbf{b}\cdot\nabla)^2[\nabla_\perp G(\mathbf{r},t)]^2}{2} + \mathbf{j}_{p\perp}\cdot\nabla_\perp G(\mathbf{r},t)\right\}. \tag{4.6}$$

Here, the curvature and gradient drift velocity of energetic particles generate the current perpendicular to the magnetic field,

$$\begin{aligned}\mathbf{b}\times\mathbf{j}_p &= q_p n_p \int d^3\mathbf{v}(\mathbf{b}\times\mathbf{v}_B)f = q_p n_p \int \frac{d^3\mathbf{v}}{\omega_c}\mathbf{b}\times(\mathbf{b}\times\kappa)(\frac{v_\perp^2}{2}+v_\parallel^2)\cdot f(\mathbf{r},\mathbf{v},t)\\ &= -q_p n_p \int \frac{d^3\mathbf{v}}{\omega_c}\kappa(\frac{v_\perp^2}{2}+v_\parallel^2)\cdot f(\mathbf{r},\mathbf{v},t), \qquad (4.7)\end{aligned}$$

where $f(\mathbf{r},\mathbf{v},t)$ is the energetic particle distribution and κ is the field line curvature where the integral covers on the velocity space $\mathbf{v}$. As the low beta approximation is being used in 4.7 we neglected the plasma pressure and used,

$$\kappa \approx \frac{\nabla_\perp B}{B}, \quad \text{for} \quad \beta \ll 1.$$

The structure of the solution $G(\mathbf{r},t)$ can now be expressed as a Fourier series in periodic magnetic coordinates, ϕ of the toroidal coordinate and θ for the poloidal coordinate. Magnetic coordinates have the property that the magnetic field is of the form $\mathbf{B} = \nabla\phi_f \times \nabla\psi - q(r)\nabla\theta_f \times \nabla\psi$ with ϕ_f and θ_f flux coordinates [21, 75]. The increment in the radial direction dr is related to the poloidal flux ψ by $d\psi = B_\theta(r,\theta=\pi/2)Rdr = B_\phi(r,\theta=\pi/2)rdr/q(r)$. The solution is represented in terms of the Fourier transform ω,

$$G(\mathbf{r},t) = \sum_{m,n}\int_{-\infty+\imath a(>0)}^{\infty+\imath a} d\omega\ g_{mn}(r,\omega)e^{-\imath(\omega t - n\phi + m\theta)},$$

where $g_{mn}(r,\omega)$ is analytic on the upper half plane which guarantees that $G(\mathbf{r},t<0)=0$. Thus the inverse transform is given by,

$$g_{mn}(r,\omega) = \frac{1}{(2\pi)^3}\int_0^\infty dt\int_0^{2\pi} d\phi\int_0^{2\pi} d\theta\ G(\mathbf{r},t)e^{\imath(\omega t - n\phi + m\theta)},$$

as $G(\mathbf{r},t)$ is real, $g_{-m,-n}(r,-\tilde{\omega})$ is the complex conjugate of $g_{mn}(r,\omega)$, or alternatively $\tilde{g}_{mn}(r,\tilde{\omega}) = g_{-m,-n}(r,-\omega)$.

Then the action integral takes the form,

$$\begin{aligned}\delta S[g_{mn}(r,\omega)] \approx (2\pi)^3 \sum_{m,n} \int_{r_m} Rdr \int_{-\infty+\imath a(<0)}^{\infty+\imath a} d\omega [\frac{\omega^2}{v_A^2} - k_{\parallel m,n}(r)^2] \\ \cdot [\frac{\partial g_{mn}(r,\omega)}{\partial r}\frac{\partial \delta g_{-m,-n}(r,-\omega)}{\partial r} + \frac{m^2}{r^2} g_{mn}(r,\omega)\delta g_{-m,-n}(r,-\omega)] \\ + 2\pi q_p n_p v_d \sum_{m,n} \int_{r_m} Rdr \int_0^{2\pi} d\phi \int_0^{2\pi} d\theta \sin\theta \int_{-\infty+\imath a(<0)}^{\infty+\imath a} d\omega \int d^3\mathbf{v} \\ \cdot f(\mathbf{r},\mathbf{v},\omega)\frac{\partial \delta g_{-m,-n}(r,-\omega)}{\partial r} e^{\imath(-n\phi+m\theta)}, \end{aligned} \tag{4.8}$$

where $\nabla_\perp$ has been expressed explicitly in our coordinates as $\nabla_\perp = \hat{\mathbf{r}}\partial/\partial r + \frac{\hat{\theta}}{r}\partial/\partial\theta$. In the vicinity of the gap, the θ derivative product on the right-hand side is order of ϵ^2 compared to the radial derivative term in the region around the TAE gap region about r_m and will be neglected in this region. The wave vector parallel to the magnetic field is $k_{\parallel m,n}(r) = (n - m/q(r))/R$. The magnitude of the curvature term $(\mathbf{b}\times\kappa)\cdot\hat{\mathbf{r}}$ is $1/R$.

In toroidal geometry, the equilibrium quantities are functions of θ but independent of ϕ, .e.g. the magnetic field strength is $B = B_0(1-\epsilon\cos\theta)$ with $\epsilon = r/R$. This leads to off-diagonal coupling among the poloidal harmonics. Although usually the coupling is weak as we assume that $\epsilon \ll 1$, in the vicinity of a TAE resonance where $\partial g_{mn}/\partial r \gg m g_{mn}/r$, there is a degeneracy in frequency, where $k_{\parallel,m} = -k_{\parallel,m+1} = \omega_A = v_A/(2q_m R)$, where $q_m = (m+1/2)/n = q(r_m)$. This degeneracy leads to strong coupling of the m and $m+1$

harmonics in the highest radial derivative terms of the resonance. When we bring in the coupling terms, we use

$$v_A(r)^{-2} = v_{A0}^{-2}\left[1+\epsilon(e^{\imath\theta}+e^{-\imath\theta})\right].$$

Then the variation of the action keeping only neighboring poloidal mode couplings of the radial derivatives becomes,

$$\begin{aligned}
\delta S[g_{mn}(r,\omega)] \approx (2\pi)^3 \sum_{m,n}\int_{r_m} Rrdr \int_{-\infty+\imath a(<0)}^{\infty+\imath a} d\omega \Bigg\{ &[\frac{\omega^2}{v_{A0}^2} - k_{\|m,n}(r)^2] \\
&\cdot[\frac{\partial g_{mn}(r,\omega)}{\partial r}\frac{\partial \delta g_{-m,-n}(r,-\omega)}{\partial r} + \frac{m^2}{r^2} g_{mn}(r,\omega)\delta g_{-m,-n}(r,-\omega)] \\
&+\epsilon\frac{\omega^2}{v_{A0}^2}[\frac{\partial g_{m+1,n}(r,\omega)}{\partial r}\frac{\partial \delta g_{-m,-n}(r,-\omega)}{\partial r} + \frac{\partial g_{m-1,n}(r,\omega)}{\partial r}\frac{\partial \delta g_{-m,-n}(r,-\omega)}{\partial r} \\
&+\frac{\partial g_{mn}(r,\omega)}{\partial r}\frac{\partial \delta g_{-m+1,-n}(r,-\omega)}{\partial r} + \frac{\partial g_{mn}(r,\omega)}{\partial r}\frac{\partial \delta g_{-m-1,-n}(r,-\omega)}{\partial r}]\Bigg\} \\
&+ 2\pi q_p n_p v_d \sum_{m,n}\int_{r_m} Rrdr \int_0^{2\pi} d\phi \int_0^{2\pi} d\theta \sin\theta \int_{-\infty+\imath a(<0)}^{\infty+\imath a} d\omega \int d^3\mathbf{v} \\
&\cdot f(\mathbf{r},\mathbf{v},\omega)\frac{\partial \delta g_{-m,-n}(r,-\omega)}{\partial r} e^{\imath(-n\phi+m\theta)}. \qquad (4.9)
\end{aligned}$$

Finally, the action 4.9 can be simplified as we just study on the coupling between two specific resonant modes (m,n) and $(m+1,n)$ due to the toroidicity

with other harmonics dropped off from the summation.

$$\delta S[g_{mn}(r,\omega), g_{m+1,n}(r,\omega)] \approx (2\pi)^3 \int_{r_m} Rrdr \int_{-\infty+\imath a(<0)}^{\infty+\imath a} d\omega \left\{ [\frac{\omega^2}{v_{A0}^2} - k_{\|m,n}(r)^2] \right.$$
$$\cdot \frac{\partial g_{mn}(r,\omega)}{\partial r} \frac{\partial \delta g_{-m,-n}(r,-\omega)}{\partial r} + [\frac{\omega^2}{v_{A0}^2} - k_{\|m+1,n}(r)^2] \frac{\partial g_{m+1,n}(r,\omega)}{\partial r} \frac{\partial \delta g_{-m-1,-n}(r,-\omega)}{\partial r}$$
$$\left. + \epsilon \frac{\omega^2}{v_{A0}^2} [\frac{\partial g_{mn}(r,\omega)}{\partial r} \frac{\partial \delta g_{-m-1,-n}(r,-\omega)}{\partial r} + \frac{\partial g_{m+1,n}(r,\omega)}{\partial r} \frac{\partial \delta g_{-m,-n}(r,-\omega)}{\partial r}] \right\}$$
$$+ 2\pi q_p n_p v_d \int_{r_m} Rrdr \int_0^{2\pi} d\phi \int_0^{2\pi} d\theta \sin\theta \int_{-\infty+\imath a(<0)}^{\infty+\imath a} d\omega \int d^3\mathbf{v}\ f(\mathbf{r},\mathbf{v},\omega)$$
$$\cdot \left(\frac{\partial \delta g_{-m,-n}(r,-\omega)}{\partial r} e^{\imath(-n\phi+m\theta)} + \frac{\partial \delta g_{-m-1,-n}(r,-\omega)}{\partial r} e^{\imath(-n\phi+(m+1)\theta)} \right). \tag{4.10}$$

Now we can use partial integration of the action integral, in attempting to evaluate the Lagrangian integrand over the m^{th} TAE gap region, between $r_m - \Delta < r < r_m + \Delta$, where $\epsilon/4nq'_m < \Delta < 1/nq'_m$. This procedure leaves us with an expression that is proportional to the Euler-Lagrange term which vanishes, and an end-point contributions at $r_m - \Delta$ and $r_m + \Delta$ that needs to be matched to the values obtained from the outer regions of the integration, which is obtained from a similar integration by parts leaving us with end-point contributions also at the points $r_m - \Delta$ and $r_m + \Delta$. To do so we define the 'flux' functions $C_m(\omega)$ and $C_{m+1}(\omega)$,

$$\frac{\imath nq'_m}{\omega_A q_m^2} C_m(r,\omega) = [\frac{\omega^2}{v_{A0}^2} - k_{\|m,n}(r)^2] \frac{\partial g_{mn}(r,\omega)}{\partial r} + \epsilon \frac{\omega^2}{v_{A0}^2} \frac{\partial g_{m+1,n}(r,\omega)}{\partial r}, \tag{4.11}$$

$$\frac{\imath nq'_m}{\omega_A q_m^2} C_{m+1}(r,\omega) = [\frac{\omega^2}{v_{A0}^2} - k_{\|m+1,n}(r)^2] \frac{\partial g_{m+1,n}(r,\omega)}{\partial r} + \epsilon \frac{\omega^2}{v_{A0}^2} \frac{\partial g_{m,n}(r,\omega)}{\partial r}. \tag{4.12}$$

Both of these $C(r,\omega)$ functions have been shown [20, 67] to be nearly spatially constant in the gap and the spatial dependence is suppressed. The kinetic

interaction term on the right-hand side of 4.10 is considered to be small, and at first neglected to this leading order. The general solution to the remaining linear Lagrangian is then obtained, as was found in [20, 67, 71]. A three point recursion relation was developed in RBV tip model, and it is this theory that will be extended to the time domain. The variation of our action without the interaction term after a partial integration leads to the Berk-Mett quadratic form of the RBV tip model.

$$-\frac{(2\pi)^3 nRr_m q'_m}{\omega_A^2 q_m^2}\int_{-\infty+\imath a(<0)}^{\infty+\imath a} d\omega\,\{[(\Delta_m+\alpha_m(\omega))C_m(\omega)+\beta_m(\omega)C_{m+1}(\omega)]\,\delta C_{-m}(-\omega) + [\beta_m(\omega)C_m(\omega)+(\Delta_m+\alpha_m(\omega))C_{m+1}(\omega)]\,\delta C_{-m-1}(-\omega))\}\,, \tag{4.13}$$

where Δ_m is the jump of g_{mn} in the outer region, which is determined from the TAE wave equation with $\epsilon = 0$. We also use the solution of the inner boundary layer equation to determine the jump in the inner layer,

$$\int_{r_m-\Delta}^{r_m+\Delta} dr' \frac{\partial g_{-m,-n}(r',-\omega)}{\partial r'} = -\alpha_m(\delta h)C_{-m}(-\omega) - \beta_m(\delta h)C_{-m-1}(-\omega).$$

Here, the frequency-like variable δh is shifted from ω_A and normalized by the Alfvén gap width $\hat{\epsilon}\omega_A/2$.

$$\delta h(\omega) = \frac{\omega^2-\omega_A^2}{\hat{\epsilon}\omega_A^2},$$

where $\hat{\epsilon} = 5\epsilon/2$ arises from a more careful treatment of the parallel current response [12]. The coefficients α_m and β_m are determined in the RBV model,

$$\begin{aligned}\alpha_m(\delta h) &= \alpha_m(\omega) = \alpha_m(-\omega) = -\frac{\delta h}{\sqrt{1-\delta h^2}},\\ \beta_m(\delta h) &= \beta_m(\omega) = \beta_m(-\omega) = -\frac{1}{\sqrt{1-\delta h^2}}.\end{aligned} \tag{4.14}$$

In our model the evolution of the amplitude of the TAE excitation is on a slow time scale compared to the TAE frequency. For the purpose of obtaining an adiabatic theory, we also need the evolution of the TAE shifted chirping frequency to be slow compared to the particle trapping frequency at the O-point of the chirping structure. This trapping frequency will be denoted as ω_{bO}. At the outset of the simulation and linear growth response develops. The nonlinear effect begins to develop when the trapping frequency is comparable to the linear growth rate γ_L. Typically, the linear solution of the TAE mode consists of both fast and slow components, where the temporal spatial dependence is assumed to be a slow component that is determined by the instantaneous frequency. The nonlinear aspect of our excitations is taken into from the nonlinear response of the energetic particle distribution function near the instantaneous resonant frequency. The linear combination of profile structure functions obtained just from MHD theory, without the influence of the kinetic contribution from the energetic particles, serves as the test functions to substitute into the action integral. When we minimize the action 4.10 with respect to the mode amplitudes, we include the nonlinear wave-particle interaction term that enables the wave amplitudes to increase and decrease in absolute magnitude and to change in frequency. We rely on the observation that the dynamics is less sensitive to a set of test functions than it is to the instantaneous frequency. To obtain the Euler-Lagrange equations, variation is taken with respect to the wave amplitudes, which then leads to the wave amplitude evolution equations as will be shown below.

4.4 TAE excitation due to the energetic particles with finite orbits

The TAE mode is generated around a gap frequency ω_A and can continue chirping $\delta\omega(t)$ through the gap frequency. We need to assume that $\delta\omega \ll \omega_A$ in our model in order for the basic assumption that the 'flux' remains independent of position.

When $n|q-q_m| \ll 1$ and taking into account the interaction of the m^{th} and $m+1^{th}$ modes, we find the relevant radial structure of a TAE mode in the vicinity of an Alfvén resonance radius r_m is of the form [12],

$$g_{mn}(r,\omega,\delta h) = \frac{\imath\Phi_m}{\omega_A}\int_{r_m}^{r} dr' \frac{a_m + b_m(r'-r_m)}{(r'-r_m)^2 + a_m^2}, \tag{4.15}$$

where $\Phi_m = (\delta h C_m(\omega) + C_{m+1}(\omega))/\sqrt{1-\delta h^2}$ and $a_m = \sqrt{1-\delta h^2}\epsilon r_m/4nq_m s_m$, $b_m = \sqrt{1-\delta h^2}C_m(\omega)/(\delta h C_m(\omega) + C_{m+1}(\omega))$. Also,

$$g_{m+1,n}(r,\omega,\delta h) = \frac{\imath\Phi_{m+1}}{\omega_A}\int_{r_m}^{r} dr' \frac{a_{m+1} + b_{m+1}(r'-r_m)}{(r'-r_m)^2 + a_{m+1}^2},$$

where $\Phi_{m+1} = -(\delta h C_{m+1}(\omega) + C_m(\omega))/\sqrt{1-\delta h^2}$ and $a_{m+1} = \sqrt{1-\delta h^2}\epsilon r_m/4nq_m s_m$, $b_{m+1} = -\sqrt{1-\delta h^2}C_{m+1}(\omega)/(\delta h C_{m+1}(\omega) + C_m(\omega))$.

The finite orbit of energetic particles Δ_b deviates from its mean flux surface position $\bar{r}$ as follows,

$$r = \bar{r} + \Delta_b \cos\theta.$$

Thus, the radial dependence of $g_{mn}(r,\omega,\delta h)$ can now be expressed as a function of the mean particle position and a periodic poloidal angle θ. Then we can

expand $g_{mn}(r, \omega, \delta h)$ in a Fourier series.

$$g_{mn}(\bar{r} + \Delta_b \cos\theta, \omega, \delta h) = \sum_{l=0}^{\infty} g_{m,l}(\bar{r}, \omega, \delta h) \cos l\theta,$$

where the Fourier components $g_{m,l}$ has been evaluated explicitly in previously derived map model [10].

$$g_{m,l}(\bar{r}, \omega, \delta h) = -\frac{\imath \Phi_m}{\omega_A l}[\imath(z_+^l - z_-^l) + b_m(z_+^l + z_-^l)], \qquad \text{for} \quad l > 0. \tag{4.16}$$

The $l = 0$ component has no contribution to the final result and $g_{m,-l} = g_{m,l}$. z_+, z_- is a function of the flux coordinate $\bar{r}$ and is analytic on the upper half complex plane of ω.

$$\begin{aligned} z_+(\bar{r}, \delta h) &= -(x + iy) + [(x + iy)^2 - 1]^{1/2}, \\ z_-(\bar{r}, \delta h) &= -(x - iy) + [(x - iy)^2 - 1]^{1/2}, \\ \text{where}, x &\equiv (\bar{r} - r_m)/\Delta_b, \quad y \equiv a_m/\Delta_b. \end{aligned} \tag{4.17}$$

Here, the branch of the square root must be chosen so that $|z_+|, |z_-| \leq 1$ and $\Delta_b = Rqv_d/v_\parallel$.

The TAE wave becomes unstable at the eigenfrequency within gap frequency centered at ω_A due to an excitation of an energy inverted energetic particle distribution.

$$0 = \omega_A - n\dot{\phi} + (m + l)\dot{\theta} = \frac{v_A}{2Rq_m} + \frac{1}{R}(\frac{m + l}{q_m} - n)v_\parallel,$$

which gives the resonant condition for the energetic particles $v_\parallel/v_A = 1/(1 - 2l)$. Therefore, the (m, l) and $(m + 1, l - 1)$ components participate in the

resonant interaction at a specified parallel velocity in Eq. 4.10. We find,

$$
\begin{aligned}
& v_d \sin\theta \left[\frac{\partial \delta g_{-m,-n}(r,-\omega,\delta h)}{\partial r} e^{\imath(-n\phi+m\theta)} + \frac{\partial \delta g_{-m-1,-n}(r,-\omega,\delta h)}{\partial r} e^{\imath(-n\phi+(m+1)\theta)} \right] \\
& \approx \frac{v_\parallel}{2Rq_m} \imath (l \delta g_{-m,-l}(\bar{r},-\omega,\delta h) + (l-1)\delta g_{-m-1,-l+1}(\bar{r},-\omega,\delta h)) e^{\imath(-n\phi+(m+l)\theta)} \\
& = -\frac{v_\parallel}{v_A} \delta \mathbf{I}_{-m,-l}^{-m-1,-l+1}(\bar{r},-\omega,\delta h) e^{\imath(-n\phi+(m+l)\theta)} \qquad (4.18)
\end{aligned}
$$

Then we substitute the forms of $\delta g_{-m,-l}$ and $\delta g_{-m-1,-l+1}$ in Eq. 4.16 into Eq. 4.18 to yield the interaction element $\delta \mathbf{I}_{-m,-l}^{-m-1,-l+1}$ between TAE and particles,

$$
\begin{aligned}
& \delta \mathbf{I}_{-m,-l}^{-m-1,-l+1}(\bar{r},-\omega,\delta h) = \delta \mathbf{I}_{-m,l}^{-m-1,l-1}(\bar{r},-\omega,\delta h) \\
& = \left[\frac{-\imath \delta h \delta C_{-m}(-\omega) - \imath \delta C_{-m-1}(-\omega)}{\sqrt{1-\delta h^2}} - \delta C_{-m}(-\omega) \right] z_+^l(\bar{r},\delta h) \\
& \quad + \left[\frac{\imath \delta h \delta C_{-m-1}(-\omega) + \imath \delta C_{-m}(-\omega)}{\sqrt{1-\delta h^2}} - \delta C_{-m-1}(-\omega) \right] z_+^{l-1}(\bar{r},\delta h) \\
& \quad + \left[\frac{\imath \delta h \delta C_{-m}(-\omega) + \imath \delta C_{-m-1}(-\omega)}{\sqrt{1-\delta h^2}} - \delta C_{-m}(-\omega) \right] z_-^l(\bar{r},\delta h) \\
& \quad + \left[\frac{-\imath \delta h \delta C_{-m-1}(-\omega) - \imath \delta C_{-m}(-\omega)}{\sqrt{1-\delta h^2}} - \delta C_{-m-1}(-\omega) \right] z_-^{l-1}(\bar{r},\delta h), \qquad (4.19)
\end{aligned}
$$

Below we use these shorthand definitions:

$$
\begin{aligned}
& sa(\delta h) = sa(\omega) = sa(-\omega) = \sqrt{\frac{1+\delta h}{2}}, \quad \delta h \geq -1, \\
& ca(\delta h) = ca(\omega) = ca(-\omega) = \sqrt{\frac{1-\delta h}{2}}, \quad \delta h \leq 1, \\
& ea(\delta h) = ca(\delta h) + \imath sa(\delta h), \quad -1 \leq \delta h \leq 1.
\end{aligned}
$$

These functions can be extended into the complex plane by the analytic continuation using the branch cuts $(-1-\imath\infty,-1]$ and $[1,1-\imath\infty)$. After a little

algebra, Eq.4.19 is simplified to,

$$
\begin{aligned}
&\delta\mathbf{I}_{-m,-l}^{-m-1,-l+1}(\bar{r},-\omega,\delta h) = \\
&\quad -\frac{1}{2}\left[ca^{-1}(\delta h)(\delta C_{-m}(-\omega)+\delta C_{-m-1}(-\omega))+\imath s a^{-1}(\delta h)(\delta C_{-m}(-\omega)-\delta C_{-m-1}(-\omega))\right] \\
&\quad \times\left[ea^{-1}(\delta h)z_{-}^{l}(\bar{r},\delta h)+ea(\delta h)z_{-}^{l-1}(\bar{r},\delta h)\right] \\
&\quad -\frac{1}{2}\left[ca^{-1}(\delta h)(\delta C_{-m}(-\omega)+\delta C_{-m-1}(-\omega))-\imath s a^{-1}(\delta h)(\delta C_{-m}(-\omega)-\delta C_{-m-1}(-\omega))\right] \\
&\quad \times\left[ea(\delta h)z_{+}^{l}(\bar{r},\delta h)+ea^{-1}(\delta h)z_{+}^{l-1}(\bar{r},\delta h)\right], \qquad (4.20)
\end{aligned}
$$

The Lagrangian terms contain the TAE wave response resulting from the coupling between m^{th} and $m+1^{th}$ components and the wave-particle resonant interaction element, $\delta\mathbf{I}_{-m,-l}^{-m-1,-l+1}$. The variation of the action with respect to the mode amplitudes of $C_{-m}(-\omega)$ and $C_{-m-1}(-\omega)$ are taken to give,

$$
\begin{aligned}
\delta S[C_m(\omega),C_{m+1}(\omega)] &= -\frac{(2\pi)^3 nRr_m q_m'}{\omega_A^2 q_m^2}\int_{-\infty+\imath a(<0)}^{\infty+\imath a} d\omega \\
&\cdot\left\{\left[(\Delta_m+\alpha_m(\delta h))C_m(\omega)+\beta_m(\delta h)C_{m+1}(\omega)\right]\delta C_{-m}(-\omega)\right. \\
&\left.+\left[\beta_m(\delta h)C_m(\omega)+(\Delta_m+\alpha_m(\delta h))C_{m+1}(\omega)\right]\delta C_{-m-1}(-\omega)\right\} \\
&-\frac{2\pi q_p n_p Rr_m v_\parallel}{v_A}\int_{r_m} d\bar{r}\int_0^{2\pi} d\phi\int_0^{2\pi} d\theta\int_{-\infty+\imath a(<0)}^{\infty+\imath a} d\omega\int d^3\mathbf{v} \\
&\cdot f(\mathbf{r},\mathbf{v},\delta h)\delta\mathbf{I}_{-m,-l}^{-m-1,-l+1}(\bar{r},-\omega,\delta h)e^{\imath(\omega_A t+\int_0^t\delta\omega(\tau)d\tau-n\phi+(m+l)\theta)}. \qquad (4.21)
\end{aligned}
$$

Here, the distribution function is shifted from the lab frame $f(\mathbf{r},\mathbf{v},\omega)$ to the chirping wave frame $f(\mathbf{r},\mathbf{v},\delta h)$ by multiplying the wave phase $e^{\imath(\omega_A t+\int_0^t\delta\omega(\tau)d\tau)}$. The coefficients of $\delta C_{-m}(-\omega)$ and $\delta C_{-m-1}(-\omega)$ will lead to the set of Euler-Lagrange equations. The explicit form of thes equations will be shown in the next section.

In general, the distribution function of energetic particles occupies a six dimensional phase space. However, in the kinetic theory we are working with, the stripping of all the resonant interactions but one, means that there are two adiabatic invariants that remain constant during the evolution, which enables the reduction of the response of the kinetic distribution function for energetic particles to depend on just one adiabatic invariant and its conjugate angle.

4.5 Dynamics of energetic particles

As we discussed in chapter 3, the unperturbed Hamiltonian, $\mathcal{H}_0(P_\phi, P_\theta, \mu)$ is considered to be of integrable form so that unperturbed distribution function depends only the adiabatic invariants of the unperturbed motion. The three adiabatic invariants (per unit mass) $v_\perp^2/\omega_c$, which to within a constant is magnetic moment, the toroidal angular momentum, P_ϕ (which is both an action variable and an exact constant of motion in a tokamak) and the poloidal action P_θ which is implicitly related to the unperturbed energy through the relation, $dP_\theta = dE/\omega_\theta$, where $\omega_\theta(E, P_\phi, \mu)$ is the mean rate of poloidal rotation around tokamak. Then the perturbed Hamiltonian takes the form for a wave whose frequency is much less that the cyclotron frequency.

$$\begin{aligned}\mathcal{H} &= \mathcal{H}_0(P_\phi, P_\theta, \mu) \\ &+ \sum_l \left\{ \delta\mathcal{H}_l(P_\phi, P_\theta, \mu, t) \exp\left[-\imath(\omega_A t + \int_0^t \delta\omega(\tau)d\tau + (m+l)\theta - n\phi) \right] + c.c. \right\}\end{aligned} \tag{4.22}$$

The coordinates ϕ and θ are the toroidal and poloidal angle variables conjugate to the action coordinates for the unperturbed orbits. The perturbative terms $\delta\mathcal{H}_l$ is an expansion in a Fourier series as we discussed in Eq. 4.16, with a time slowly varying dependence in $\delta\mathcal{H}_l$ and a fast oscillation appearing in the phase term. As the magnetic moment, μ, remains a constant of motion this perturbed Hamiltonian does not have any dependence on the gyrating action angle. Thus μ can be treated as a constant parameter which we often suppress below.

We focus on resonant particle behavior of a single TAE resonance response, which is allowable under the assumption that the characteristic trapping frequency is small compared to the separation of different resonances. If the amplitude is low enough, so that there is no overlap of resonances in the particle's phase space, we can approximate this Hamiltonian for the resonant interactions by dropping all but the resonant terms with m^{th} and $m+1^{th}$ TAE modes. And the Hamiltonian takes the form,

$$\begin{aligned}\mathcal{H} = \mathcal{H}_0(P_\phi, P_\theta) + [\delta\mathcal{H}_{m,l}(P_\phi, P_\theta, t) + \delta\mathcal{H}_{m+1,l-1}(P_\phi, P_\theta, t)] \\ \cdot \exp\left[-\imath(\omega_A t + \int_0^t \delta\omega(\tau)d\tau + (m+l)\theta - n\phi)\right] + c.c. \end{aligned} \tag{4.23}$$

In principle at the same frequency other l-values can resonate with different groups of particles in the energetic particle phase space, but for simplicity we neglect this possibility throughout this work.

As we have discussed, we view the resonance condition as a function of energy E and because the Hamiltonian is a function of $n\phi - \omega t$ it follows that

$\omega dP_\phi/n = dE \approx m_p v_\parallel dv_\parallel$, with the latter approximation applicable because the magnetic moment is conserved.

The form of the Hamiltonian 4.23 enables the identification of another constant of motions by the following procedure. A canonical transformation, that will be shown below, is taken from the old canonical variable pair (ϕ, P_ϕ) to the new coordinates (ξ, Ω), where $\xi = -(\omega_A t + \int_0^t \delta\omega(\tau)d\tau + (m+l)\theta - n\phi)$ is the wave phase in the wave frame and the toroidal momentum of energetic particles $P_\phi = m_p(Rv_\parallel - \int_{r_m}^{r} \frac{\omega_c(r')r'dr'}{q(r')})$ is transformed into the wave frame through,

$$n\Omega = P_\phi - m_p R v_\parallel + \frac{m_p \omega_c(r_m) r_m R}{n v_\parallel q'_m}\delta\omega(t), \tag{4.24}$$

where is shown that Ω is proportional to the deviation from the resonant condition of chirping wave, $\omega_A + \delta\omega - n\dot{\phi} + (m+l)\dot{\theta}$. The type 2 generating function that leads to these transformation coordinates is:

$$\begin{aligned} F_2(\phi, \Omega, t) = &- \left(\Omega + \frac{m_p R v_\parallel}{n} - \frac{m_p \omega_c(r_m) r_m R}{n^2 v_\parallel q'_m}\delta\omega(t)\right) \\ &\times \left(\omega_A t + \int_0^t \delta\omega(\tau)d\tau + (m+l)\theta - n\phi\right). \end{aligned} \tag{4.25}$$

The new Hamiltonian system $\mathcal{K}(\xi, \Omega)$ for the instantaneous wave frame is,

$$\begin{aligned} \mathcal{K}(\xi, \Omega, t) =& \mathcal{H}(P_\phi(\Omega), P_\theta, \xi, t) + \frac{\partial F_2}{\partial t} \\ =& \mathcal{H}_0(P_\phi(\Omega), P_\theta) + 2\Re\left[(\delta\mathcal{H}_{m,l} + \delta\mathcal{H}_{m+1,l-1})e^{\imath\xi}\right] \\ &- (\omega_A + \delta\omega(t))\left(\Omega + \frac{m_p R v_\parallel}{n} - \frac{m_p \omega_c(r_m) r_m R}{n^2 v_\parallel q'_m}\delta\omega(t)\right) \\ &- \frac{m_p \omega_c(r_m) r_m R}{n^2 v_\parallel q'_m}\frac{d\delta\omega}{dt}\xi, \end{aligned} \tag{4.26}$$

where $\Re$ denotes the real component. As this Hamiltonian is independent of the action coordinate, θ, it follows that P_θ is an invariant. As it is constant, the Hamiltonian $\mathcal{K}$, can be considered only as function in a truncated two dimension space for Ω and ξ. Hence we only need to deal with a two dimensional Hamiltonian, $\mathcal{K}(\xi, \Omega, t)$ with the dependence on P_θ suppressed too.

The rotational frequency of particles deeply trapped on the resonant surface is equal to the instantaneous wave frequency in accord with the resonance condition.

$$\frac{\partial \mathcal{K}_0}{\partial \Omega} = \frac{\partial \mathcal{H}_0}{\partial \Omega} - (\omega_A + \delta\omega) \approx 0. \tag{4.27}$$

The deviation from the resonant condition is proportional to the particle excursion from the resonant surface. Near the resonance surface, the unperturbed Hamiltonian written as, $\mathcal{H}_0$, can be determined up to quadratic terms Ω,

$$\begin{aligned} \mathcal{H}_0(P_\phi(\Omega)) &= \frac{\partial \mathcal{H}_0}{\partial \Omega}\Omega + \frac{1}{2}\frac{\partial^2 \mathcal{H}_0}{\partial \Omega^2}|_{\Omega=0}\Omega^2 \\ &= (\omega_A + \delta\omega)\Omega + \frac{1}{2M_r}\Omega^2, \end{aligned} \tag{4.28}$$

where M_r is an effective mass of an resonant energetic particle in the TAE wave field, which is set to be one as a mass unit in the following discussion. This is the form of the unperturbed Hamiltonian that is substituted into the entire Hamiltonian, $\mathcal{K}$, which then yields, with constant terms excluded,

$$\mathcal{K}(\xi, \Omega, t) = \frac{\Omega^2}{2} - \frac{m_p \omega_c(r_m) r_m R}{n^2 v_\parallel q'_m}\frac{d\delta\omega}{dt}\xi + 2\Re\left[(\delta\mathcal{H}_{m,l} + \delta\mathcal{H}_{m+1,l-1})e^{\imath\xi}\right],$$

where the first quadratic term is effectively a kinetic energy term of the energetic particles in the vicinity of the resonant surface and the second one is

the term is the one that allows the calculation to remain in the wave frame. The third term generates the wave-particle interaction, where the interaction element is found in Eq. 4.20. The resulting Hamiltonian that governs the form of the Vlasov equation is,

$$\mathcal{K}(\xi,\Omega,t)=\frac{\Omega^2}{2}-2\Re\left[\frac{v_\parallel}{v_A}\mathbf{I}_{m,l}^{m+1,l-1}(\bar{r},\omega_A+\delta\omega(t),\delta\omega(t))e^{\imath\xi}\right]+\alpha(t)\xi, \quad (4.29)$$

where $\alpha(t)=-\frac{m_p\omega_c(r_m)r_mR}{n^2v_\parallel q'_m}\frac{d\delta\omega}{dt}$ is the chirping rate of the frequency shifting from ω_A. The energy of particles is not conserved because of the implicit time dependence in the Hamiltonian form of Eq. 4.29. However, the slow varying implicit time dependences of $\mathbf{I}_{m,l}^{m-1,l+1}(\bar{r},\delta\omega(t))$ and $\alpha(t)$ provide a new adiabatic invariant, which will be constructed numerically in next section.

It is convenient to choose an energetic particle distribution that is a delta function in μ and energy E,

$$f(\xi,\Omega,\mu,P_\theta,\omega)\approx f(\xi,\Omega,\delta\omega(t))\delta(\mu-\mu_\alpha)\delta(E-E_\alpha),$$

where $\delta(x)$ is the Dirac delta function. To solve for the distribution function, we treat each instant of the distribution as constant in amplitude, chirping rate, and spatial profile and solve for the 'steady state' in the wave frame, as we did in chapter 3, but now for a more complex Hamiltonian, and with two mode amplitudes to solve for.

We build the basic equations of this systematic model for TAE chirps based on the variation of the action 4.21, where the wave-particle interaction is added into the linear TAE Berk-Mett variational form as the perturbation. The linear mode structure functions g_{mn} and $g_{m+1,n}$ are used as the test

functions to extremize the action functional with respect to $C_{-m}(-\omega)$ and $C_{-m-1}(-\omega)$,

$$\begin{aligned}\delta S[C_m(\omega), C_{m+1}(\omega)] = &-\frac{(2\pi)^3 n R r_m q'_m}{\omega_A^2 q_m^2} \int_{-\infty+\imath a(<0)}^{\infty+\imath a} d\omega \\ &\cdot \{[(\Delta_m + \alpha_m(\delta h))C_m(\omega) + \beta_m(\delta h) C_{m+1}(\omega)]\, \delta C_{-m}(-\omega) \\ &+ [\beta_m(\delta h) C_m(\omega) + (\Delta_m + \alpha_m(\delta h))C_{m+1}(\omega)]\, \delta C_{-m-1}(-\omega)\} \\ &- \frac{2(2\pi)^2 q_p n_p R r_m v_\parallel \Delta}{v_A} \int_{-\infty+\imath a(<0)}^{\infty+\imath a} d\omega \int d\xi d\Omega \\ &\cdot f(\xi, \Omega, \omega - \omega_A - \delta\omega) \delta \mathbf{I}_{-m,-l}^{-m-1,-l+1}(\bar{r}, -\omega, \delta h) e^{-\imath\xi}. \end{aligned} \tag{4.30}$$

Because the arbitrary choice of the variations $\delta C_{-m}(-\omega)$ and $\delta C_{-m-1}(-\omega)$, the integrands are zero according to the fundamental lemma of calculus of variations. The Euler-Lagrangian equations for TAE waves are derived with the excitation of the energetic particles,

$$\begin{aligned}(\Delta_m + \alpha_m(\delta h))C_m(\omega) + \beta_m(\delta h) C_{m+1}(\omega) = &\frac{\eta}{\pi} \int d\Omega d\xi f(\xi, \Omega, \omega - \omega_A - \delta\omega) e^{-\imath\xi} \\ &\times \left\{ ca^{-1}(\delta h) \left[ea(\delta h)(z_+^l(\bar{r}, \delta h) + z_-^{l-1}(\bar{r}, \delta h)) + ea^{-1}(\delta h)(z_-^l(\bar{r}, \delta h) + z_+^{l-1}(\bar{r}, \delta h)) \right] \right. \\ &\left. + \imath s a^{-1}(\delta h)) \left[ea(\delta h)(-z_+^l(\bar{r}, \delta h) + z_-^{l-1}(\bar{r}, \delta h)) + ea^{-1}(\delta h)(z_-^l(\bar{r}, \delta h) - z_+^{l-1}(\bar{r}, \delta h)) \right] \right\}, \end{aligned} \tag{4.31}$$

$$\begin{aligned}(\Delta_m + \alpha_m(\delta h))C_{m+1}(\omega) + \beta_m(\delta h) C_m(\omega) = &\frac{\eta}{\pi} \int d\Omega d\xi f(\xi, \Omega, \omega - \omega_A - \delta\omega) e^{-\imath\xi} \\ &\times \left\{ ca^{-1}(\delta h) \left[ea(\delta h)(z_+^l(\bar{r}, \delta h) + z_-^{l-1}(\bar{r}, \delta h)) + ea^{-1}(\delta h)(z_-^l(\bar{r}, \delta h) + z_+^{l-1}(\bar{r}, \delta h)) \right] \right. \\ &\left. - \imath s a^{-1}(\delta h)) \left[ea(\delta h)(-z_+^l(\bar{r}, \delta h) + z_-^{l-1}(\bar{r}, \delta h)) + ea^{-1}(\delta h)(z_-^l(\bar{r}, \delta h) - z_+^{l-1}(\bar{r}, \delta h)) \right] \right\}, \end{aligned} \tag{4.32}$$

where $\eta = (\Delta/8nR^2 q'_m) q_p n_p v_\parallel v_A$ determines the linear growth rate of TAE mode due to the energetic particles. The term $\bar{r} - r_m$ in z_+ and z_- is proportional to the momentum variable Ω around the resonant surface $r = r_m$.

Because the wave-particle interaction in our chirping model is localized in the frequency domain, to the lowest order, the WKB equations are found for a wave being excited at a frequency $\omega = \omega_A + \delta\omega(t)$ in the frequency representation for the wave evolution without the interaction term.

The linear mode structures are substituted into the action as test functions in the interaction term and the variation with respect to the wave amplitudes C_m and C_{m+1} to obtain the Euler-Lagrange equations. The new decoupled pair of wave amplitude variables A_e and A_o without interactions is found to be,

$$A_e(\omega) = \frac{C_m(\omega) + C_{m+1}(\omega)}{2},$$
$$A_o(\omega) = \frac{C_m(\omega) - C_{m+1}(\omega)}{2\imath}.$$

In previous studies of TAE modes [31], $A_e(\omega)$ is referred to as the even component and $A_o(\omega)$ the odd TAE component. The driving of the odd TAE mode is usually weak for the large aspect ratio tokamak due to the cancellation of contributions from energetic particles. Then we obtain the wave equations in terms of $A_e(\omega)$ and $A_o(\omega)$ using a WKB-like approximation which leads to the conclusion that to lowest order we replace form of the frequency by the

instantaneous frequency of the wave $\delta\omega(t)$. The equations then take the form,

$$\begin{aligned}(\Delta_m ca(\delta h) - sa(\delta h))A_e(\omega_A + \delta\omega(t)) \\ =&\frac{\eta}{\pi}\int d\xi d\Omega f(\xi,\Omega,\omega-\omega_A-\delta\omega(t))e^{-\imath\xi}g_e(\Omega,\delta h), \\ (\Delta_m sa(\delta h) + ca(\delta h))A_o(\omega_A + \delta\omega(t)) \\ =&\frac{\eta}{\pi}\int d\xi d\Omega f(\xi,\Omega,\omega-\omega_A-\delta\omega(t))e^{-\imath\xi}g_o(\Omega,\delta h),\end{aligned} \quad (4.33)$$

where the interaction kernels in the integrals of the right-hand terms are,

$$\begin{aligned}g_e(\Omega,\delta h) &= ea(\delta h)(z_+^l(\bar{r},\delta h) + z_-^{l-1}(\bar{r},\delta h)) + ea^{-1}(\delta h)(z_-^l(\bar{r},\delta h) + z_+^{l-1}(\bar{r},\delta h)), \\ g_o(\Omega,\delta h) &= ea(\delta h)(-z_+^l(\bar{r},\delta h) + z_-^{l-1}(\bar{r},\delta h)) + ea^{-1}(\delta h)(z_-^l(\bar{r},\delta h) - z_+^{l-1}(\bar{r},\delta h)).\end{aligned} \quad (4.34)$$

In addition we need to add to these equations dissipation terms, in exactly the same way they were introduced in chapter 3.

We now discuss the solution of the Vlasov equation which in this studies, has been developed in absence of collisional diffusion and drag. Hence we need to solve,

$$\frac{\partial f}{\partial t} + [f,\mathcal{K}] = 0, \quad (4.35)$$

where

$$\begin{aligned}\mathcal{K} = \frac{\Omega^2}{2} + \frac{2v_\parallel}{v_A}\Re\big[\big(&ca^{-1}(\delta h)g_e(\Omega,\delta h)A_e(\delta\omega(t)) \\ &-sa^{-1}(\delta h)g_o(\Omega,\delta h)A_o(\delta\omega(t))\big)e^{\imath\xi}\big] + \alpha(t)\xi,\end{aligned} \quad (4.36)$$

where $[f,g]$ is the classical possion bracket $\frac{\partial f}{\partial\xi}\frac{\partial g}{\partial\Omega} - \frac{\partial f}{\partial\Omega}\frac{\partial g}{\partial\xi}$. Using the adiabatic approximation, the solution of distribution is derived in a manner similar to

what was developed in chapter 3,

$$\delta f(\xi, \Omega, \delta\omega(t)) = \delta f(J(t)) = f(J(t)) - F(\omega_A + \delta\omega(t))$$

In our adiabatic approximation treatment, the perturbation of energetic particles are only followed in the phase space region that is within the separatrix hence we are only interested in the distribution function in the vicinity of resonance frequency.

4.6 Linear analysis

The linear analysis of the above described model of TAE wave and energetic particle interactions will give the relation between the linear growth rate γ_L and the physical parameters. First, the linearize Vlasov equation is obtained by using the Hamiltonian $\mathcal{K}$ without the chirping term,

$$\frac{\partial \delta f}{\partial \tau} + [\delta f, \mathcal{K} - \mathcal{K}_{res}] = -[F, \mathcal{K}_{res}],$$

where F is the inverted equilibrium distribution, which provides the free energy to excite the TAE waves. The inverted equilibrium distribution, is taken to have a constant slope in the region of the energetic particle interaction and is normalized so that $\partial F/\partial\Omega$ =1 in the following discussion. We observe that if $\Delta_m \geq 0$, which is case for the normal $q(r)$ profile that increases with radius, the even mode $A_e(\omega)$ is linearly excited by the energetic particles but the odd mode $A_o(\omega)$ always stays stable. The linear TAE frequency and the growth

rate are calculated from the dispersion relation.

$$\omega_0 = \frac{\Delta_m^2 - 1}{\Delta_m^2 + 1}$$
$$\gamma_L = \frac{4\pi\eta\Delta_m v_\parallel}{(\Delta_m^2 + 1)v_A} \int d\Omega \; g_e^2(\Omega, \delta h = \omega_0).$$

However, a negative magnetic shear leads to a Δ_m that becomes negative and then the odd mode $A_o(\omega)$ is linearly excited in the gap and the even mode A_e is stable. We confine our studies to the normal shear case so that only the even TAE mode is excited during the linear stage of evolution.

4.7 Numerical algorithm on the adiabatic model

TAE waves and their interactions with the energetic particles are difficult to handle in the time domain because in the equation of evolution a history of both the wave amplitude and in values of the energetic particle distribution in its phase space is needed. This leads to the need of keeping the time history of the time dependence of the distribution in its phase space evolution as well as the mode amplitude evolution. As the time kernels are Bessel-like functions, which decays as slowly as $1/\sqrt{t}$ asymptotically, a long time history is needed. Further, though the relevant kernel could be expressed analytically in our model analysis in chapter 2, the kernel needed for the propagation of the distribution function needs to be calculated numerically. Hence, a direct computation of the equations we have derived, is computationally intensive with regard to the time to complete a calculation, with the added concern that the calculation would be memory intensive. All of which leads to a very

large computational cost.

The adiabatic model we developed solves the time evolution problem if the evolution is slow enough to satisfy the adiabatic condition which is a WKB-like approximation. The TAE wave equations are localized in the frequency domain where the mode spectrum is localized to the instantaneous chirping frequency. Physically, the energetic particles are trapped in the wave field and to cause a libration of the phase space where particles and holes are trapped by wave fields. It is often the case that the particle's bounce time in the wave field is much shorter than other time scales in the system and the chirping rate hardly varies in one bounce period. This allows us to view each point of the evolution as having a quasi-steady mode amplitude and chirping rate.

As we discussed previously in the absence of collision, the approximation that the particles' adiabatic invariant is constant, which implies that the distribution function is a function only of J as long as J is less than the separatrix value. The distribution only changes due to the changing value of J at the separatrix. At the separatrix $f(J_{sep})$ takes on the value of the ambient distribution function in a field where the separatrix value is rising in time. If J_{sep} is decreasing in time, only the distribution within the new separatrix is accounted for, and the trapping region rapidly moves away from its 'excrement' which very rapidly homogenizes.

The action variable J is usually constructed from the Hamiltonian where $J = 1/(2\pi) \oint \Omega d\xi$ as we did in chapter 3. However, the interaction term we study now is not only a function of angle but also a function of canonical

momentum, an effect which is especially pronounced when the separatrices are in the vicinity of the tip points of the continuum. Hence, the Hamiltonian is non-separable in its coordinates, as we cannot explicitly express the canonical momentum as function of ξ and an instantaneous energy E. To help solve this problem, a numerical method was developed to calculate the action J using a series of ordinary differential equations. Quantities are normalized by the bounce frequency ω_{bO} at the O-point (there is no uniform bounce frequency in the trapped structure due to the momentum dependent interaction term).

$$\mathcal{K} \to \omega_{bO}^2 k, \quad E \to \omega_{bO}^2 e, \quad J \to \omega_{bO} j, \quad \Omega \to \omega_{bO}\Omega, \quad \alpha \to \alpha/\omega_{bO}^2,$$
$$t \to t/\omega_{bO}, \quad (M_e, M_o) \to \omega_{bO}(m_e, m_o), \quad (A_e, A_0) \to \omega_{bO}^2(a_e, a_o).$$

A significant observation is the emergence of a discontinuity of $\partial k/\partial\Omega$ when $z_+ = 1$ or $z_- = 1$, where the bifurcation of the O-point takes place and generates the new internal X- and O-point pair. The bifurcation usually is localized in a very small phase space area which is difficult to resolve accurately. We found the bifurcation of the O point vanishes when an artificial dissipation is added into the imaginary component of wave frequency $\Im(\omega)$, which is required to be greater than $0.165\omega_{bO}^{5/2}$ in our numerical study. For instance, in the case of $\gamma_L = 0.1$ with a saturation level $\omega_{bO} \approx \gamma_L/2 = 0.05$, if we take an artificial imaginary component of frequency greater than 9.2×10^{-5}, this is enough to eliminate the bifurcation. Further, as the bifurcated region remains small, any alteration of the dynamics we have followed is expected to be negligible.

With the canonical transformation from the conventional phase space to the action-angle variables, the interaction integrals in the TAE wave equations become,

$$\int d\xi d\Omega \delta f(\xi,\Omega,\delta\omega(t)) e^{-\imath\xi} \begin{pmatrix} g_e(\Omega,\delta h) \\ g_o(\Omega,\delta h) \end{pmatrix} = \int dJ \delta f(J) \int dt \frac{dE}{dJ} e^{-\imath\xi} \begin{pmatrix} g_e \\ g_o \end{pmatrix}$$
$$= \int dJ \delta f(J) \frac{d}{dJ} \begin{pmatrix} M_e(J) \\ M_o(J) \end{pmatrix} \quad (4.37)$$

where $M_e(J) = \int dE \oint dt e^{-\imath\xi} g_e(\Omega,\delta h)$ and $M_o(J) = \int dE \oint dt e^{-\imath\xi} g_o(\Omega,\delta h)$.

Geometrically, the actions $J(E)$ are areas of phase space, which in the adiabatic limit are the trajectories of a set trapped particles at various energies enclosing an O-point with the higher energy trajectories enclosing the lower energy ones. We introduce a new polar coordinates (ρ,ψ) inside the trapped region, where the origin is the O-point (ξ_O,Ω_O) of the trapped structure and then the function $\rho(\psi)$ depicts one of trajectories of trapped particles. We then calculate many trajectory curves $\rho(\psi)$ to construct the action-angle variable inside the trapped structure,

$$\xi = \rho\cos\psi + \xi_O,$$
$$\Omega = \rho\sin\psi + \Omega_O.$$

As the angle ψ might not be monotonic when the particles move along the trajectories following the Hamiltonian equations. We use an arclength $ds = \sqrt{d\xi^2 + d\Omega^2} = dt\sqrt{k_\xi^2 + k_\Omega^2}$ as a new dependent variable, where the subscript under the normalized Hamiltonian k means that we take the first derivative with respect to the corresponding variable. The equations for the trajectory

of a trapped particle are then given by (ρ, ψ) coordinates,

$$\sqrt{k_\xi^2 + k_\Omega^2}\frac{d\rho}{ds} = \cos\theta k_\Omega - \sin\psi k_\xi,$$
$$\sqrt{k_\xi^2 + k_\Omega^2} r\frac{d\psi}{ds} = -\sin\theta k_\Omega - \cos\psi k_\xi.$$

An ordinary differential equation for the area $\mathcal{A}$ enclosed by the trajectory is constructed from the polar coordinates,

$$\frac{d\mathcal{A}}{ds} = \frac{1}{2}\rho^2\frac{d\psi}{ds}.$$

Then the normalized action j is then the area when the angle reaches 2π, i.e. $j = |\mathcal{A}(\psi = 2\pi)|/(2\pi)$.

Other important constructions as the functions are of m_e and m_o, which are calculated indirectly through the equalities $m_e = \int_{e_O}^{e} de' u_e(e', \psi = 2\pi)$ and $m_o = \int_{e_O}^{e} de' u_o(e', \psi = 2\pi)$. We found that u_e, u_o can be evaluated from the following differential equations,

$$\sqrt{k_\xi^2 + k_\Omega^2}\frac{du_e}{ds} = g_e(\delta h)e^{-\imath\xi}$$
$$\sqrt{k_\xi^2 + k_\Omega^2}\frac{du_o}{ds} = g_o(\delta h)e^{-\imath\xi}.$$

As in the previous adiabatic model described in section 4.5, the chirping rate α can be expressed explicitly in the wave equations. Similarly, an identity integrating over a closed loop in phase space is found to be given by,

$$0 = \oint d\xi\frac{d\Omega}{d\xi} = -\oint \frac{d\xi}{k_\Omega}k_\xi = -\oint \frac{d\xi}{k_\Omega}\left\{\frac{2v_\parallel}{v_A}\Re[\imath e^{\imath\xi}(\frac{a_e g_e}{ca} - \frac{a_o g_o}{sa})] + \alpha\right\}.$$

and then α is obtained,

$$\alpha = -\frac{2v_\parallel}{v_A}\Im[ca^{-1}a_e\frac{dm_e}{dj} - sa^{-1}a_o\frac{dm_o}{dj}].$$

In contrast to our previous models, there are two independent wave amplitudes a_e and a_o evolving in the present system of equations. Therefore, four unknowns ω_{bO}, α and a_e (a complex wave amplitude) need to be solved in following adiabatic wave equations rather than two amplitudes.

$$\begin{aligned}
a_o &= \frac{ca^{-1}a_e g_e - \frac{v_A}{2v_\parallel}}{sa^{-1}g_o}, \\
\Re\left[(\Delta_m ca(\delta h) - sa(\delta h))\, a_e\right]\omega_{bO} &= \frac{\eta}{\pi}\int_0^{jx} dj\delta f(\omega_{bO}j)\frac{d}{dj}\Re[m_e(j)], \\
\Im\left[(\Delta_m ca(\delta h) - sa(\delta h))\, a_e\right]\omega_{bO} &= \frac{\eta}{\pi}\int_0^{jx} dj\delta f(\omega_{bO}j)\frac{d}{dj}\Im[m_e(j)], \\
\Re\left[(\Delta_m sa(\delta h) + ca(\delta h))\, a_o\right]\omega_{bO} &= \frac{\eta}{\pi}\int_0^{jx} dj\delta f(\omega_{bO}j)\frac{d}{dj}\Re[m_o(j)], \\
\Im\left[(\Delta_m - \frac{sa(\delta h)}{ca(\delta h)})a_e^2 - (\Delta_m + \frac{ca(\delta h)}{sa(\delta h)})a_o^2\right]\omega_{bO} &= -\frac{\alpha\eta v_A}{2\pi v_\parallel}\int_0^{jx} dj\delta f(\omega_{bO}j),
\end{aligned} \tag{4.38}$$

where $\delta f(\omega_{bO}j)$ is the perturbed distribution function inside the trapped structure, which is updated by j value of separatrix as we mentioned before.

4.8 Results and discussion

We have developed a Fortran code to calculate the nonlinear algebraic equations 4.38 as we increment the chirping frequency. We observe two modes born from the linear excitation $\omega_0 = \omega$ as shown in Fig. 4.8. Previously, where we had a fixed mode structure, the odd TAE is not induced during the

nonlinear evolution due to a cancellation of the interaction integral for the odd mode. When we take the self-consistent mode structure into account in our new model, the odd TAE also is nonlinearly excited and interplays with the even TAE during the chirp into the Alfvén continuum. However, in the vicinity of the continuum the amplitude of the even TAE is again more dominant than the odd one. It is observed that the odd TAE almost vanishes near the lower Alfvén tip and the resonance jump $z_+ = 1$ (indeed it would exactly vanish if we had not added the artificial dissipation).

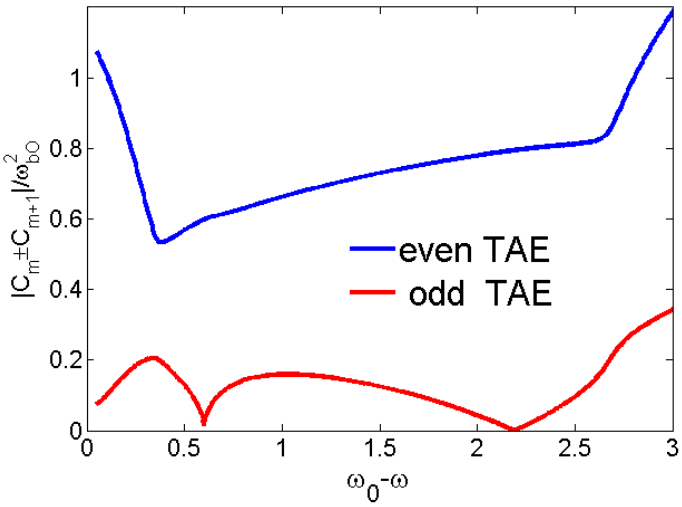

Figure 4.2: Both even and odd TAE modes are excited in the Alfvén gap in forming the clump and hole structures in phase space. The downward chirp is sometimes able to chirp to the deep continuum. The parameters are chosen as $\gamma_L = 0.1, \gamma_d = 0.08$ for the even mode, $\omega_0 = -0.4$ in the Alfvén gap and $\Delta_b/\Delta_{Gp} = 3$.

The dynamics of holes are similar to what was shown in our simple adiabatic model, where the hole cannot penetrate the upper Alfvén tip. The

hole only chirps in the gap and the spatial variation of mode structure changes only slightly from our predictions in chapter 3. Here, our work will focus on the dynamics of clump, which chirp towards to lower tip and sometimes penetrates the lower tip to propagate into a significant part of the continuum and then apparently the chirp stops (in contrast to previous model) which also happens to be where the adiabatic approximation fails. Hence, what happens around these points needs to be determined by a dynamic code that has not as yet been developed.

We have scanned various values of the ratio of the particle orbit width to TAE gap width Δ_b/Δ_{Gp} in Fig. 4.3. It is seen that downward chirps terminate within the gap when $\Delta_b/\Delta_{Gp} < 1$. When $\Delta_b/\Delta_{Gp} > 1$, the downward chirps can penetrate below the lower tip into the Alfvén continuum with increasing amplitude until the chirping frequency reaches a critical frequency $\omega_{cr} = (\Delta_b^2 + \Delta_{Gp}^2)/(2\Delta_b\Delta_{Gp})$. We can show that the equation around the continuum for the orbits with large widths is almost the same as the one in our generic model of chapter 3. However, deeper into the continuum, the frequency chirp is suddenly significantly suppressed just where the chirp reaches a critical frequency. At the critical frequency, the orbits of the trapped particles have a sudden transition from a double to a single crossing in the continuum.

A check of the adiabaticity criterion using Eq. 4.1 is made during the entire evolution of chirps. Figure 4.8 shows the adiabatic parameter is always below 0.1 when the TAE structure chirps in the gap. When the ratio Δ_b/Δ_{Gp} is large, the clump penetrates the lower tip where the adiabatic parameter

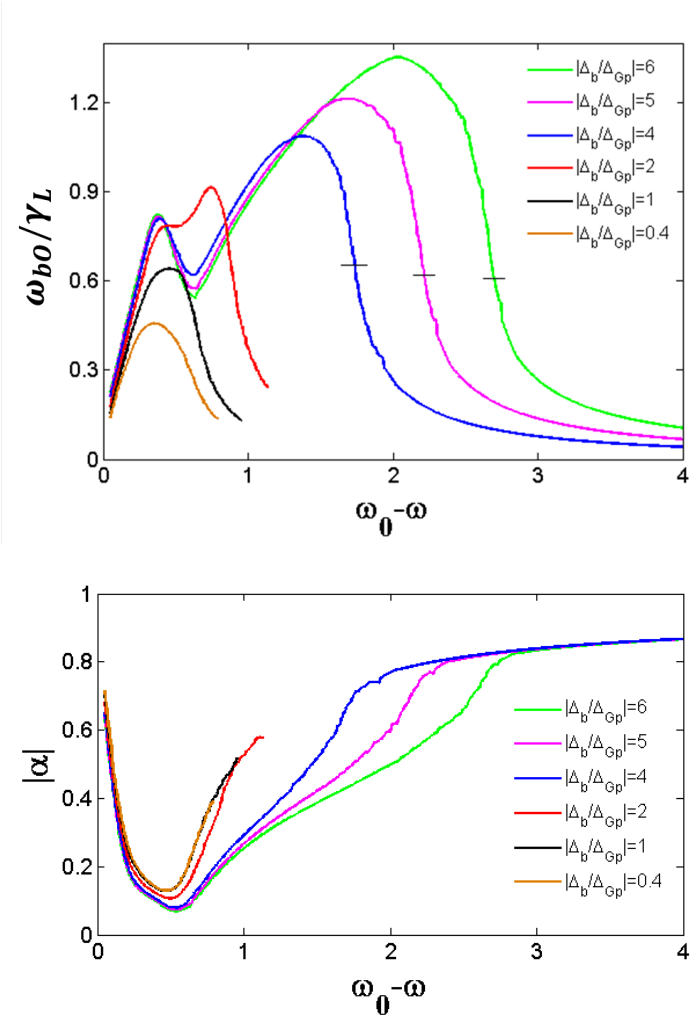

Figure 4.3: Induced trapping frequency at O-point ω_{bO} and chirping rate α of TAE modes for various ratios of orbit width to spatial width of gap Δ_b/Δ_{Gp}. Tic marks in the top figure denote where the motion of trapped particle has a transition from two to a single crossing of the continuum.

still remains small. However, near the critical frequencies, the transition from two orbit crossing to one sudden increases on the adiabatic parameters occur. Thus, the validity of the evolution is verified until just before the particle orbit goes from two continuum crossing to a single crossing. Then, due to the relatively large adiabatic parameters, our model based on the adiabatic approximation is highly suspect. To resolve whether chirping continues a kinetic simulation is needed. This is calculation that is considerably more complicated and time consuming than the kinetic simulation presented in chapter 2 and is a possible post-thesis project.

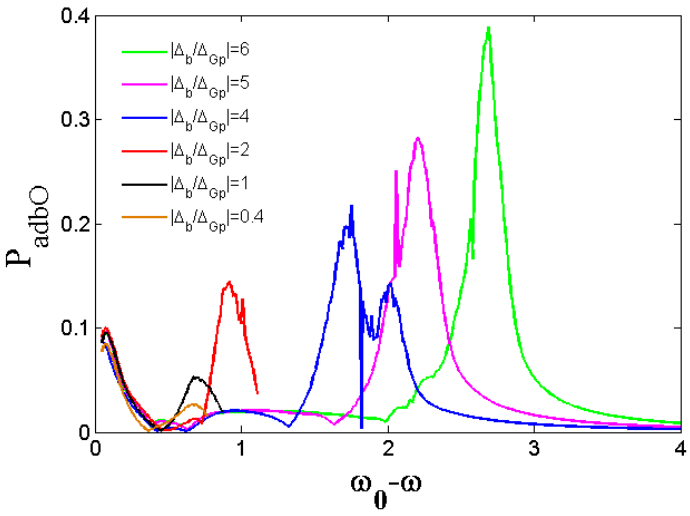

Figure 4.4: The adiabatic criteria for the trapped structure with the various values of Δ_b/Δ_{Gp}.

4.9 Summary

The tip model for the TAE mode in the large aspect ratio limit, conceived by Rosenbluth et. al. [67] in the frequency domain, together with an interaction term in the frequency domain based on a map model [9], has been extended into the time domain. We have presented the formal basis for the model starting with a MHD Lagrangian with coupling between m^{th} and $m+1^{th}$ poloidal components and adding the particle-wave interaction as a perturbation. Two independent mode structure functions with a spatial variation are derived analytically and substituted into the action. Taking a variation with respect to the wave amplitudes, we can construct the TAE wave equations in the frequency domain, where the interaction terms arise naturally from the variational principle and which is a convenient representation for the adiabatic response.

In this chapter we have presented self-consistent solutions in the adiabatic limit in a manner similar, by extending the adiabatic method discussed in chapter 3 where a simplified generic Hamiltonian was used. A numerical code has been developed to construct the adiabatic action from the non-separable Hamiltonian of resonant particles, update the distribution on the separatrix of trapped structure and solve the nonlinear algebraic equations with four unknowns.

The results show the particle excursion from the resonant surface plays an important role in the frequency chirps. The chirping range is determined by the drift orbit width of the energetic particles. However, in experiment

other mechanisms may suppress downward chirps, such as the diffusion or penetration into a low frequency GAM gap in experiments. More information from experiments is needed, such as the position of continuum, drift orbit width and diffusion. Further, there is the realization that our model of large aspect ratio may be of limited applicability in experiments, especially for the small aspect ratio spherical tokamak experiments, where chirping phenomena have been particularly prolific.

Chapter 5

Conclusion and Discussion

Weak instabilities in the presence of damping from the background plasma, often give rise to spontaneous chirps associated with the formation of trapped clump and/or hole structures in phase space[4, 27, 54, 67]. This phenomenon, which has often been described for the electrostatic bump-on-tail model, extends to more general kinetically driven instabilities, where the linearized wave is essentially arbitrary, as long as the particle/wave resonances have non-zero 'winding numbers'. In this thesis, we show how to generalize to a more realistic model that incorporates a frequency gap and continuum damping, where the TAE modes are found to sweep spontaneously through the Alfvén gap with a rapid frequency chirping rate. Frequency chirps are associated with the momentum and energy transfer between the waves and resonant particles, which allow the energetic particles to diffuse efficiently along lines in phase space of (P_ϕ, E).

In chapter 2 we formulated a simulation model for TAE waves that are excited by energetic particles in the Alfvén gap, chirp towards the Alfvén continuum, reach the gap-continuum boundary and chirp into the continuum. Previous theoretical descriptions of chirping TAE modes were limited to fre-

quency shifts small compared to the TAE gap frequency interval. In our simulation, the wave-particle interaction is taken into account in time domain and is incorporated consistently into the time evolution of the TAE mode in a large aspect ratio circular tokamak limit, which produces frequency shifts comparable to and even larger than the gap frequency interval. On achieving high accuracy and reliability, we designed a calculated wave frame where the dynamics of hole/clump in phase space and the responses from the chirping TAE wave are numerically solved. The results exhibit that a long range frequency chirp sweeps downward through the Alfvén gap and even accelerates its chirping rate when the chirping wave penetrates the lower tip, but the chirping frequency range for the upward chirping TAE is found to be constrained in the gap with the disintegration of the hole structure in the vicinity of the upper tip.

In chapter 3 we provided an adiabatic description of the simulation model developed in chapter 2, where the trapped particle is assumed to evolve in a slowly varying wave field allowing their actions to remain invariant during the chirp. The adiabatic theory quantitatively replicates the simulation for the down-chirping dynamics which even exhibits an explosive response in the continuum. For the up-chirping signal, it reproduces the simulation until its frequency approaches the upper continuum. Two extrinsic dissipation models are employed to show that the hole smoothly vanishes as it goes into the upper continuum. However, the hole in the simulations suddenly disintegrates before reaching the upper continuum for one case and smoothly decays for the other.

The discrepancy is apparently explained from the calculation of an adiabatic validity parameter that implies that hole disintegration has taken place when the adiabatic condition breakdowns as the upper continuum is approached. Compared with the simulation, the adiabatic model captures the essential physics of the frequency chirps and removes the unnecessary noise from the particles. Based on this adiabatic approximation, the analytic results are derived near the lower and upper tips and the numerical code is very efficient in the entire frequency domain.

Chapter 4 is a further improvement on TAE modeling, where the spatial profile variation of mode structure as predicted by a reduced MHD theory in the large aspect ratio limit and finite orbit excursion from the resonant flux surfaces are taken into account . As in the previous model, the up-chirping hole does not penetrate into the continuum. However, a finite drift orbit width is found to suppress the explosive wave response in the lower continuum. When the trapped particles intersect from two resonant points to one, the mode amplitudes rapidly fall off which effectively ends the chirping range in the adiabatic theory, though the justification for the adiabatic theoretical description in this region breaks down. Future work needs to develop the temporal responses of the energetic particles and TAE modes in a simulation, such as has been done in the simplified model in chapter 2. The temporal kernels for TAE modes can be calculated analytically from the Berk-Mett variational from. However, the temporal kernel for the wave-particle interaction appears too complicated to obtain an analytic form for the kernel. Instead, when

we are interested on the neighboring frequency regions where the adiabatic approximation is shown not to be satisfied, it may be possible to use an approximate interaction kernel which would have a compatible analytical form in the vicinity of the breakdown. Then as an initial condition, an adiabatic solution before entering the breakdown region is used to start the simulation and if a structure survives the non-adiabatic region, the adiabatic approximation can be reinstated for the subsequent evolution.

Our study may have application to the observations of strong sweeping events in MAST [35]. It is possible that the results of this simulation, which indicate that downward chirp originating in the gap is capable of sweeping through a large frequency range while upward frequency chirp has a limited range of sweeping, captures a property that is common in experimental data. Here, and in the experiment, there is preferential frequency sweeping into the lower continuum where then there is further enhancement of the chirping signal as it moves through the continuum. Perhaps this pattern captures an essential physics feature that is responsible for the experimental data. However, the basic physics of our modeling of the energetic particles and wave interaction must still be improved before the mechanism of the wave penetration into the continuum can be considered numerical duplicated. In addition our model is for a large aspect ratio tokamak, while MAST is a small aspect ratio tokamak. Nonetheless, the mechanisms we are uncovering may well be independent of the aspect ratio.

Our present studies have neglected the particle collisions. They lead to

diffusion and drag terms on the right hand of Vlasov equation and these terms can readily be implemented in our simulation code. The collisions have an important role when the collision rate is large enough during the evolution of frequency chirps that the particles near the separatrix can diffuse in and out of the hole/clump structure and thus the difference in distribution across the separatrix becomes less. Thus the adiabatic invariant J is not conserved but decays into smaller enclosed areas occupied by trapped trajectories. However, our adiabatic theory can readily be altered to include a bounce average diffusion equation as a function of the action allowing the distribution to change within the separatrix [24, 58].

An additional interesting enhancement is to include the couplings among the contributions from the various nearby tips. Our model approximates a single Alfvén gap, which excludes the possibility that the chirping TAE propagates across the multiple gaps and for the TAE modes to be excited in the neighboring gaps, as is usually the case in linear theory. The technique we developed in chapters 2 and 4 are easy to extend to the multiple gap case when considering the contributions from more m components of wave excitation. Additionally, it may be possible to generate the mode structure functions from a linear ideal MHD code [78] in a realistic geometry, which can then serve as test functions in our action 4.21 integral.

Bibliography

[1] Paul Murray Bellan. *Fundamentals Of Plasma Physics*. Cambridge University Press, 2006.

[2] C.M. Bender and S.A. Orszag. *Advanced Mathematical Methods for Scientists and Engineers I: Asymptotic Methods and Perturbation Theory*. Advanced Mathematical Methods for Scientists and Engineers. McGraw-Hill, 1999.

[3] H. L. Berk. Overview of nonlinear kinetic instabilities. In S. Benkadda, N. Dubuit, and Z. Guimara˜es-Filho, editors, *American Institute of Physics Conference Series*, volume 1478 of *American Institute of Physics Conference Series*, pages 29–49, September 2012.

[4] H. L. Berk, B. N. Breizman, J. Candy, M. Pekker, and N. V. Petviashvili. Spontaneous hole-clump pair creation. *Physics of Plasmas*, 6:3102–3113, August 1999.

[5] H. L. Berk, B. N. Breizman, and M. Pekker. Numerical simulation of bump-on-tail instability with source and sink. *Physics of Plasmas*, 2:3007–3016, August 1995.

[6] H. L. Berk, B. N. Breizman, and M. Pekker. Nonlinear Dynamics of a

Driven Mode near Marginal Stability. *Physical Review Letters*, 76:1256–1259, February 1996.

[7] H. L. Berk, B. N. Breizman, and M. S. Pekker. Simulation of Alfven-wave-resonant-particle interaction. *Nuclear Fusion*, 35:1713–1720, December 1995.

[8] H. L. Berk, B. N. Breizman, and N. V. Petviashvili. Spontaneous hole-clump pair creation in weakly unstable plasmas [Erratum on Physics Letters A 238 (1998) 408]. *Physics Letters A*, 234:213–218, February 1997.

[9] H. L. Berk, B. N. Breizman, and H. Ye. Finite orbit energetic particle linear response to toroidal Alfven eigenmodes. *Physics Letters A*, 162:475–481, March 1992.

[10] H. L. Berk, B. N. Breizman, and H. Ye. Map model for nonlinear alpha particle interaction with toroidal Alfvén waves. *Physics of Fluids B*, 5:1506–1515, May 1993.

[11] H. L. Berk, R. R. Mett, and D. M. Lindberg. Arbitrary mode number boundary-layer theory for nonideal toroidal Alfvén modes. *Physics of Fluids B*, 5:3969–3996, November 1993.

[12] H. L. Berk, J. W. Van Dam, Z. Guo, and D. M. Lindberg. Continuum damping of low-n toroidicity-induced shear Alfvén eigenmodes. *Physics of Fluids B*, 4:1806–1835, July 1992.

[13] I. B. Bernstein, J. M. Greene, and M. D. Kruskal. Exact Nonlinear Plasma Oscillations. *Physical Review*, 108:546–550, November 1957.

[14] B. N. Breizman. Nonlinear travelling waves in energetic particle phase space. *Nuclear Fusion*, 50(8):084014, August 2010.

[15] B. N. Breizman, J. Candy, F. Porcelli, and H. L. Berk. On the theory of internal kink oscillations. *Physics of Plasmas*, 5:2326–2333, June 1998.

[16] B. N. Breizman and S. E. Sharapov. Energetic particle drive for toroidicity-induced Alfven eigenmodes and kinetic toroidicity-induced Alfven eigenmodes in a low-shear Tokamak. Technical report, October 1994.

[17] B. N. Breizman and S. E. Sharapov. Major minority: energetic particles in fusion plasmas. *Plasma Physics and Controlled Fusion*, 53(5):054001, May 2011.

[18] J. Candy, H. L. Berk, B. N. Breizman, and F. Porcelli. Nonlinear modeling of kinetic plasma instabilities. *Physics of Plasmas*, 6:1822–1829, May 1999.

[19] L. Chen, R. B. White, and M. N. Rosenbluth. Excitation of Internal Kink Modes by Trapped Energetic Beam Ions. *Physical Review Letters*, 52:1122–1125, March 1984.

[20] C. Z. Cheng and M. S. Chance. Low-n shear Alfvén spectra in axisymmetric toroidal plasmas. *Physics of Fluids*, 29:3695–3701, November 1986.

[21] W.D. D'haeseleer. *Flux coordinates and magnetic field structure: a guide to a fundamental tool of plasma structure*. Springer series in computational physics. Springer-Verlag, 1991.

[22] I. Y. Dodin and N. J. Fisch. Adiabatic nonlinear waves with trapped particles. I. General formalism. *Physics of Plasmas*, 19(1):012102, January 2012.

[23] C. Eckart. Variation Principles of Hydrodynamics. *Physics of Fluids*, 3:421–427, May 1960.

[24] D. Eremin. *Self-consistent dynamics of nonlinear phase space structures*. PhD thesis, The University of Texas at Austin, 2004.

[25] S. Ferraz-Mello, editor. *Canonical Perturbation Theories - Degenerate Systems and Resonance*, volume 345 of *Astrophysics and Space Science Library*, January 2007.

[26] N. J. Fisch. Elementary processes underlying alpha channeling in tokamaks. In S. Benkadda, N. Dubuit, and Z. Guimara˜es-Filho, editors, *American Institute of Physics Conference Series*, volume 1478 of *American Institute of Physics Conference Series*, pages 80–90, September 2012.

[27] E. D. Fredrickson, R. E. Bell, D. S. Darrow, G. Y. Fu, N. N. Gorelenkov, B. P. Leblanc, S. S. Medley, J. E. Menard, H. Park, A. L. Roquemore, W. W. Heidbrink, S. A. Sabbagh, D. Stutman, K. Tritz, N. A. Crocker, S. Kubota, W. Peebles, K. C. Lee, and F. M. Levinton. Collective fast

ion instability-induced losses in National Spherical Tokamak Experiment. *Physics of Plasmas*, 13(5):056109, May 2006.

[28] E. D. Fredrickson, N. A. Crocker, R. E. Bell, D. S. Darrow, N. N. Gorelenkov, G. J. Kramer, S. Kubota, F. M. Levinton, D. Liu, S. S. Medley, M. Podestá, K. Tritz, R. B. White, and H. Yuh. Modeling fast-ion transport during toroidal Alfvén eigenmode avalanches in National Spherical Torus Experiment. *Physics of Plasmas*, 16(12):122505, December 2009.

[29] B. D. Fried, C. S. Liu, R. W. Means, and R. Z. Sagdeev. Nonlinear evolution and saturation of an unstable electrostatic wave. Technical Report AD0730123, , 1971.

[30] G. Y. Fu and C. Z. Cheng. Excitation of high-n toroidicity-induced shear Alfvén eigenmodes by energetic particles and fusion alpha particles in tokamaks. *Physics of Fluids B*, 4:3722–3734, November 1992.

[31] G. Y. Fu, R. Nazikian, R. Budny, and Z. Chang. Alpha particle-driven toroidal Alfvén eigenmodes in Tokamak Fusion Test Reactor deuterium-tritium plasmas: Theory and experiments. *Physics of Plasmas*, 5:4284–4291, December 1998.

[32] G. Y. Fu, W. Park, H. R. Strauss, J. Breslau, J. Chen, S. Jardin, and L. E. Sugiyama. Global hybrid simulations of energetic particle effects on the n=1 mode in tokamaks: Internal kink and fishbone instability. *Physics of Plasmas*, 13(5):052517, May 2006.

[33] G. Y. Fu and J. W. Van Dam. Excitation of the toroidicity-induced shear Alfvén eigenmode by fusion alpha particles in an ignited tokamak. *Physics of Fluids B*, 1:1949–1952, October 1989.

[34] D. Gottlieb and C.-W. Shu. On the Gibbs Phenomenon and Its Resolution. *SIAM Review*, 39:644–668, January 1997.

[35] M. P. Gryaznevich and S. E. Sharapov. Perturbative and non-perturbative modes in START and MAST. *Nuclear Fusion*, 46:942, October 2006.

[36] M.E. Gurtin. Variational principles for linear initial-value problems. *Quart. Appl. Math*, 22(3):252–256, 1964.

[37] A. Hasegawa and L. Chen. Plasma Heating by Alfvén-Wave Phase Mixing. *Physical Review Letters*, 32:454–456, March 1974.

[38] R.D. Hazeltine and J.D. Meiss. *Plasma Confinement*. Dover Books on Physics Series. Dover, 2003.

[39] R.D. Hazeltine and F.L. Waelbroeck. *The Framework Of Plasma Physics*. Frontiers in Physics. Westview Press, Advanced Book Program, 2004.

[40] W. W. Heidbrink. Basic physics of Alfvén instabilities driven by energetic particles in toroidally confined plasmas. *Physics of Plasmas*, 15(5):055501, May 2008.

[41] W. W. Heidbrink and G. J. Sadler. REVIEW PAPER: The behaviour of fast ions in tokamak experiments. *Nuclear Fusion*, 34:535–615, April 1994.

[42] JW Herivel. The derivation of the equations of motion of an ideal fluid by hamiltons principle. *Math. Proc. Cambridge Philos. Soc*, 51:344–349, 1955.

[43] K. Ikeda. PREFACE: Progress in the ITER Physics Basis. *Nuclear Fusion*, 47, June 2007.

[44] J.D. Jackson. *Classical Electrodynamics*. Wiley, 1998.

[45] A. N. Kaufman. Quasilinear Diffusion of an Axisymmetric Toroidal Plasma. *Physics of Fluids*, 15:1063–1069, June 1972.

[46] L.L.D. Landau and E.M.A. LIFSHITZ. *Course of Theoretical Physics. - 1: Mechanics*. Pergamon Press, 1976.

[47] M. Lesur, Y. Idomura, and X. Garbet. Fully nonlinear features of the energetic beam-driven instability. *Physics of Plasmas*, 16(9):092305, September 2009.

[48] M. Lesur, Y. Idomura, K. Shinohara, X. Garbet, and The JT-60 Team. Spectroscopic determination of kinetic parameters for frequency sweeping Alfvén eigenmodes. *Physics of Plasmas*, 17(12):122311–+, December 2010.

[49] M. K. Lilley and B. N. Breizman. Convective transport of fast particles in dissipative plasmas near an instability threshold. *Nuclear Fusion*, 52(9):094002, September 2012.

[50] M. K. Lilley, B. N. Breizman, and S. E. Sharapov. Destabilizing Effect of Dynamical Friction on Fast-Particle-Driven Waves in a Near-Threshold Nonlinear Regime. *Physical Review Letters*, 102(19):195003, May 2009.

[51] M. K. Lilley, B. N. Breizman, and S. E. Sharapov. Effect of dynamical friction on nonlinear energetic particle modes. *Physics of Plasmas*, 17(9):092305–+, September 2010.

[52] S. M. Mahajan and C. Y. Chen. Plasma kinetic theory in action-angle variables. *Physics of Fluids*, 28:3538–3545, December 1985.

[53] M. E. Manuel. Laboratory Observations of Wave-Induced Radial Transport within an "Artificial Raditation Belt". In *Laboratory Space Science Workshop*, page 193, 1998.

[54] D. Maslovsky, B. Levitt, and M. E. Mauel. Observation of Nonlinear Frequency-Sweeping Suppression with rf Diffusion. *Physical Review Letters*, 90(18):185001, May 2003.

[55] P. J. Morrison. Hamiltonian and action principle formulations of plasma physics. *Physics of Plasmas*, 12(5):058102, May 2005.

[56] V. Mukhovatov, M. Shimada, A. N. Chudnovskiy, A. E. Costley, Y. Gribov, G. Federici, O. Kardaun, A. S. Kukushkin, A. Polevoi, V. D. Pustovitov, Y. Shimomura, T. Sugie, M. Sugihara, and G. Vayakis. Overview of physics basis for ITER. *Plasma Physics and Controlled Fusion*, 45(26):A260000–A252, December 2003.

[57] C. Nguyen, H. Lütjens, X. Garbet, V. Grandgirard, and M. Lesur. Existence of metastable kinetic modes. *Phys. Rev. Lett.*, 105(20):205002, Nov 2010.

[58] R. M. Nyqvist, M. K. Lilley, and B. N. Breizman. Adiabatic description of long range frequency sweeping. *Nuclear Fusion*, 52(9):094020, September 2012.

[59] A. Ödblom, B. N. Breizman, S. E. Sharapov, T. C. Hender, and V. P. Pastukhov. Nonlinear magnetohydrodynamical effects in precessional fishbone oscillations. *Physics of Plasmas*, 9:155–166, January 2002.

[60] T. M. O'Neil, J. H. Winfrey, and J. H. Malmberg. Nonlinear Interaction of a Small Cold Beam and a Plasma. *Physics of Fluids*, 14:1204–1212, June 1971.

[61] F. Peinetti, W. Bertsche, J. Fajans, J. Wurtele, and L. Friedland. Numerical studies of driven, chirped Bernstein, Greene, and Kruskal modes. *Physics of Plasmas*, 12(6):062112, June 2005.

[62] N. V. Petviashvili. *Coherent Structures in Nonlinear Plasma Dynamics*. PhD dissertation, University of Texas at Austin, Department of Physics, May 1998.

[63] S. D. Pinches, H. L. Berk, M. P. Gryaznevich, S. E. Sharapov, and J.-E. Contributors. Spectroscopic determination of the internal amplitude of

frequency sweeping TAE. *Plasma Physics and Controlled Fusion*, 46:47, July 2004.

[64] M. Podestà, W. W. Heidbrink, D. Liu, E. Ruskov, R. E. Bell, D. S. Darrow, E. D. Fredrickson, N. N. Gorelenkov, G. J. Kramer, B. P. Leblanc, S. S. Medley, A. L. Roquemore, N. A. Crocker, S. Kubota, and H. Yuh. Experimental studies on fast-ion transport by Alfvén wave avalanches on the National Spherical Torus Experiment. *Physics of Plasmas*, 16(5):056104, May 2009.

[65] W. H. Press, S. A. Teukolsky, W. T. Vetterling, and B. P. Flannery. *Numerical recipes in FORTRAN. The art of scientific computing.* 1992.

[66] M. N. Rosenbluth, H. L. Berk, J. W. Van Dam, and D. M. Lindberg. Continuum damping of high-mode-number toroidal Alfvén waves. *Physical Review Letters*, 68:596–599, February 1992.

[67] M. N. Rosenbluth, H. L. Berk, J. W. Van Dam, and D. M. Lindberg. Mode structure and continuum damping of high-n toroidal Alfvén eigenmodes. *Physics of Fluids B*, 4:2189–2202, July 1992.

[68] C.E. Shannon. Communication in the presence of noise. *Proceedings of the IRE*, 37(1):10–21, 1949.

[69] L. N. Tao. On Variational Principles for Electromagnetic Theory. *Journal of Mathematical Physics*, 7:526–530, March 1966.

[70] R. G. L. Vann, H. L. Berk, and A. R. Soto-Chavez. Strongly Driven Frequency-Sweeping Events in Plasmas. *Physical Review Letters*, 99(2):025003, July 2007.

[71] G. Vlad, F. Zonca, and S. Briguglio. Dynamics of Alfvén waves in tokamaks. *Nuovo Cimento Rivista Serie*, 22:1–97, July 1999.

[72] G. Wang and H. L. Berk. Model for spontaneous frequency sweeping of an Alfvén wave in a toroidal plasma. *Communications in Nonlinear Science and Numerical Simulations*, 17:2179–2190, May 2012.

[73] G. Wang and H. L. Berk. Simulation and theory of spontaneous TAE frequency sweeping. *Nuclear Fusion*, 52(9):094003, September 2012.

[74] J. Wesson. *Tokamaks*. International Series of Monographs on Physics. OUP Oxford, 2011.

[75] R.B. White. *The Theory of Toroidally Confined Plasmas*. Imperial College Press, 2006.

[76] R.B. White. *Asymptotic Analysis of Differential Equations*. Imperial College Press, 2010.

[77] H. Ye and P. J. Morrison. Action principles for the Vlasov equation. *Physics of Fluids B*, 4:771–777, April 1992.

[78] L.-J. Zheng and M. Kotschenreuther. AEGIS: An adaptive ideal-magnetohydrodynamics shooting code for axisymmetric plasma stability. *Journal of Computational Physics*, 211:748–766, January 2006.

[79] F. Zonca and L. Chen. Theory of toroidal Alfvén modes excited by energetic particles in tokamaks. *Physics of Plasmas*, 3:323–343, January 1996.

Vita

Ge Wang was born in Xiashi, Zhejiang on 8 May 1978, the son of Wang Xueqing and Xu Xinbao. He received the Bachelor of Science degree in Applied Physics from the University of Science and Technology of China (USTC). He has taken a lecturer position in USTC since his graduation of 2001. He also received the Master of Science degree in Plasma Physics from USTC during this period. When the five year contract was completed, he applied to the University of Texas at Austin for enrollment in their physics program. He was accepted and started graduate studies in August, 2006.

Permanent address: 1628 W 6TH ST APT A
Austin, Texas 78703

This dissertation was typeset with LaTeX[†] by the author.

[†]LaTeX is a document preparation system developed by Leslie Lamport as a special version of Donald Knuth's TeX Program.